THE THERMOMECHANICAL RESPONSE OF PARTICULATE COMPOSITE ENERGETIC MATERIALS UNDER MECHANICAL VIBRATION

A Dissertation

Submitted to the Faculty

of

Purdue University

by

Allison R. Range

In Partial Fulfillment of the

Requirements for the Degree

of

Doctor of Philosophy

December 2019

Purdue University

West Lafayette, Indiana

THE PURDUE UNIVERSITY GRADUATE SCHOOL
STATEMENT OF DISSERTATION APPROVAL

Dr. Jeffrey Rhoads, Chair

School of Mechanical Engineering

Dr. Patricia Davies

School of Mechanical Engineering

Dr. J. Stuart Bolton

School of Mechanical Engineering

Dr. Bryan Boudouris

Charles D. Davidson School of Chemical Engineering

Approved by:

Dr. Nicole Key

Head of the Mechanical Engineering Graduate Program

ACKNOWLEDGMENTS

With great appreciation, I'd like to acknowledge my advisor, Jeffrey Rhoads, for providing guidance and support throughout my graduate education. I would also like to thank Patricia Davies and J. Stuart Bolton for their contributions to my success in this field, as well as the staff of Herrick Laboratories for always being there to help students when possible. Also, thank you to my friends in the research group for the moral support both in the lab and in life.

To my family members and friends, especially Brenda Range and Troy Odstrcil—thank you for the constant encouragement and understanding throughout the course of this work, even during the difficult moments. It is my sincere hope that I have made you proud.

This work was funded by the Air Force Research Laboratory through Grant No. FA8651-16-D-0287 entitled "Hysteretic Heating of Polymer Crystal Composites through Mechanical Vibration" and Grant No. FA8651-18-2-0004 entitled "Exploring the Thermomechanics of Energetic and Mock Energetic Composite Materials Under Quasi-Static and Near-Resonant Excitation".

Distribution statement A: Approved for public release. Distribution unlimited. (96TW-2019-0454)

TABLE OF CONTENTS

LIST OF TABLES

LIST OF FIGURES

Figure Page

Figure Page

Figure Page

Figure Page

Figure Page

Figure Page

ABSTRACT

Range, Allison R. Ph.D., Purdue University, December 2019. The Thermomechanical Response of Particulate Composite Energetic Materials Under Mechanical Vibration. Major Professor: Jeffrey F. Rhoads, School of Mechanical Engineering.

Polymer-bonded, particulate composite energetic materials are widely used in the defense and energy sectors for munitions systems and explosive devices, yet their thermomechanical behavior is not well understood. In this work, the macroscale, thermomechanical response of energetic materials to contact mechanical excitation was studied at frequencies spanning 1 Hz to 100 kHz. The effects of formulation variation, thermal boundary conditions, excitation amplitude, and intentional stress concentrations within large composite plate samples were examined when the samples were excited at various resonances. Initial experiments focused primarily on the first structural resonance of a plate geometry, as determined experimentally using laser Doppler vibrometry. Excitation at frequencies up to 1000 Hz resulted in heating, attributable to the viscoelastic nature of the polymeric binder, on the order of 2-3°C/hr, and the propagation of structural defects such as cracks. At frequencies above 10 kHz, the heat generation within the material increased, potentially due to a combination of viscoelastic heating, particle / binder interactions, and conduction with exterior mounting components. Experiments were performed utilizing laser Doppler vibrometry and infrared thermography on both inert and fully-loaded energetic material variants in order to analyze the thermal and mechanical response due to the mechanical excitation using a piezoelectric shaker. The thermal analysis of various sample formulations revealed temperature changes on the order of 4°C/min, with several samples reaching 100°C within a 15 min window. Due to significant material softening observed during the thermal cycling, the resonant frequency was found to shift over the course of the experimental analysis. Potential applications may require the energetic materials to sustain extreme temperature environments coupled with vibratory loads. In an effort to characterize this effect, a custom enclosure was fabricated to maintain an ambient air temperature around the sample of up to 70°C. Distinctions between ambient

and elevated temperature environment experiments on a preliminary sample set were noted in regard to rate of change of temperature, and several samples exhibited maximum surface temperatures in excess of 100°C. Finally, an analytical model was developed to estimate the heat generation associated with the observed experimental results. The cylindrical sample geometry was modeled as a longitudinal rod subjected to harmonic base excitation, and the resulting mechanical response was used to estimate the rate of mechanical energy expended per unit length at the predicted resonant frequencies. The thermal response was obtained by numerical integration of the heat transfer equation accounting for energy generation in the system, and the resulting axial temperature profiles predicted maximum temperatures on the order of 120°C after 60 seconds of excitation at the first predicted resonant frequency.

1. INTRODUCTION

Due to their prevalant use in improvised explosives devices and munition systems, energetic and inert particulate composite materials are of interest for numerous national security, defense, and energy applications. An energetic material is characterized by a large amount of stored chemical energy with the potential for ignition in response to a stimulus. This class of material spans propellants, explosives, and fuels. Proper functionality and safety must be ensured when designing, fabricating, and handling munition systems, as mechanical excitation can induce heating within the material [1,2]. The micrograph in Figure 1.1 shows a cross-section of this type of material produced by van der Heijden *et al.* [3], in which energetic particles are held within an elastic polymer binder. The inhomogeneity of this composition presents unique challenges with regard to the thermomechanical behavior of the material, and can give rise to important phenomena, such as hot-spot formation and particle debonding at the crystal-binder interface [4]. It has been observed that these polymer-bonded materials exhibit stiffening as their age increases [5], an effect that must be accounted for when utilizing classic thermomechanical models for polymer-based composites responding to mechanical excitation. The materials also exhibit dramatically varying bulk thermal and mechanical moduli when particle/binder ratios are changed and these materials can rapidly decompose, both thermally and mechanically, under comparatively weak external loads [6–9]. These examples provide a subset of the qualities that contribute to the distinct thermal and mechanical behavior exhibited by polymer-bonded energetic materials.

1.1 Thermomechanical Response of Polymer and Composite Materials to Applied Vibration

The mechanical response of polymeric materials to mechanical vibration has been widely researched in open literature. Polymers exhibit several distinct properties, including high levels of internal energy dissipation and low thermal conductivities, that provide pathways

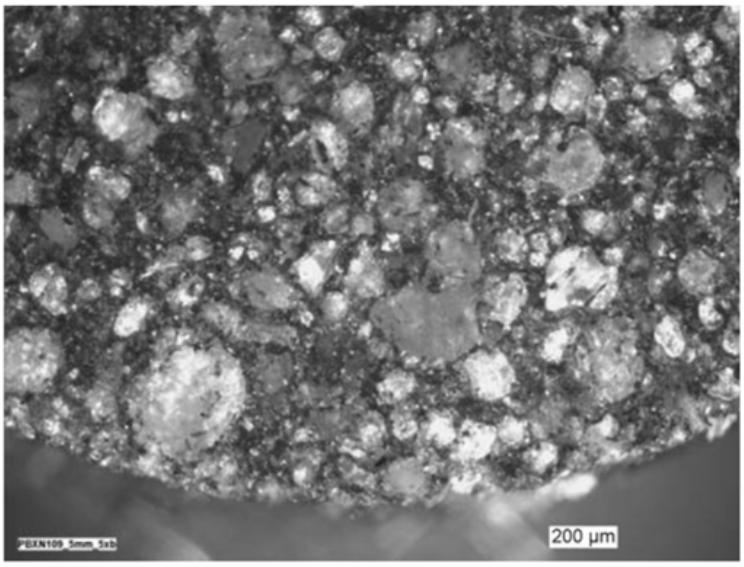

Figure 1.1. : Optical micrograph of a polished cross-section of PBXN-109 containing conventional RDX [3].

for significant heat generation when under load. Ratner *et al.* investigated the self-heating of polymers due to hysteretic heating and heat losses during cyclic deformation in which two significant zones of steady-state heating were identified, described as a low temperature and a high temperature zone, separated by a discontinuous zone in which heating is impossible [10]. Under the assumption of constant stress amplitude, the softening of the material results in an increased strain amplitude and, consequently, an increased work of deformation, or rate of heat release, with each cycle. The heat release rate due to hysteretic heating has a temperature dependence that is not monotonic, whereas heat losses to the environment have a direct, linear temperature-dependence assuming a constant heat transfer coefficient. At temperatures in which these two closely interact, thermal equilibrium is unstable or discontinuous and the system will tend toward the high-temperature zone. Additional work, performed by Dinzart *et al.*, modeled the thermomechanical response of thermoplastic beams undergoing cyclic bending utilizing a temperature and frequency dependent viscoelastic model [11]. The authors cited an amplification of thermal softening effects in the high-frequency regime due to the reduced loss of dissipated energy to the surroundings.

Furthermore, the characterization of fiber and particulate composite materials and structures has been increasingly studied due to their ability to generate heat on a bulk scale. Under mechanical load, the internal dissipation results in energy losses converted to heat that are commonly observed in regions of high stress. Thus, the resulting temperature profiles will depend upon the modal response of the system under mechanical vibration. This phenomenon was studied by Dimarogonas and Syrimbeis for rectangular metal plates [12]. Gibson utilized modal vibration measurements in response to impulsive excitation to determine the mechanical properties of fiber-reinforced composite materials [13]. In a similar approach, Botelho *et al.* estimated the damping properties of a hybrid fiber-metal laminate, validated against the analytical predictions of the composite micromechanics approach [14]. Katunin *et al.* performed studies involving glass fiber-reinforced laminate plates, which revealed appreciable heating at modal architectures in response to resonant excitation [15]. Finally, Cady *et al.* performed compression experiments on cylindrical pellet samples to investigate the temperature and strain rate dependence of the mechanical response of hydroxyl-terminated polybutadiene [16]. In the context of the present work, the potential for thermal response

in polymer and composite materials will be exploited through near-resonant, modal vibration in an attempt to observe the heating of energetic materials in response to mechanical vibration.

With regard to energetic materials, characterization methods are largely focused on particle-scale experiments and shock behavior with only a minor focus on vibration qualification testing. Prior to fabrication, energetic crystals are characterized by temperature and humidity tests as well as imaging methods, such as scanning electron microscopy (SEM) and micro-CT analysis to allow for the observation of particle morphology, chemical composition, orientation, and scale. Techniques such as these can be used to analyze homogeneity, porosity, and the defects present in a specific sample. Shock behavior is typically ascertained through a variety of impact experiments, characterized by high strain rate excitation on relatively small time scales. Tokmakoff *et al.* investigated the shock sensitivity of energetic molecular materials by transferring large quantities of energy into the molecules' internal vibrations using multiphonon up-pumping [17]. The study focused on weak shock waves indicative of accident scenarios that can couple with low frequency molecular vibration in the material to result in up-pumping. These methods provide information utilized primarily in the classification and design of energetic material components, however, they do not quantify the effects of prolonged high strain rate excitation in polymer-bonded explosives. Vibration qualification tests have been focused on examining the material's sensitivity to current operational environments which are characterized by low-frequency, low-amplitude excitation. Little is known about material sensitivity to this low-frequency, low-amplitude testing environment, and there are concerns regarding the potential for unintended deflagration at high-amplitude, high-frequency excitation in application.

1.2 Heat Generation in Solid Materials

The mechanically-induced heat generation of solids is a well-studied effect for pure materials and alternative composites. One such example is that of particle-filled elastomers used in systems such as tires and shock absorbers that are subjected to cyclic loading in application. The work of Bhenke *et al.* in this area is representative of many investigations on carbon-

black filled elastomers responding to cyclic strains up to 60% at frequencies on the order of 10 Hz [18]. The dominance of viscoelastic heating at relatively low heating rates allowed the authors to accurately predict the surface temperature of dumbbell-shaped specimens by using measurements of hysteresis. In addition, Bhenke *et al.* [18] noted an increase in surface temperature when increasing the forcing frequency from 1 to 10 Hz, but excitation frequencies larger than this range were outside of the scope of this application. The method developed by Bhenke also presents challenges due to the strain rate- and temperature-dependence of the mechanical material properties characteristic of polymers and composites, as well as the potential for damage accumulation at relatively low strain amplitudes. The most prevalent resolution to this challenge is referred to as time-temperature superposition (TTS) in which a representative data set of mechanical properties at varying temperatures and strain rates is measured and fit to produce a master curve of each property as a function of the two aforementioned variables. Walid and Liang applied this method to the elastic modulus, ultimate stress, and ultimate strain of an HTPB-based composite propellant at temperatures from -60 to 76°C and strain rates of 5 mm/min, 50 mm/min, and 500 mm/min [19]. Although some success has been noted for energetic materials with this technique, it is uncertain whether this method is valid for materials in which the adhesion of the particle-binder interface is altered as a result of temperature changes.

While it is not comprehensive, there exists a small body of work related to the influence of mechanical vibrations at low and high frequencies on particulate composite materials such as polymer-bonded explosives. The works of Loginov *et al.* [20,21] provide useful insight into the phenomenological nature of the vibration-induced heating of energetic materials. Initial experiments by Loginov and collaborators sought to characterize the initiation of explosives under vibration, citing important features such as inelastic deformation and non-uniform temperature distributions. Their later experiments focused on the structural and physicochemical changes in RDX crystals under vibrational excitation, concluding that vibration accelerates the formation of crystal defects, thus allowing for the progression of inelastic deformation, fracture, and dispersion. Although they capture the essential phenomena of decomposition at a coarse level, these works neglect investigation of the role of various struc-

tural or material properties, such as material formulation. The influence of thermal boundary conditions on this heat generation has also not been significantly investigated in prior work.

Although the method has not been usually applied to energetic materials, the use of high-frequency mechanical excitation as a means of inducing localized heating has been demonstrated in a variety of materials. Under mechanical load, the thermomechanical coupling in the system can be described using the thermodynamic theory of solids to incorporate both reversible and irreversible effects, such as thermoelastic and damping effects, respectively [22]. Vibrothermography, a nondestructive testing method utilizing this thermomechanical coupling behavior at high-frequency excitation, has been applied to various polymer and composite materials to identify impact damage, inclusions, voids, delaminations, and cracks [23,24]. Renshaw *et al.* [25] provided additional insight into high frequency excitation, citing friction and viscoelastic losses as significant components of heat generation. Renshaw *et al.* [25], as well as others [26–30], cited higher-frequency excitation as an effective mechanism for inducing a thermal response near stress concentrations in various materials. A similar application of mechanical loads in the realm of particulate composite energetic materials may induce localized heating that can have detrimental consequences in the operational environments for energetic materials. Thus, a thorough understanding of the thermal behavior in response to low and high frequency mechanical excitation is imperative in energetic material applications.

In prior work, Mares *et al.* characterized the internal heat generation of individual energetic particles embedded in elastic binder samples at ultrasonic frequencies (100 kHz - 20 MHz) [31]. At frequencies near 215 kHz, Mares observed the chemical decomposition of specific energetic crystals, including ammonium perchlorate and cyclotetramethylenetetranitramine (HMX), and attributed this significant heat generation to frictional effects and potential delamination between the particle and the polymer binder [32]. Chen *et al.* used infrared microscopy to observe energy localization in RDX crystals embedded in two polymeric binder materials in response to an ultrasonic horn vibrating at 20 kHz. The authors observed that several samples in the study exhibited signs consistent with energetic decomposition within 120 ms of the start of the test, and performed additional testing to approximate the onset of the heat generation at, or near, the particle-binder interface [33].

The importance of the interface led You *et al.* to continue the investigation using the ultrasonic horn to excite embedded energetic crystals with and without liquid coating, and observe rapid heating rates in coated crystals [34]. In further investigations, the response of fully-loaded composite materials resulted in significant heat generation in PBX 9501 samples when undergoing excitation in similar frequency ranges, concluding that the heating mechanisms observed were dependent on the excitation frequency [1]. Experiments have also been performed to characterize the localized heating, or "hot spot" formation, behavior of particulate composite explosives, using a modified Kolsky bar and high speed synchrotron X-ray phase contrast imaging to identify the fracture of crystals and frictional heating [32]. Results of previous experiments confirmed the existence of heat generation in composite beams and plates undergoing low-frequency inertial excitation. Temperature increases on the order of 1-2°C/hr were observed for plate samples fabricated from surrogate energetic material at varying ratios of crystal to binder [2,35]. In both studies, the composite material was shown to exhibit heating at modal architectures when excited near resonant frequencies.

In addition to experimental observations of heating within pure and composite materials, numerous methods have been proposed for analytically estimating heat dissipation under various loading conditions. It is well known that plastic work induced by mechanical deformation results in energy generation and storage within the material. The ratio of energy converted to heat to the overall mechanical energy due to deformation is commonly referred to in the literature as β. Although this parameter is difficult to measure due to its strain and strain-rate dependence, it is well studied in metals, and several methods have been proposed to accurately measure and predict the quantity during high-strain-rate split Hopkinson bar tests [36–38]. Tong *et al.* applied similar principles to solid propellants to characterize the surface-temperature evolution during strain-controlled tensile fatigue tests [39]. The authors utilized an assumption of adiabatic conditions during the initial rapidly increasing temperature stage of cyclic fatigue and an assumption of isothermal conditions at the temperature stabilization stage in order to compare the rate of mechanical energy converted to heat to the energy storage rate of the material. At large values of strain (greater than 5%), a phenomenon known as the Mullins Effect has been incorporated to capture the strain-induced softening in filled rubbers [40, 41]. A particular body of work performed by Schapery and

Farris [42–45] explored the application of this effect to the mechanical modelling of particulate composite energetic materials, inferring that the Mullins effect contributes primarily to the nonlinear portion of the response prior to the formation of voids. In addition, Schapery and Farris concluded that the majority of the overall energy dissipation (approx. 90%) can be predicted using linear theory; thus, only a minor percentage of the energy dissipation is provided by the Mullins effect [45]. These studies provide a solid foundation to the theoretical determination of the rate of heat generation within both pure and composite materials.

Throughout the course of the present research, experiments were performed to characterize the thermal behavior of polymer-bonded energetic materials in response to both low (below 1 kHz) and high frequency (1-80 kHz) excitation. An extended study on the macroscale thermomechanics of composite mock energetic plates under low frequencies of excitation is presented in Chapter 2, in particular exploring the effects of formulation variation, thermal boundary conditions, increased excitation amplitude, and intentional stress concentrations. A study characterizing similar thermal and mechanical behavior in response to excitation at frequencies above 1 kHz of small mock energetic cylinders is presented in Chapter 3, with significant focus on the heat generation associated with various material formulations. Due to the large heating rates exhibited in the mock energetic material study at high frequencies, the transition of the experiment from mock to fully-loaded, live energetic cylinders with RDX crystals embedded is discussed in Chapter 4. Energetic materials in application may be transported or stored in extreme temperature environments, thus the design, fabrication, and functional verification of a custom enclosure to characterize the mechanical and thermal response of inert and live energetic materials under elevated ambient air temperatures up to 60°C is discussed in Chapter 5. A method of analytically determining the heat dissipation evident in the experimental results to theoretically validate the observed material behavior is presented in Chapter 6. Finally, the overarching conclusions from the research, as well as recommendations for work to be explored in the future, are provided in Chapter 7.

2. LOW–FREQUENCY RESONANT EXCITATION OF MOCK ENERGETIC MATERIALS

The majority of this chapter was published as 'The influence of formulation variation and thermal boundary conditions on the near-resonant thermomechanics of mock explosives' in *Fracture, Fatigue, Failure and Damage Evolution, Volume 7*, 2017, and as 'The influence of macroscale stress concentrations on the near-resonant thermomechanics of mock energetic materials' in the *Summer Undergraduate Research Fellowship (SURF) Symposium, Paper 7*, 2017.

2.1 Introduction

In an effort to characterize the macroscale thermal and mechanical behavior of a polymer-bonded energetic material, low-frequency vibration experiments were performed on inert plate samples. The study described in this chapter was performed as an extension of initial experiments performed by Miller and Woods [2,35]. In the original study, the effect of crystal to binder ratio used in particulate composite plate samples on the plate response to low-frequency excitation was studied. These plates were fabricated with hydroxyl-terminated polybutadiene (HTPB) and ammonium chloride (NH_4Cl). The new experiments were conducted to extend the characterization method to plates of alternate energetic material compositions and to investigate effects caused by the inclusion of additive content materials, changing thermal boundary conditions, increasing the amplitude of the vibration excitation, and introducing intentional stress concentrations.

2.2 Experimental Techniques

The sample preparation and experimental set-up, including the measurement procedures, are described.

2.2.1 Sample Preparation

The samples of mock energetic explosive material were prepared using an HTPB binder, sucrose particles, and spherical aluminum powder. The sucrose particles, sieved to a diameter range of 106 to 355 μm, are comparable in size to particles of RDX, a common energetic material. The spherical aluminum powder has an average particle diameter of 25 μm. In real world applications, the weight ratio of particles to binder can vary drastically, thus motivating the investigation of the responses resulting from various formulations.

To fabricate the test samples, the HTPB binder was combined with a curing agent, isophorone diisocyanate (IPDI), and other constituents. The binder was then mixed in a Resodyn^{TM} acoustic mixer for 5 min to ensure a homogeneous mixture. The mixture was then degassed in a vacuum chamber to remove unwanted gasses from the liquid mixture and to prevent bubbles from forming in the final sample. The solid constituents were then added to the binder mixture and the Resodyn^{TM} was again used to mix the constituents for 5 min. For samples with low particle-to-binder weight ratios, the sample was again degassed, after which the particle and binder mixture was poured into a custom plate mold. The plates were cured in an oven for a period of 7 days at 60°C. The final dimension of each plate was 25.4 cm by 17.8 cm by 1.27 cm.

The formulation variations are based upon the PBXN-109 formulation given by Lochert *et al.* [51], but substituting sucrose particles for the RDX to render the plate inert. A summary of this base formulation is given in Table 2.1.

Plates were prepared with 85% solids loading. Three formulation variations were made with 0%, 15%, and 30% weight ratios of aluminum additive content. Solids loading defines the weight ratio of solid crystals to polymer binder in the overall formulation. Additive content provides the weight ratio of spherical aluminum powder to mock RDX crystals (sucrose) in the solids. The mass and density of each plate is presented in Table 2.2.

In an attempt to provide a comparison to the plates with significant solids loading, two plates were fabricated of pure binder; however, the resulting sample was far to pliable to mount and test in the experimental setup. The ratio of polybutadiene resin to plasticizer in

Table 2.1. : PBXN-109 mock formulation

Constituent	Weight Percent
RDX/Sucrose	64
Aluminum	20
R45-HT (Hydroxyl-terminated Polybutadiene resin)	7.346
Dioctyl Adipate (DOA)	7.346
Antioxidant 2246	0.100
Dantocol® DHE	0.260
Triphenylbismuth	0.020
Isophorone Diisocyanate (IPDI)	0.950

Table 2.2. : Plate sample characteristics

Solids Loading-Additive Content-Sample	Mass (kg)	Density (kg/m^3)
85-00-1	0.7025	1225
85-00-2	0.6400	1275
85-15-1	0.8148	1421
85-15-2	0.8027	1400
85-30-1	1.0392	1611
85-30-2	0.9200	1604

the binder formulation would need to be significantly increased to produce a polymer binder with sufficient stiffness for this type of testing.

2.2.2 Experimental Setup

Experiments were performed according to the methodology developed in Miller *et al.* [2]. A TIRA 59335/LS AIT-440 electrodynamic shaker was used to mechanically excite the plates at low excitation levels. The parallel short ends of the plate were clamped to the shaker using a plate fixture to simulate clamped-free-clamped-free (CFCF) mechanical boundary conditions with an unsupported sample area of 22.9 cm by 17.8 cm. An accelerometer mounted to the shaker head provided direct feedback to the VibeLab VL-144 vibration controller. The transient and steady-state thermal responses were recorded at the sample surface using a FLIR A325 thermal camera with a temperature sensitivity of 0.07°C at 30°C and an accuracy of ± 2°C or ± 2%. Note that the emissivity of each sample was calibrated by determining the reflected apparent temperature of a perfect emitter and then calibrating the sample temperature to that of a known emissivity. A Polytec PSV-400 scanning laser Doppler vibrometer was used to record the frequency response of each plate. The experimental setup is presented in Figure 2.1.

Frequency response functions, relating the support vibration to the measured velocity at points on the plate, were estimated in response to broadband (10-1000 Hz) white noise applied at various forcing levels. H1 estimators were used to estimate the system frequency response by comparing the estimated cross spectral density between the accelerometer on the shaker head and the differentiated vibrometer reading (converted in the frequency domain using the forcing frequency) to the estimated power spectral density of the accelerometer. The estimated frequency response functions were calculated for both the response at the geometric center of the plate and at an offset point. The offset point was half of the distance from the free and clamped edges to the center of the plate, measured as 4.4 cm and 5.7 cm, respectively.

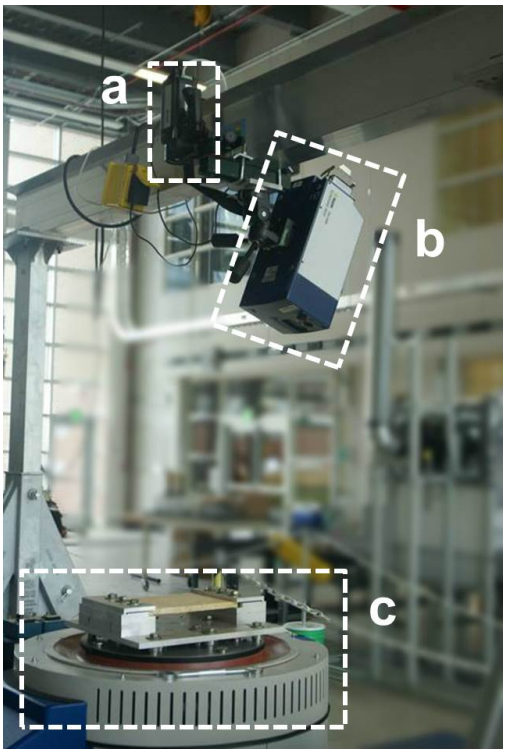

Figure 2.1. : The experimental setup with a (a) FLIR A325 infrared camera and (b) Polytec PSV-400 scanning laser Doppler vibrometer positioned above a plate mounted to the (c) TIRA shaker by the CFCF clamping mount.

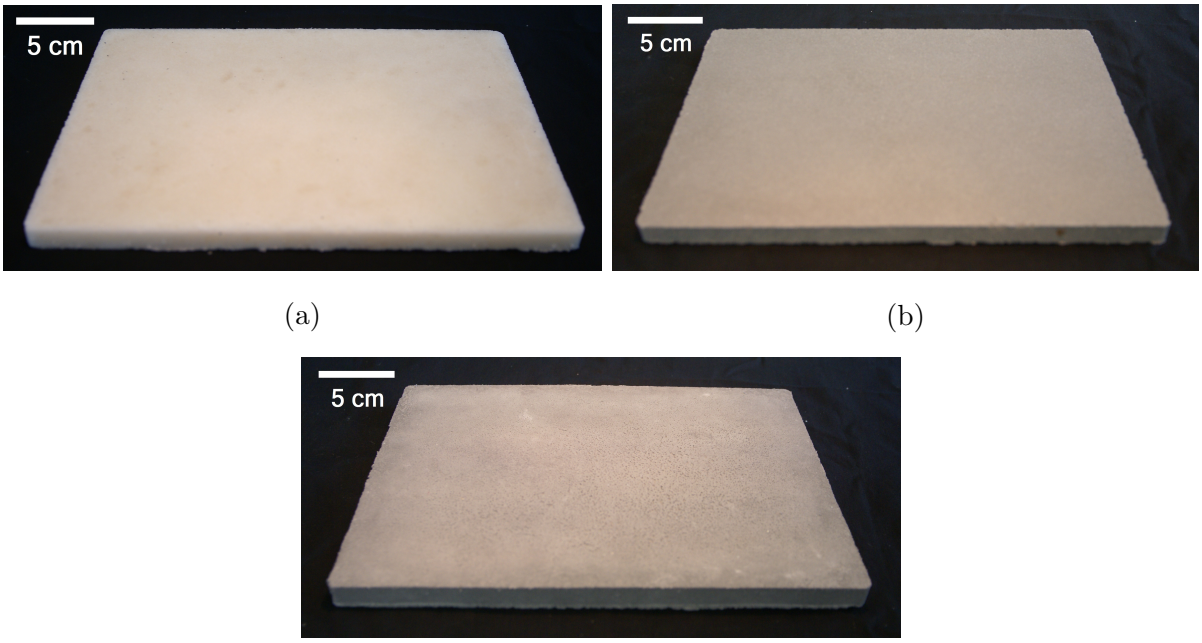

(a) (b)

(c)

Figure 2.2. : Representative plate samples of 85% solids loading with (a) 0% (b) 15% and (c) 30% additive content.

2.3 Results and Discussion

2.3.1 Formulation Variation

The effect of formulation variation on the near-resonant thermomechanical response of the mock energetic materials was observed using the three variations of aluminum additive content mentioned above (0%, 15%, and 30%). Each plate was tested under convective boundary conditions 43 days after curing to avoid inconsistencies due to aging effects of the polymer composite in the observed mechanical responses. The data presented in this section applies to the plates pictured in Figure 2.2a-2.2c.

Mechanical Response

The magnitude of the H1 frequency response estimates and corresponding coherence functions for representative plates of 85% solids loading with 0, 15, and 30% additive content

in response to three levels of excitation are given in Figures 2.3-2.5. As noted earlier, the frequency responses relate the base accelerations to the accelerations measured on top of the plate samples. The H1 estimates were calculated using Hann windowed segments with a frequency resolution of 1.25 Hz. Frequency response estimates for the additional plates of identical formulation ratios are not presented here for the sake of brevity but appear qualitatively similar to those presented below. All of the plates exhibit clear resonant behavior at multiple frequencies within the excited range of 10 to 1000 Hz. Softening behavior is also exhibited in all of the formulation variations, as evidenced by the decrease in both frequency and amplitude with increased forcing levels. With regard to sample variation, the amplitude and general trend of each estimated frequency response magnitude appears similar for each of the three additive content levels. It should be noted that signal return from the laser Doppler vibrometer improved with the addition of aluminum due to its increased reflectivity.

The experimentally obtained peak frequencies and estimated quality factors for each plate (measured from the highest excitation level utilized in the random vibration tests) are presented in Table 2.3. The magnitude of the frequency response estimate at the first resonant frequency for plates with identical formulation ratios appear to coincide, suggesting that the sample fabrication was consistent across various mixing days. The quality factors were estimated using the bandwidth at half-power, and the damping was low enough to observe distinct peaks in the estimated frequency response magnitude. The loss factors, designated as η, are estimated by definition as the reciprocal of the quality factor.

Interestingly, each of the frequency response estimates presented above exhibit a significant peak in amplitude at approximately 700 Hz that was not expected based upon previous experiments for plates of this geometry. In an attempt to characterize the high frequency resonance, the operational deflection shape was recorded in response to a 6 g mechanical excitation for plates of 85% solids loading with 0% and 30% additive content by the laser Doppler vibrometer. Deflection behavior in each case can be approximated as a 3-1 plate mode, indicated by 3 distinct peaks in the longitudinal direction with 1 row of peaks in the transverse direction, as shown in Figure 2.6.

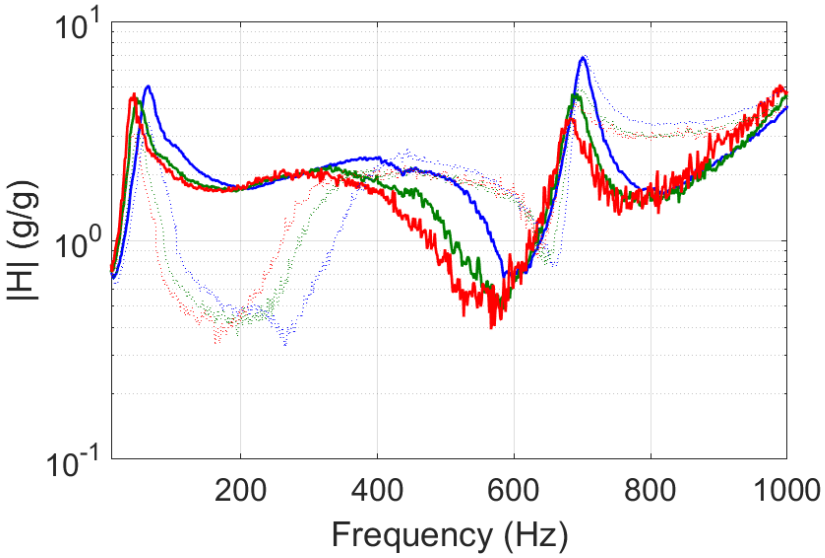

(a)

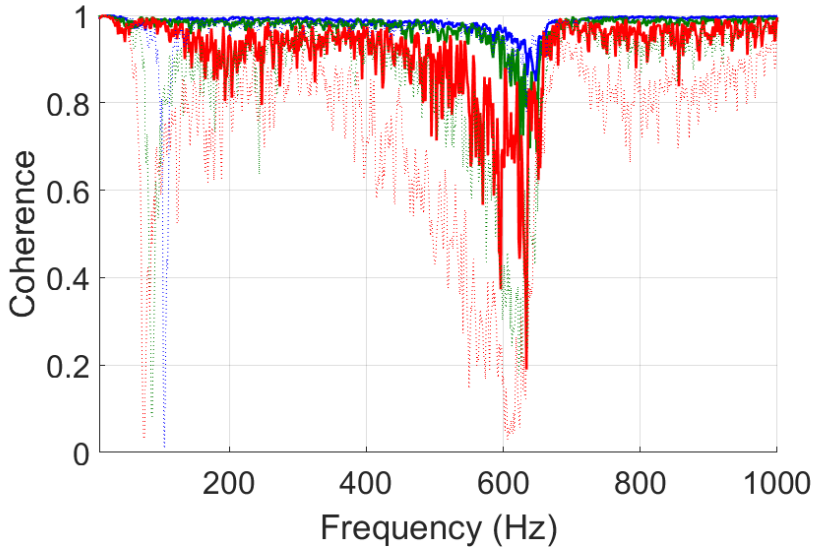

(b)

Figure 2.3. : Experimental (a) H1 estimate of the frequency response magnitude and (b) coherence estimate of a 85% solids loading - 0% additive plate at three levels of excitation. The red, green, and blue curves depict responses at 2.44, 1.86, and 1 g RMS, respectively. Solid lines represent data from the geometric center, and dashed lines represent data from the offset point. Data is presented for the first 85-0% plate.

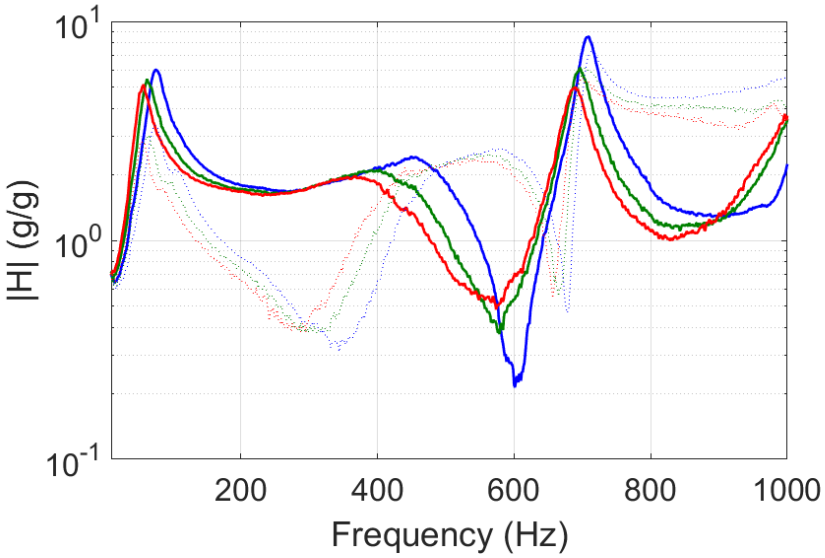

(a)

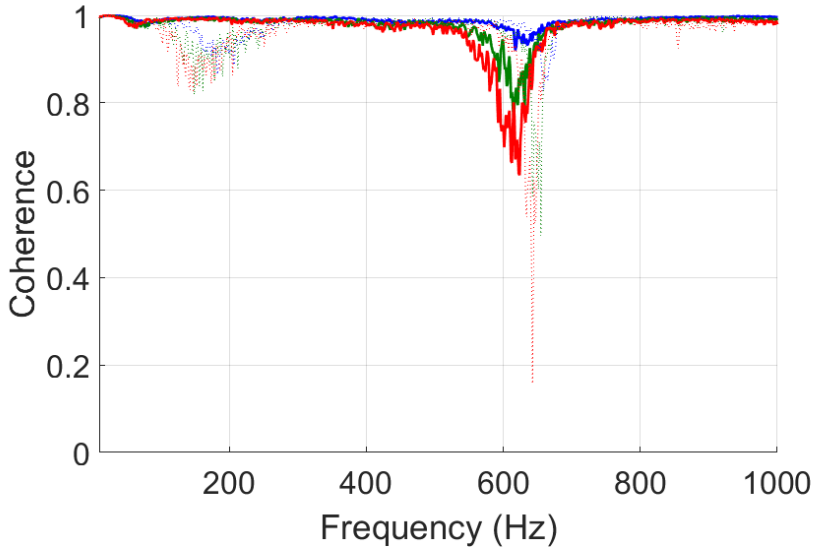

(b)

Figure 2.4. : Experimental (a) H1 estimate of the frequency response magnitude and (b) coherence estimate of a 85% solids loading - 15% additive plate at three levels of excitation. The red, green and blue curves depict responses at 2.44, 1.86, and 1 g RMS, respectively. Solids lines represent data from the geometric center, and dashed lines represent data from the offset point. Data is presented for the first 85-15% plate.

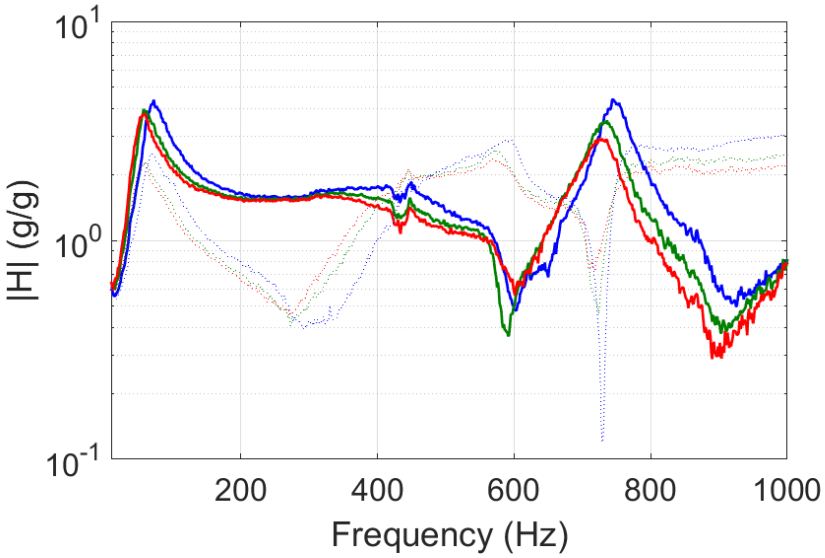

(a)

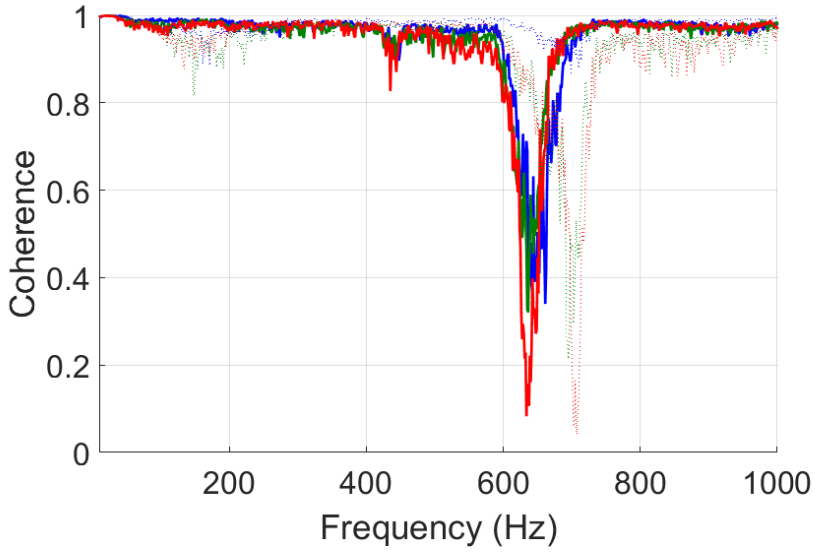

(b)

Figure 2.5. : Experimental (a) H1 estimate of the frequency response magnitude and (b) coherence estimate of a 85% solids loading - 30% additive plate at three levels of excitation. The red, green, and blue curves depict responses at 2.44, 1.86, and 1 g RMS, respectively. Solid lines represent data from the geometric center, and dashed lines represent data from the offset point. Data is presented for the first 85-30% plate.

Table 2.3. : First resonant frequencies with associated quality and loss factors for each of the plate samples in the analysis.

Solids Loading- Additive Content-Sample	f_{11} (Hz)	Q_{11}	η
85-00-1	39.2	2.33	0.43
85-00-2	37.5	2.50	0.40
85-15-1	55.2	2.56	0.39
85-15-2	56.1	2.37	0.42
85-30-1	51.6	1.67	0.60
85-30-2	52.1	1.77	0.56

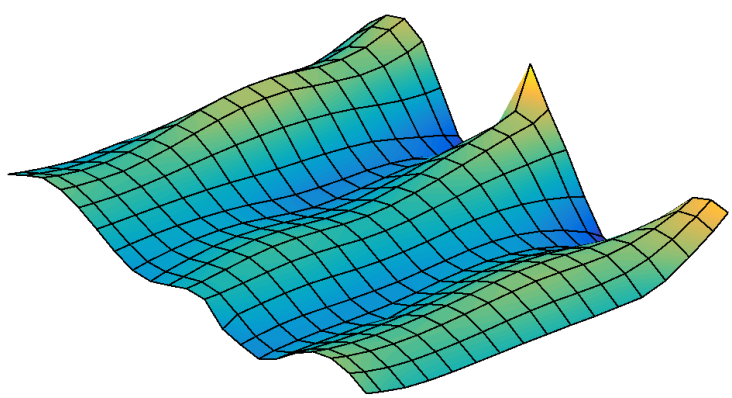

Figure 2.6. : Operational deflection shape of a 85% solids loading - 0% additive plate in response to 6 g harmonic excitation at 695 Hz.

Thermal Response

The spatial average and maximum surface temperature of each plate over the 60 min window when excited at the first resonant frequency (see Table 2.3) under convective boundary conditions are presented in Figures 2.7a and 2.7b, respectively. The data appears to asymptotically approach steady state within the duration of the data measurement. Each plate exhibits a similar upward trend, but little distinction can be drawn between the various levels of additive content. Note that the negative lower bound of average temperature increase at the start of the experiment can be attributed to minor discrepancies between the spatial average temperature of the plate and the ambient temperature recorded on a reference material in proximity to the experiment. Within the 60 min experiment, the observed spatial average and maximum plate surface temperature increased by approximately 0.5°C and 1.2°C, respectively. The magnitude of temperature increase does correlate well with the trends exhibited by plates of high solids loading content in prior work [2].

2.3.2 Thermal Boundary Conditions

Constant harmonic excitation was used to obtain the thermal response at the top surface of the plates under two different boundary conditions. The first of which was characterized by convection with the open air on the four largest surfaces and conduction with the aluminum clamping fixture on the remaining small ends, referred to herein as the 'convective' condition. In contrast, the second thermal boundary condition, referred to as 'insulated', utilized an insulated boundary offset from all sides of the plates. A thermally-insulated box was constructed to roughly simulate an insulated environment, as shown in Figure 2.8. The structural integrity of the box was ensured by using acrylic panes with a 3.8 cm clearance relative to the top surface of the plate, and additional thermal insulation was provided by 1.9 cm thick foam with a K-factor of 0.25 at 24°C attached on all of the sides. The box was attached to the outside of the clamping fixture of the plate and moved with the shaker head during the course of experimentation.

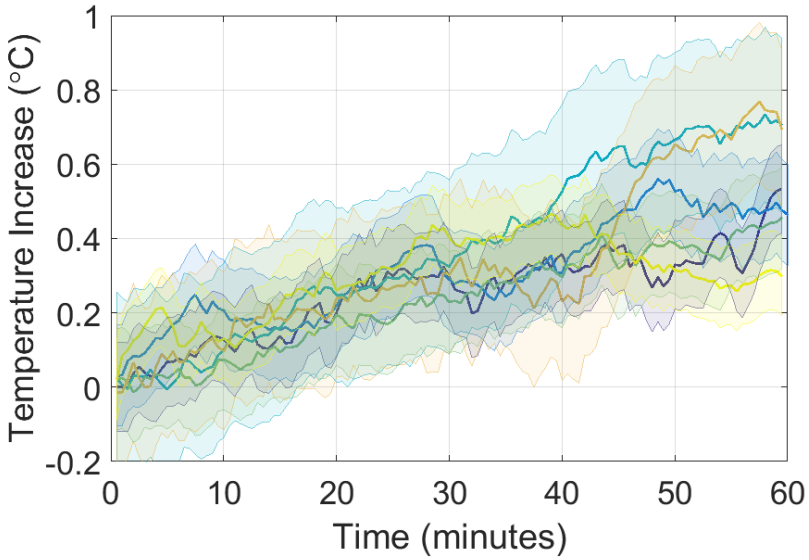

(a)

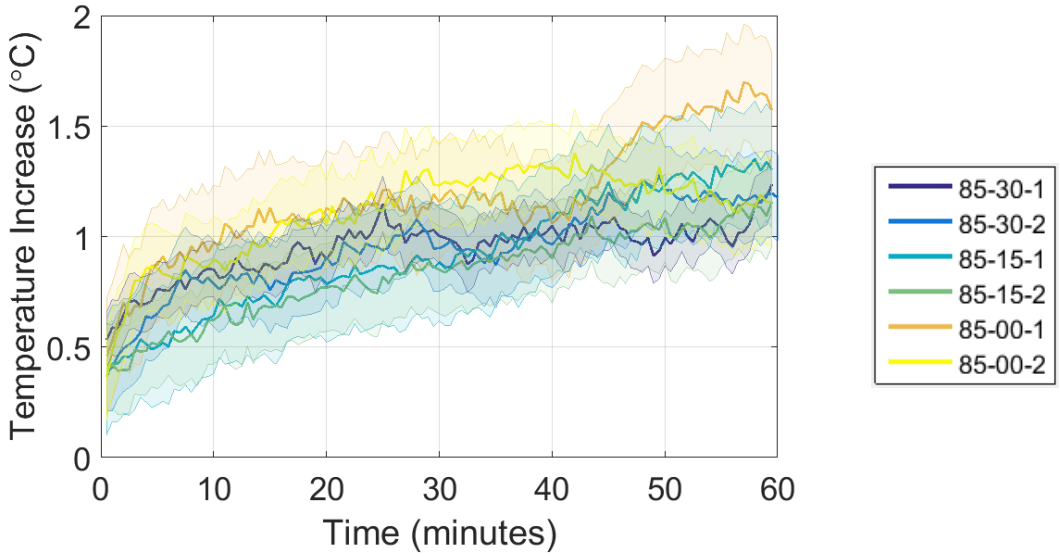

(b)

Figure 2.7. : A comparison of the experimentally obtained plate surface temperature versus time in response to a 2 g harmonic excitation near the first resonant frequency for all of the plates. Solid lines indicate experimental data. The colored envelope indicates the error associated with the thermal camera measurement. Data are presented for the (a) mean and (b) maximum plate surface temperatures versus time. The legend indicates: solids loading - additive content - sample number.

Figure 2.8. : The acrylic box with foam insulation used to create an insulated boundary condition for the plates.

Table 2.4. : A comparison of the mean and maximum temperature increase under convective and insulated thermal boundary conditions for the minimum and maximum additive content samples.

Solids Loading-Additive Content-Sample	Mean Surface Temperature (°C)		Maximum Surface Temperature (°C)	
	Convective	Insulated	Convective	Insulated
85-00-01	0.52	1.26	0.90	1.51
85-30-01	0.81	1.60	0.97	1.77

Thermal Response

A forcing level of 2 g was used to obtain the thermal response under both the convective and insulated boundary conditions. Due to the opaque nature of the insulated box, the transient temperature profile as a function of time could not be obtained with the infrared thermal camera as described in the previous section. As a result, the thermal camera was used to collect a snapshot of data at the beginning and end of the 60 min time interval. The temperature increase of the plate was determined as the difference between the two recorded temperature values.

Application of the insulated boundary condition to the various plates yielded increased heat generation as expected. The temperature increases for the convective and insulated experiments for a single plate of minimum and maximum additive content is given in Table 2.4. As previously noted, the values presented are determined as the temperature difference between the initial and final profiles recorded using the infrared camera. Note that the temperature increases presented here for the 85-00 plate sample were modeled and results are given in the following section. Inconsistencies were present between the experimental results and a simple bulk-scale heat transfer model prediction. These inconsistencies may be attributable to either experimental error within the thermal measurements or, more likely, the variations in the particulate composite nature of the material itself.

Thermal Simulation

In order to predict the temperature responses observed in the experiment, a thermal simulation was performed with a commercial finite element package for both the convective and insulated boundary conditions. The theory and assumptions used to model the simulation are outlined in Miller *et al.* [2] in which the heat source is given by

$$r_{avg} = \frac{\omega}{2\pi} \int_{t_0}^{t_0+\frac{2\pi}{\omega}} \sigma \frac{\partial \epsilon}{\partial \tau} d\tau = \pi_0 \left(\eta\omega\right) \tag{2.1}$$

where η is the material loss factor, ω is the frequency of excitation, and π_0 is the strain energy density given by

$$\pi_0 = \frac{E' \epsilon_0^2}{2\left(1-\nu^2\right)} \tag{2.2}$$

where E' is the real part of the dynamic modulus of the plate, ν is Poisson's ratio, and ϵ_0 is the strain magnitude. The dynamic modulus was estimated using a system identification approach developed by Paripovic [5]. Specifically, the technique relies on acceleration data from uniaxial compression tests to estimate stiffness and damping coefficients that are then used to identify dynamic mechanical properties. Transient thermal properties for each representative plate were determined using the transient plane source technique [46]. The dynamic modulus (E'), thermal conductivity (k), and thermal diffusivity (α) were measured as 3.02 MPa, 0.35 W/(m-K), and 2.84×10^{-7} m^2/s, respectively, for a representative plate of 85% solids loading with 0% additive content. The density of 1250 kg/m^3 was taken as the average of the two 85-00 plate sample densities given in Table 2.2, and the structural loss factor was estimated as the inverse of the experimental quality factors for the two 85-00 plate samples given in Table 2.3.

Thermal behavior for a representative plate of the minimum additive content formulation was simulated using a commercial finite element package in response to the heat source in Eq. (2.1). In the convective simulations, insulated clamped ends were assumed with convective boundary conditions on all of the other surfaces. In the insulated boundary condition simulations, all of the surfaces were assumed to be perfectly insulated. The transient average and maximum simulated temperature response for a representative plate of 85% solids load-

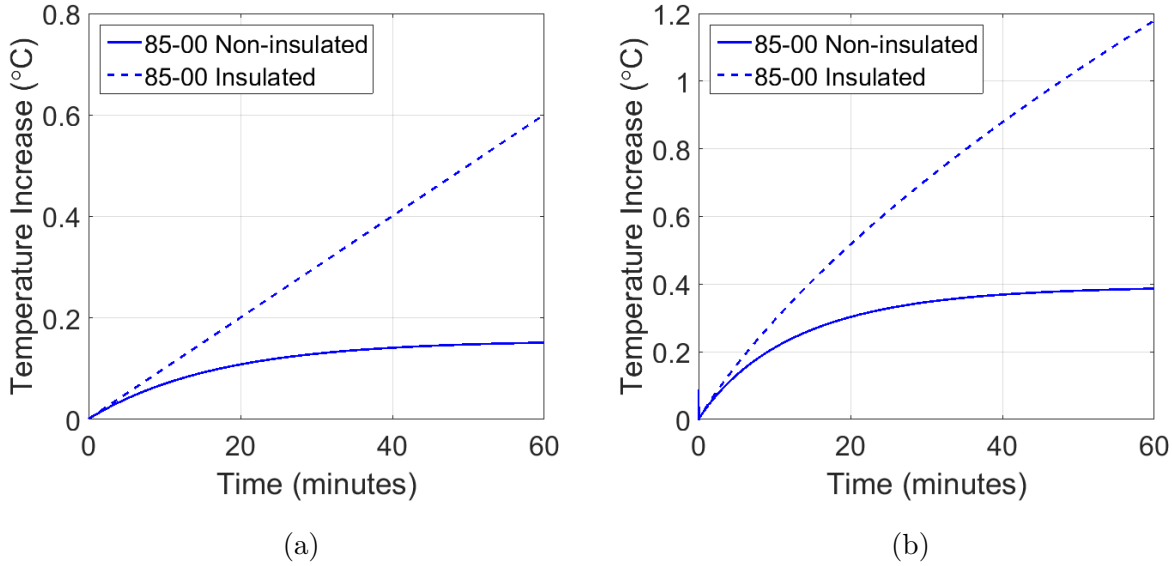

Figure 2.9. : Numerically simulated plate surface temperatures versus time in response to a 2 g excitation near the first resonant frequency for a representative plate of 85% solids loading with 0% additive content. Solid lines indicate results with insulated boundary conditions on all of the surfaces. Dotted lines indicate results under convective boundary conditions. Data are presented for the (a) mean and (b) maximum plate surface temperatures over time.

ing with 0% additive content over the 60 min time period is presented in Figures 2.9a and 2.9b. Note that the assumption of perfectly insulated plate boundaries provides an upper bound of temperature increase for the experimental results presented above. As expected, the insulated surface condition results in a significantly greater temperature rise than the convective condition.

Interestingly, the thermal simulation under-predicts the temperature increase observed for both the mean and maximum surface temperature for the simulated 85-00 plate, as evident when comparing the temperatures in the first row of Table 2.4 with the final temperatures in Figures 2.9a and 2.9b. This may be due to the presence of particle-scale interactions that are not accounted for in the simulation, such as friction between particles or de-bonding of the particle-binder interface [4, 47].

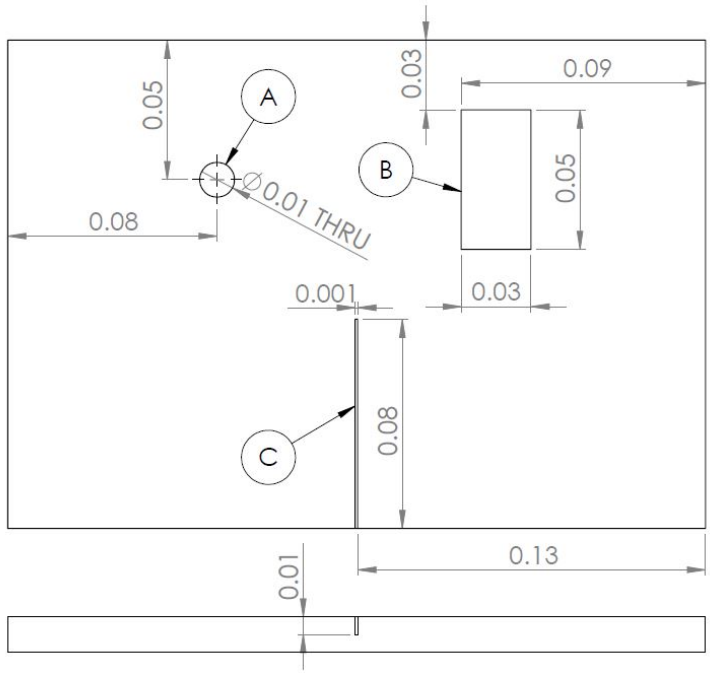

Figure 2.10. : A dimensioned drawing of the plate sample highlighting the size and placement of (a) hole, (b) step, and (c) crack stress concentrations. All dimensions are reported in meters.

2.3.3 Intentional Stress Concentrations

In order to observe the effect of intentional stress concentrations on the thermomechanical behavior of mock energetic plates, three unique features were incorporated into the samples– a hole, step, and crack. The plates were fabricated with a solids loading of 85% with 0% and 15% aluminum additive content. The dimensions and placement of each intentional stress concentration are depicted in Figure 2.10. The overall dimensions were consistent with the pristine samples, measuring 25.4 cm by 17.8 cm by 1.27 cm. Each plate was tested 27 days after curing to account for aging effects of the polymer composite present in the mechanical response. The data presented in this section is from experiments on the plates pictured in Figure 2.11. Note that the white substance that appears around the crack in Figure 2.11b is the mold-release agent applied to the metal insert to aid in the removal of the plate from the Teflon mold.

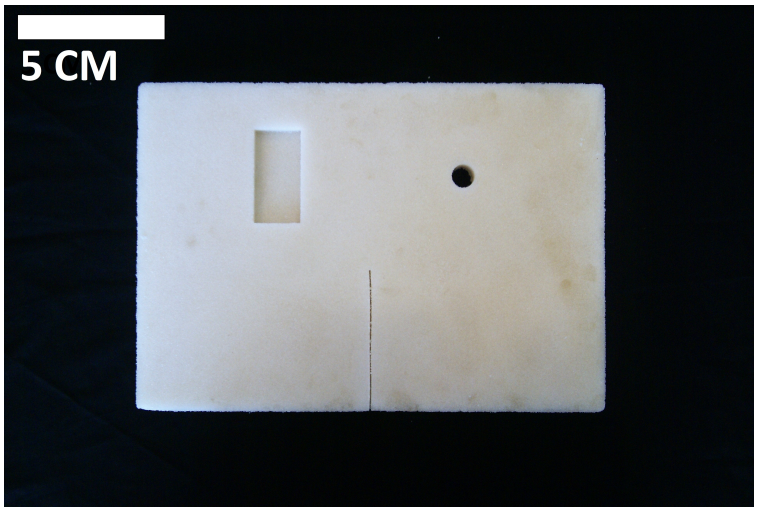

(a)

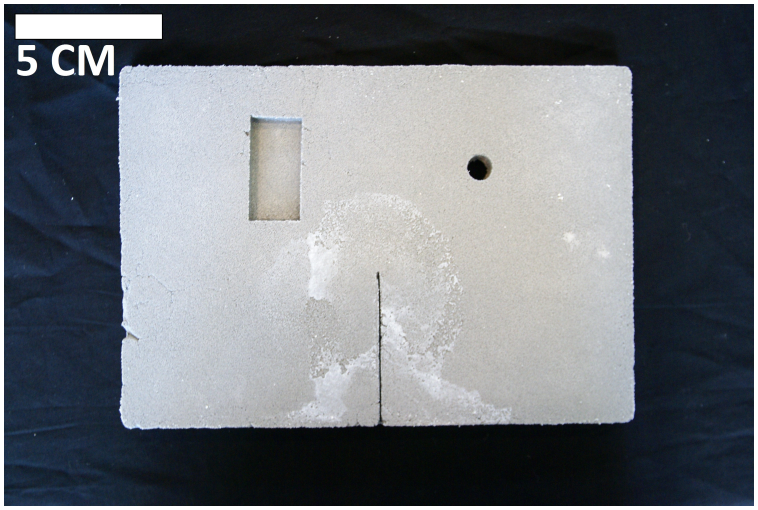

(b)

Figure 2.11. : Representative plate samples with intentional stress concentrations of 85% solids loading with (a) 0% and (b) 15% additive content.

Mechanical Response and Simulation

Preceding the thermal experiment, the laser Doppler vibrometer was used to record the mechanical response of the plate samples with intentional stress concentrations under random excitation to observe the resonant frequencies. The H1 frequency response estimates for an 85-00 plate and an 85-15 plate in response to three levels of random excitation are presented in Figure 2.12. The mechanical response of the plate with intentional stress concentrations exhibits similar trends to the pristine plate responses shown in Figures 2.3-2.5.

As a point of comparison, a mechanical simulation was performed using a commercial finite element package to characterize the operational deflection shapes of this geometryclose to resonance as compared to the pristine plate samples. The simulation modeled harmonic excitation perpendicular to the plate, with the two short ends constrained in all directions. The resulting operational deflection shapes at the first resonance for the pristine and intentional stress concentration plate are shown in Figure 2.13, respectively. Red areas correspond to high levels of displacement, whereas blue corresponds to low levels of displacement. Qualitatively, both contours appear to coincide with the experimental results, exhibiting a classic half sign displacement across the length of the plate in both the pristine and intentional stress concentration plate.

Thermal Response

The transient temperature profiles for a 60 min window when the plate samples with stress concentrations were excited sinusoidally near resonance at 2 g under convective boundary conditions were recorded using a FLIR thermal camera. To characterize the local heating near the intentional stress concentrations, the spatial average and maximum temperature of the 85-00 and 85-15 plates over the 60 min window are presented in Figures 2.14a and 2.14b, respectively, at the tip of the crack, the circumference of the hole at the top surface, and the step in thickness. Note that the minor temperature decreases in the bulk scale temperature profile during the first several minutes of excitation can be attributed to minor discrepancies between the spatial average temperature of the plate and the ambient temperature recorded on a reference material in proximity to the experiment. The samples were each excited at the

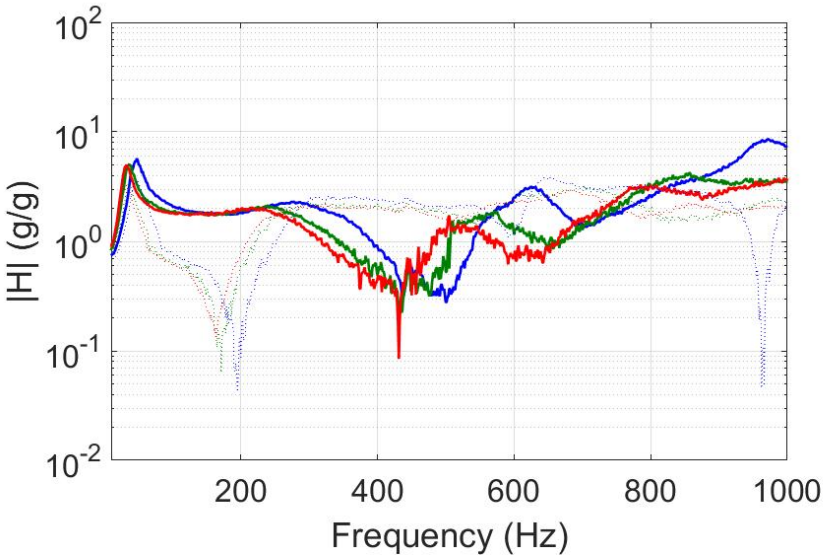

(a)

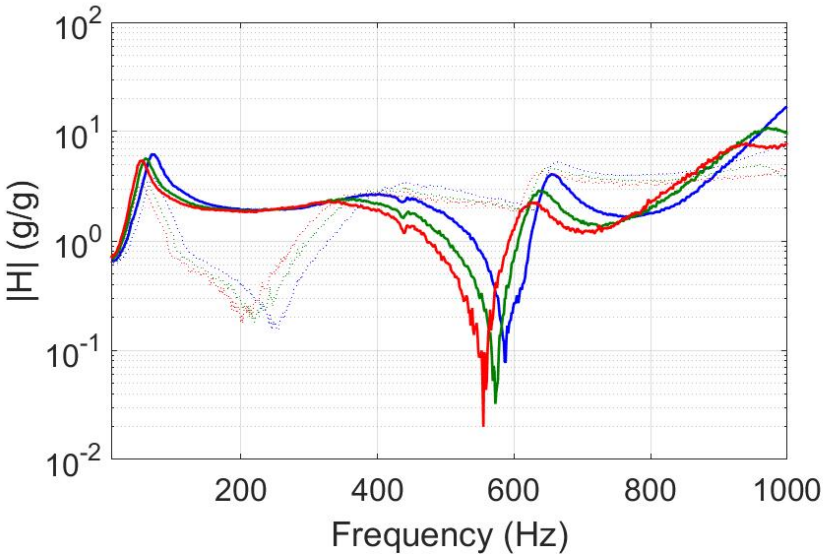

(b)

Figure 2.12. : Experimental H1 estimate of the frequency response magnitude of an (a) 85% solids loading - 0% additive plate and an (b) 85% solids loading - 15% additive plate with structural defects at three levels of excitation. The red, green, and blue curves depict responses at 2.44, 1.86, and 1 g RMS, respectively. Solid lines represent estimates for the response at the geometric center, and dashed lines represent results for the offset point placed near the corner adjacent to the crack and step.

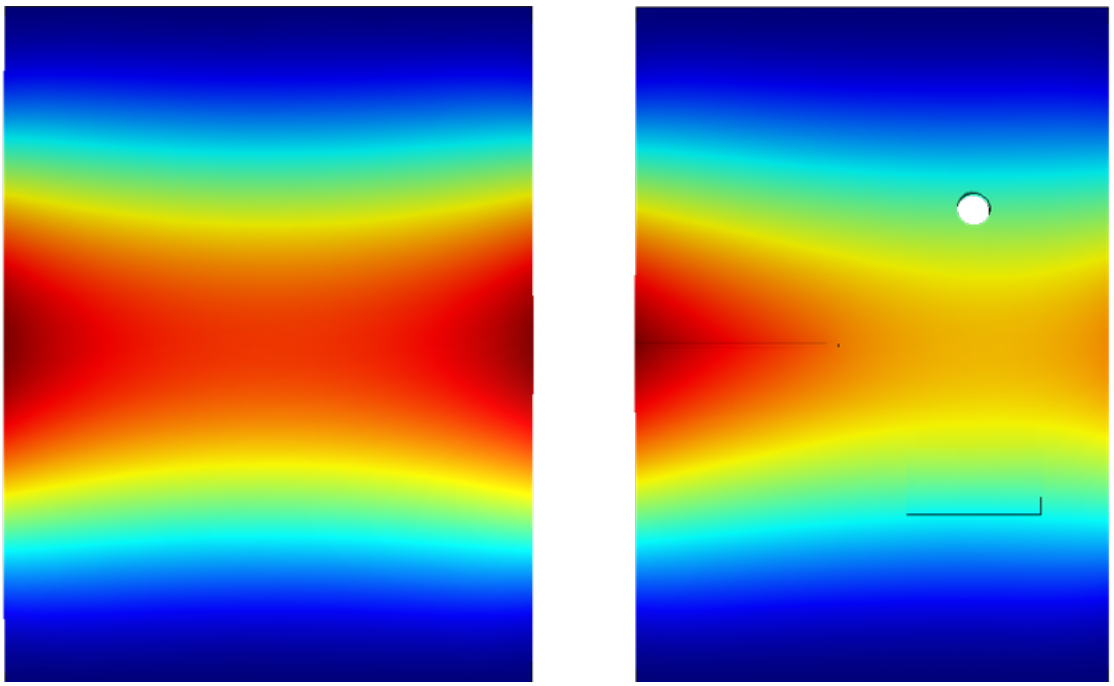

(a) (b)

Figure 2.13. : Simulated operational deflection shape in response to harmonic excitation close to the first resonance for (a) a pristine plate sample and (b) a plate with intentional stress concentrations.

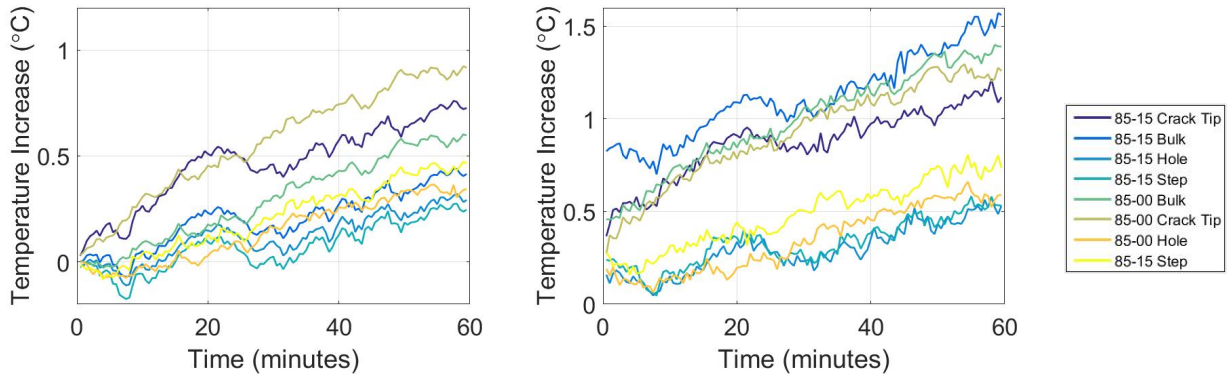

(a) (b)

Figure 2.14. : Comparison of the experimentally obtained plate surface temperature versus time in response to a 2 g harmonic excitation near the first resonant frequency for plates of 85% solids loading with 0% additive content and 85% solids loading with 15% additive content. Data is presented for the (a) mean and (b) maximum plate surface temperatures versus time. The legend indicates the plate sample tested for each profile, and the physical location on the top surface of the plate.

respective first resonant frequency. Bulk scale average and maximum temperature increase are also presented for comparison. In regards to mean temperature, the crack tip exhibits the greatest temperature increase in each formulation. However, the bulk scale temperature increase appears to be greater when analyzing the maximum temperature across the surface of the plate. The magnitude of temperature rise exhibited for these plates with intentional stress concentrations appears to agree with the bulk temperature increase observed in pristine plate samples. An additional test was performed at the same forcing level in an attempt to "exercise" the crack itself at the higher-order 3-1 mode exhibited at approximately 700 Hz presented previously. The transient temperature profile over a 60 min window did not appear significantly different than the resulting plot at the first mode of excitation. This suggests the stress concentrations do not result in significantly greater heat generation when excited in this frequency range.

2.3.4 Material Behavior in Response to Increased Excitation Amplitude

The transient thermal response results presented up to this point have been in response to a 2 g sinusoidal excitation at resonance; however, it has been hypothesized that the heat generation would increase significantly as the forcing level was increased. To this end, a set of increased amplitude experiments were conducted on a representative pristine plate sample of each 85% solids loading formulation (0%, 15%, and 30% additive content).

Mechanical Response

As in previous experiments, the laser Doppler vibrometer was used to record the mechanical response of the plate under random excitation to monitor resonant frequency shifts and potential structural damage to the sample. The H1 frequency response magnitude estimate for a single plate of each formulation in response to 2.44 g RMS random excitation are presented in Figures 2.15-2.17. The signal processing parameters utilized for data acquisition were identical to the previous experiments. The legend indicates the forcing level used in the thermal response test following the recording of the respective frequency response. Note that the sample of 0% additive exhibits softening effects as the tests progress, shifting the first resonant frequency to the left, as evident in Figure 2.15b. In contrast, the first resonant frequency of the remaining samples with 15% and 30% additive content does not appear to shift significantly as the forcing level increases.

Thermal Response

The spatial average and maximum surface temperature of all three of the representative plate samples over the 60 min window when excited at the first resonant frequency under convective boundary conditions at 2, 3, 4, and 5 g forcing levels are presented in Figure 2.18. Note that the maximum temperature increases displayed at the onset of the experiment in Figures 2.18b, 2.18d, and 2.18f can be attributed to minor discrepancies between the maximum temperature of the plate and the ambient temperature recorded on a reference material in proximity to the experiment. The temperature rise observed in each subsequent

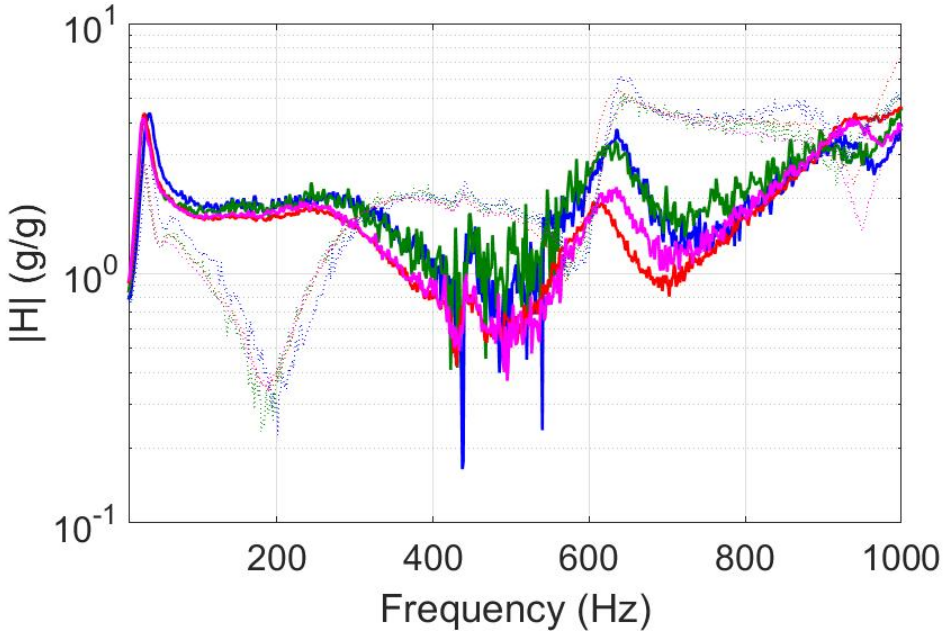

(a)

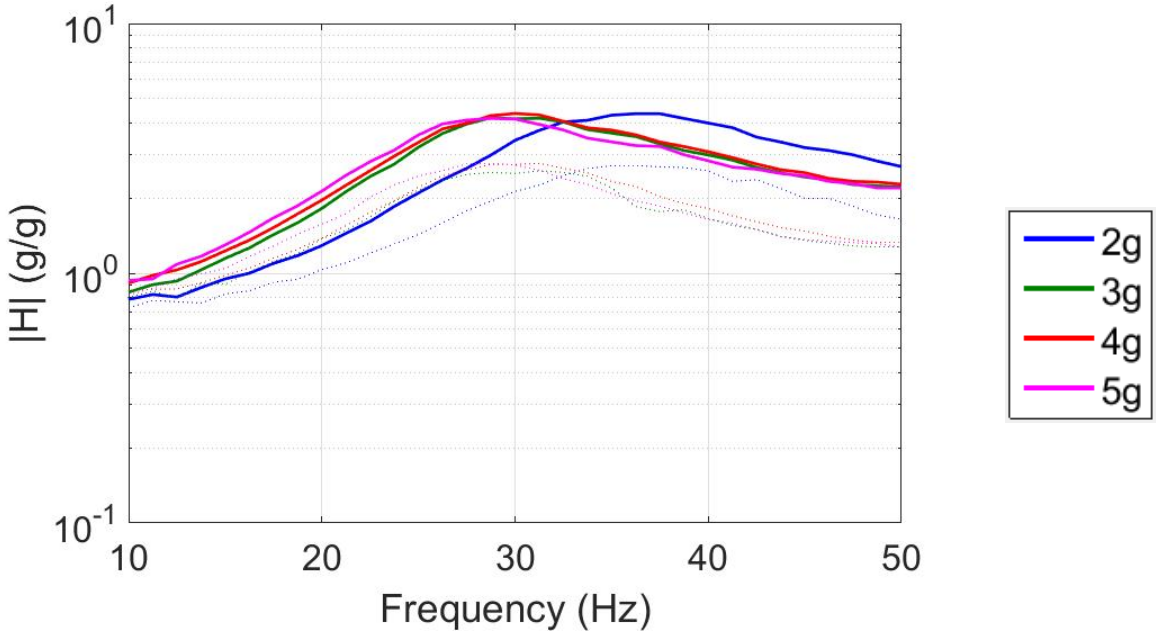

(b)

Figure 2.15. : Experimental H1 estimate of the frequency response magnitude of a 85% solids loading - 0% additive plate at 2.44 g RMS excitation from 10 to 1000 Hz. The legend indicates the forcing level used in the thermal experiment performed immediately following the frequency response estimate. The solid lines represent data from the geometric center, and the dashed lines represent data from the offset point. Data is presented (a) over the entire excited range and (b) over the 40 Hz region surrounding the first resonant frequency.

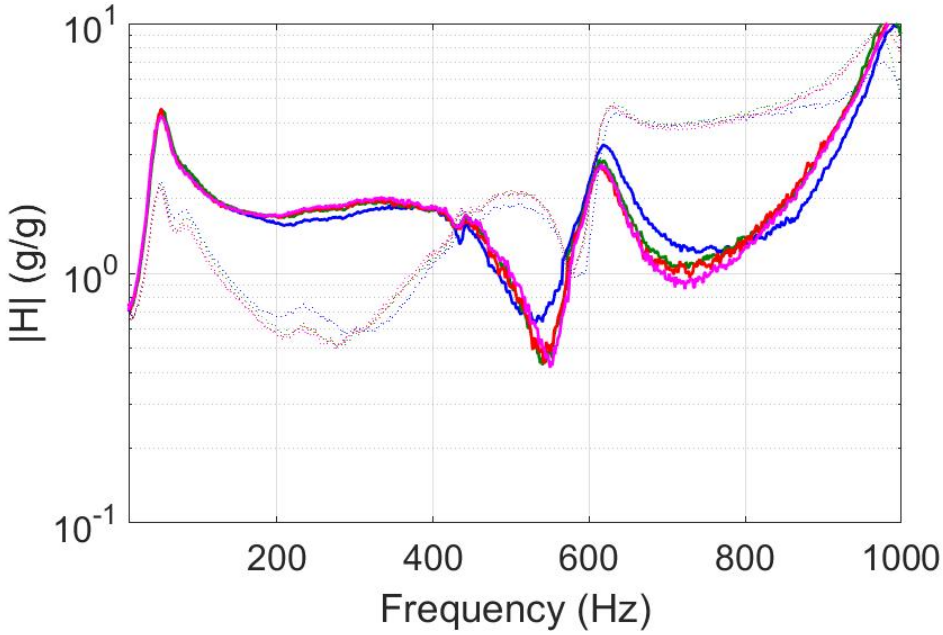

(a)

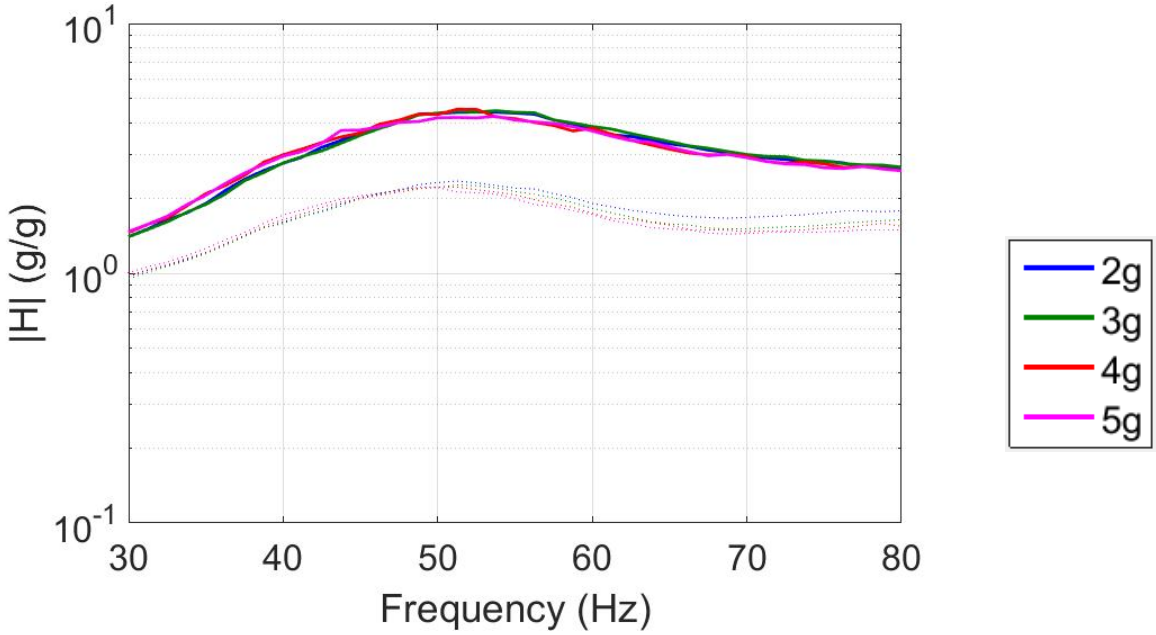

(b)

Figure 2.16. : Experimental H1 estimate of the frequency response magnitude of a 85% solids loading - 15% additive plate at 2.44 g RMS excitation from 10 to 1000 Hz. The legend indicates the forcing level used in the thermal experiment performed immediately following the frequency response estimate. The solid lines represent data from the geometric center, and the dashed lines represent data from the offset point. Data is presented (a) over the entire excited range and (b) over the 50 Hz region surrounding the first resonant frequency.

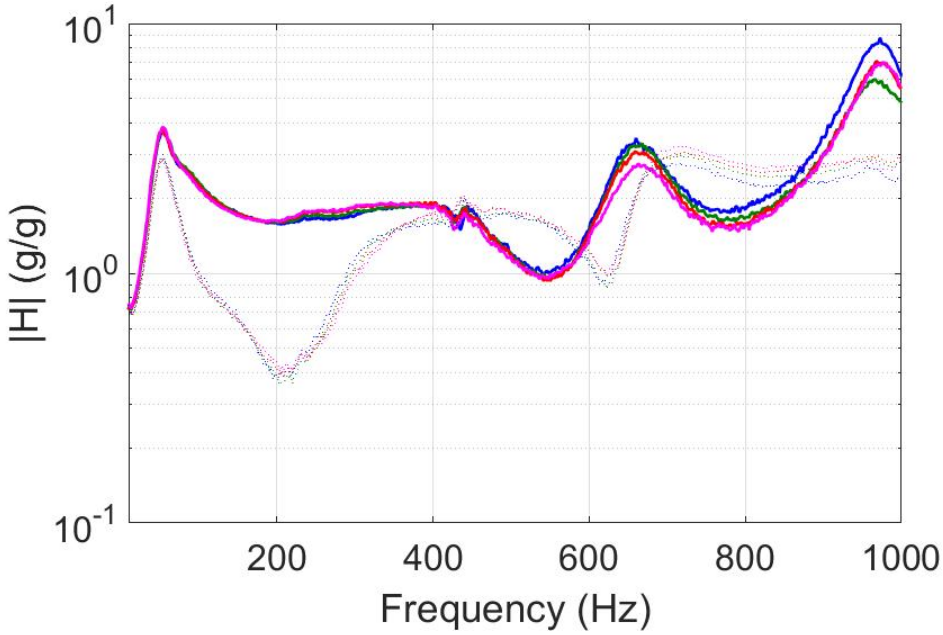

(a)

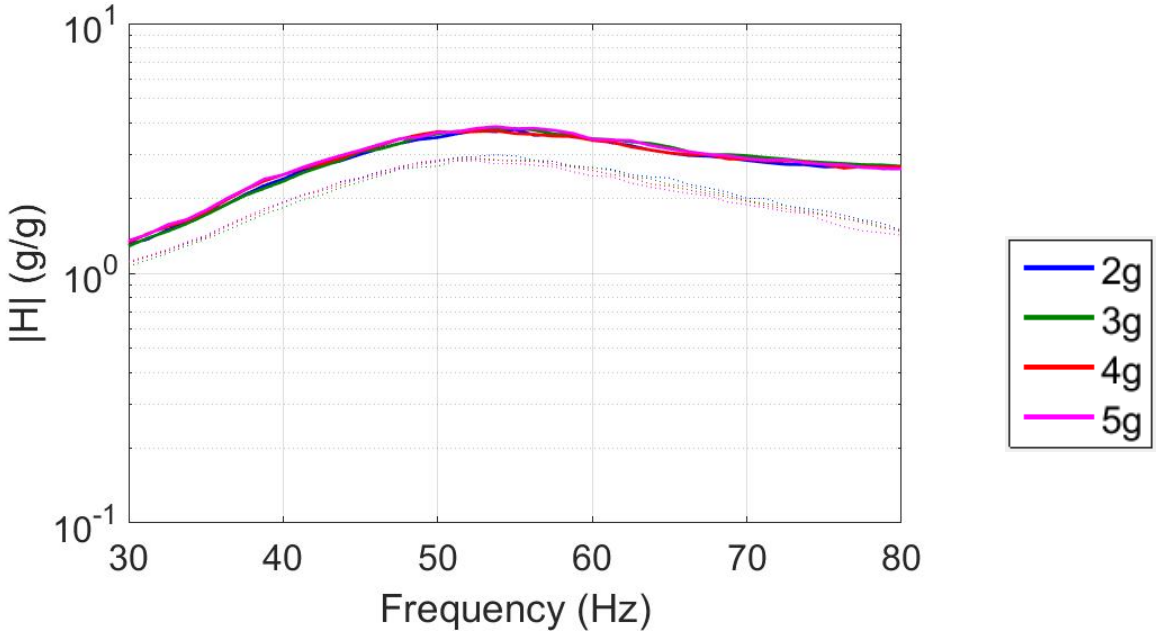

(b)

Figure 2.17. : Experimental H1 estimate of the frequency response magnitude of a 85% solids loading - 30% additive plate at 2.44 g RMS excitation from 10 to 1000 Hz. The legend indicates the forcing level used in the thermal experiment performed immediately following the frequency response estimate. The solid lines represent data from the geometric center, and the dashed lines represent data from the offset point. Data is presented (a) over the entire excitation range and (b) over the 50 Hz region surrounding the first resonant frequency.

test does increase with forcing level; however, the rise is quite gradual. Interestingly, the temperature rise exhibited throughout the experiment does not appear to have a significant dependence on the additive content of the sample, as the magnitude is approximately equal in each case.

2.4 Conclusions

The thermal and mechanical responses of particulate composite mock energetic plates, comprised of varying ratios of HTPB binder, sucrose particles, and spherical aluminum powder, under contact excitation have been presented. Clear resonant behavior was observed in each of the three formulation variations, differing solely based on the amounts of additive content.

The reported transient surface temperature patterns appear to approach steady-state over the 60 min window of harmonic excitation at an amplitude of 2 g, resulting in temperature increases on the order of 0.5-1°C, as expected from prior work with high solids loading composite materials [2]. These temperature increases provide insight into the thermal characterization of the particulate composite material itself for applications in munitions systems, as well as aid in the effort towards the detection and defeat of hidden explosive devices due to the temperature dependence of vapor pressure in many explosive materials.

The comparison of temperature profiles of different aluminum additive content plates yielded variations on the order of 0.5°C, suggesting that increased additive content does not result in significantly increased heat generation at a forcing level of 2 g. The extension to increased amplitudes of excitation yielded temperature increases on the same order as before (up to 4°C), with minor variations between the three formulations analyzed. However, the increase in excitation amplitude was more likely to promote physical damage within the samples, especially near boundary constraints as the onset of crack propagation was observed at amplitudes greater than 5 g.

The insulated boundary condition resulted in a temperature increase approximately 0.7°C higher than the corresponding convective experiment in all of the plate formulations, as expected. However, the observed trends appear to be inconsistent with simple bulk-scale heat

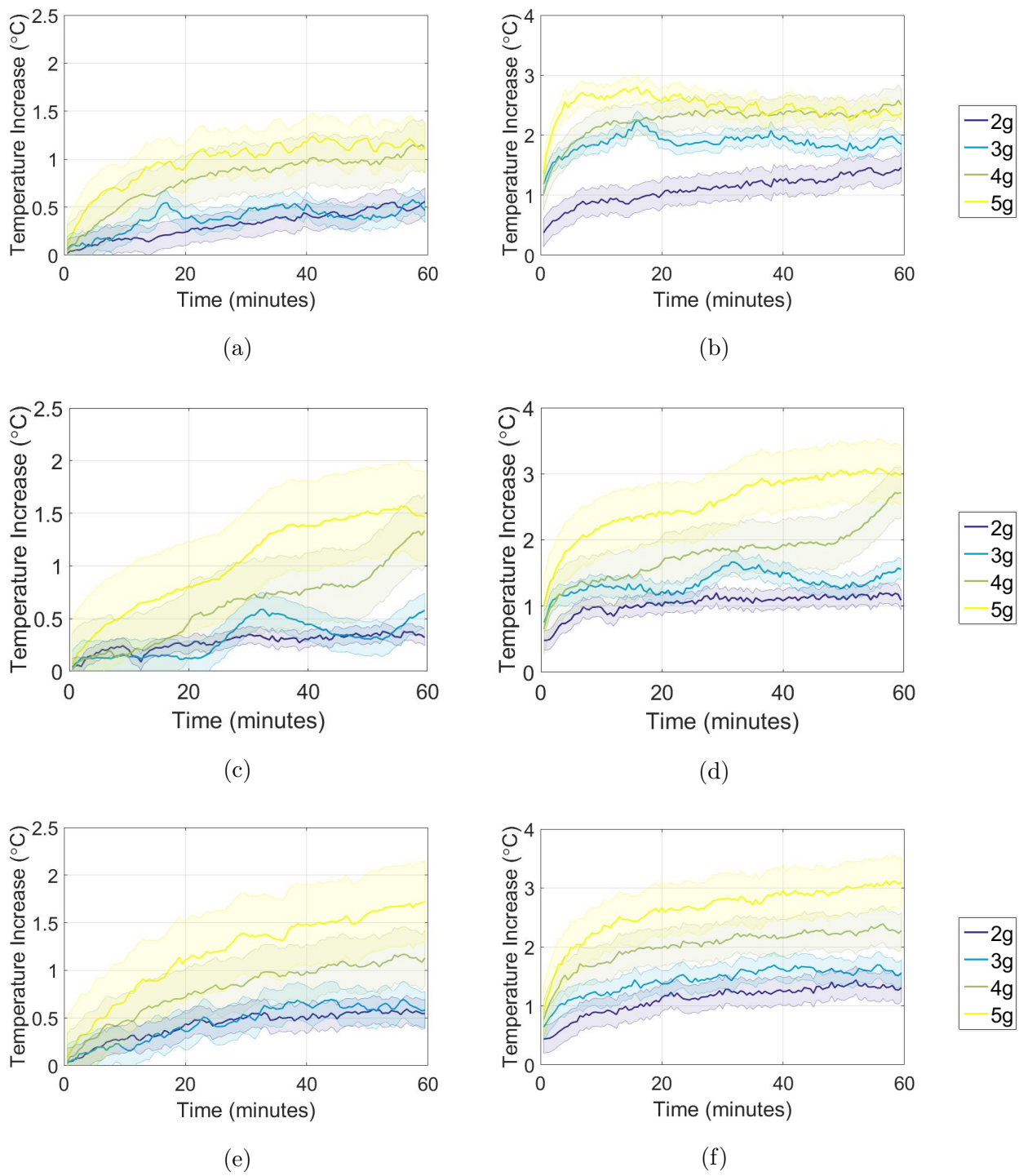

Figure 2.18. : Experimentally obtained plate surface temperature versus time in response to increasing harmonic excitation near the first resonant frequency for a plate with (a,b) 85% solids loading - 0% additive content, (c,d) 85% solids loading - 15% additive content, and (e,f) 85% solids loading - 30% additive content. The colored envelope indicates the error associated with the thermal camera measurement. Data are presented for the (a,c,e) mean and (b,d,f) maximum plate surface temperatures versus time. The legend indicates the forcing level for each respective test.

transfer models. Future efforts will investigate whether this behavior is due to experimental error (i.e., measuring small temperature changes via an infrared camera), or, as is more likely, directly attributable to the particulate composite nature of the material.

Thermal simulation of the heat generation within a sample of 85% solids loading with 0% additive content resulted in temperature increases significantly lower than experimentally-observed values. This effect may also be attributable to particle-particle interactions at the micro-scale, such as friction and de-bonding between the particle and the binder, which are not accounted for in the current heat generation simulation due to the assumption of homogeneous material behavior in the volume of interest.

As a whole, the work summarized in this chapter provides a solid foundation of knowledge with regard to the thermal and mechanical behavior of particulate composite energetic materials at low frequencies (below 1000 Hz). For the design of munition systems, the likelihood of physical damage and potential heating due to prolonged excitation in this frequency regime would likely present a challenge, as the damage induced in the material may reduce and/or eliminate the functionality of the device. Thus, the design for systems under long-duration, low-frequency mechanical vibration must identify and avoid the potential material damage to ensure safe handling and proper performance.

3. HIGH–FREQUENCY RESONANT EXCITATION OF MOCK ENERGETIC MATERIALS

3.1 Introduction

As aircraft technology advances, the frequency range in which significant vibration is experienced by various munitions systems during transportation continues to expand. A review of the current literature reveals that there has been little characterization of energetic material behavior between 1 and 100 kHz, aside from several works by Dlott, Fayer, and others [48–50]. In previous experiments, researchers have explored discrete energetic particles embedded in an elastic binder [31, 32], or fully-loaded composite propellants excited at low frequency [1, 2, 35], however, the response of energetic materials to excitations above 1 kHz is of great interest within the defense and energy sectors. The research presented here is an attempt to bridge this knowledge gap, and is focused on characterizing the thermomechanical behavior of mock energetic materials to contact mechanical excitation at frequencies between 1 and 80 kHz.

3.2 Experimental Techniques

3.2.1 Sample Preparation

The samples of mock explosive material were prepared using sucrose particles and spherical aluminum powder, held within a hydroxyl-terminated polybutadiene (HTPB) binder. The sucrose particles were sieved to a diameter range of 106-355μm in order to be comparable in size to particles of RDX, a common energetic material. The spherical aluminum powder was purchased from Valimet, Inc. and had an average particle diameter of 25 μm. Particle size analysis was performed to verify the aforementioned particle distributions on a Malvern Mastersizer 3000 using air, as opposed to a liquid solvent.

In real world applications, the weight ratio of particles to binder can vary considerably, motivating the investigation of multiple formulations. Similarly to the plate samples described in the previous chapter, the formulation variations are based upon the PBXN-109 formulation given by Lochert *et al.* [51], with sucrose particles substituted for RDX to render the samples inert. A summary of this base formulation is given in Table 2.1.

Cylinders were prepared with 85% solids loading. Three variations were made with 0%, 15%, and 30% weight ratios of aluminum additive content. Solids loading describes the weight ratio of solid crystals, encompassing both sucrose and aluminum particles, to polymer binder in the overall formulation. Additive content indicates the weight ratio of spherical aluminum powder to sucrose crystals in the solids loading ratio.

To fabricate test samples, the HTPB resin was combined with a curing agent, isophorone diisocyanate (IPDI), and various other constituents. The binder was then mixed in a Resodyn^{TM} acoustic mixer for 3 min to ensure a homogeneous mixture. This mixture was then degassed in a vacuum chamber to remove unwanted gases from the liquid binder and to prevent bubbles from forming in the final sample. The solid constituents were then added to the binder mixture and the Resodyn^{TM} was again used to mix the constituents for 3 min. The combined particle and binder mixture was then poured into a custom Teflon mold. The mold features 10 cylindrical cavities, each used to cast a cylinder with a final diameter of 2.54 cm and a height of 2.54 cm. The cylinders, held within the mold, were cured in an oven for a period of 7 days at 60°C. The cylinders were then cut down using a lathe to final heights of 1.27 cm and 0.64 cm for experimental purposes. The mass and density of each cylinder after being cut down are given in Table 3.1.

The samples were then epoxied to elevator bolts for attachment to the shaker. The bolts were painted a matte black to reduce radiation during thermal experiments. Representative cylinders of each formulation are presented in Figures 3.1a-3.1c.

As noted with the plate samples described in Chapter 2, attempts were made to fabricate cylinders of pure binder for comparison purposes; however, the soft and pliable nature of the polymer binder meant that it was not strong enough to withstand the force of separating the mold without tearing.

Table 3.1. : Cylinder sample characteristics.

Solids Loading - Additive Content - Identification	Height (cm)	Mass (g)	Density (g/cm^3)
85-00-1	1.27	9.88	1.54
85-00-2	1.27	10.12	1.57
85-00-3	0.64	5.26	1.64
85-00-4	0.64	5.01	1.56
85-15-1	1.27	8.82	1.37
85-15-2	1.27	9.05	1.41
85-15-3	0.64	5.08	1.58
85-15-4	0.64	4.39	1.36
85-30-1	1.27	7.89	1.23
85-30-2	1.27	8.76	1.36
85-30-3	0.64	4.03	1.25
85-30-4	0.64	3.83	1.19

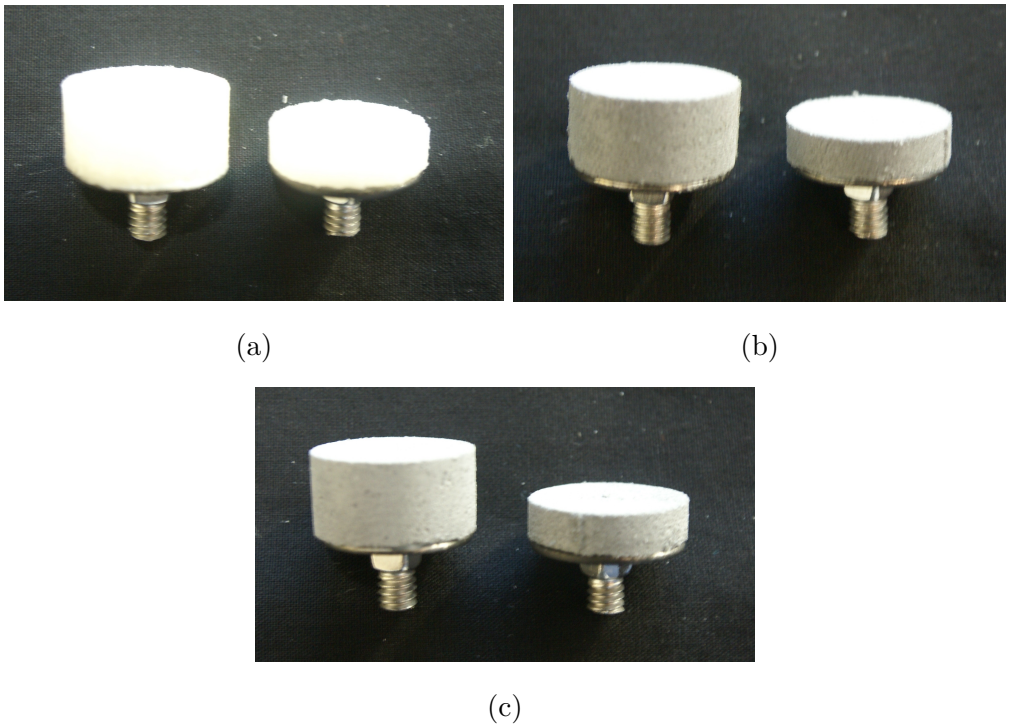

Figure 3.1. : Representative cylinder samples of 85% solids loading with (a) 0% (b) 15% and (c) 30% additive content.

3.2.2 Experimental Setup

A Meggitt F7-1 piezoelectric shaker was used to mechanically excite the cylinders at moderate excitation levels on the order of 1000 g. The elevator bolts epoxied on the bottom of the cylinders were fastened to a baseplate mounted atop the shaker head. Similar to the elevator bolts, the baseplate was painted matte black to reduce radiation. A Keysight 33509B Waveform Generator provided the sinusoidal input signal to the Wilcoxon Research® PA8HF power amplifier with a maximum input signal of 1.25 V_{rms}. The signal was then routed to the Wilcoxon Research® N8HFS impedance matching network and through to the shaker head. The shaker is characterized by a frequency range of 1 to 80 kHz with a maximum force output of 50 N. The thermal response was recorded using a FLIR A325 above the sample and a FLIR A6507 thermal camera at the side of the sample with an accuracy of ± 2°C or ± 2%. A Polytec PSV-400 scanning laser Doppler vibrometer was used to record the velocity response of the top of each cylinder.

Frequency responses were obtained in response to sinusoidal excitation swept from 1 to 80 kHz at a peak amplitude of 500 mV. The laser Doppler vibrometer was used to record the velocity response at the geometric center on the top of the cylinder for the duration of the sweep. Although the measurement at the center point would miss anti-symmetric deflection shapes / resonances, it is expected that the largest response amplitude will be captured as well as the majority of the anti-symmetric deflection shapes due to the imperfections associated with the experimental measurement and sample heterogeneity. Data was recorded with a sampling frequency of 204.8 kHz, and the linear sweep rate was held constant at 125 Hz/s. This velocity measurement was then differentiated and transformed to determine the instantaneous amplitude of acceleration present at the corresponding instantaneous frequency of the sinusoidal excitation input to the shaker, and the various resonant frequencies were identified. The digital filters used for the differentiation and the Hilbert transform were designed to suit the 80 kHz maximum frequency of interest, and the response for each filter in the frequency and time domain is included for reference in Figure 3.2. The experimental set up for the mechanical experiments is depicted in Figure 3.3.

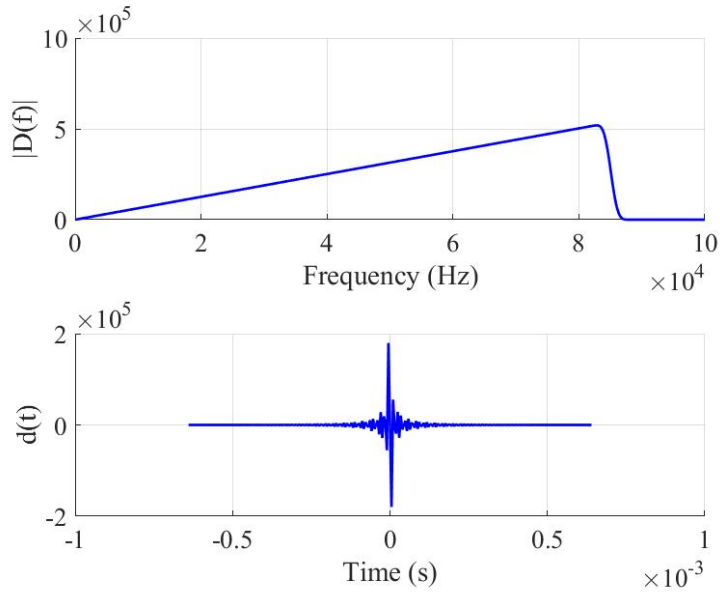

(a)

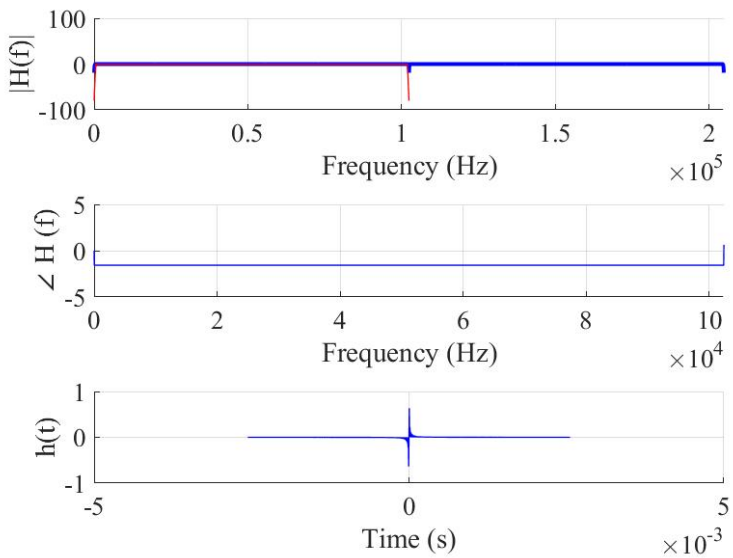

(b)

Figure 3.2. : Frequency and time domain response of the (a) differentiation and (b) Hilbert transform digital filters developed for the post-processing of the velocity data measured at the top surface of the cylinder.

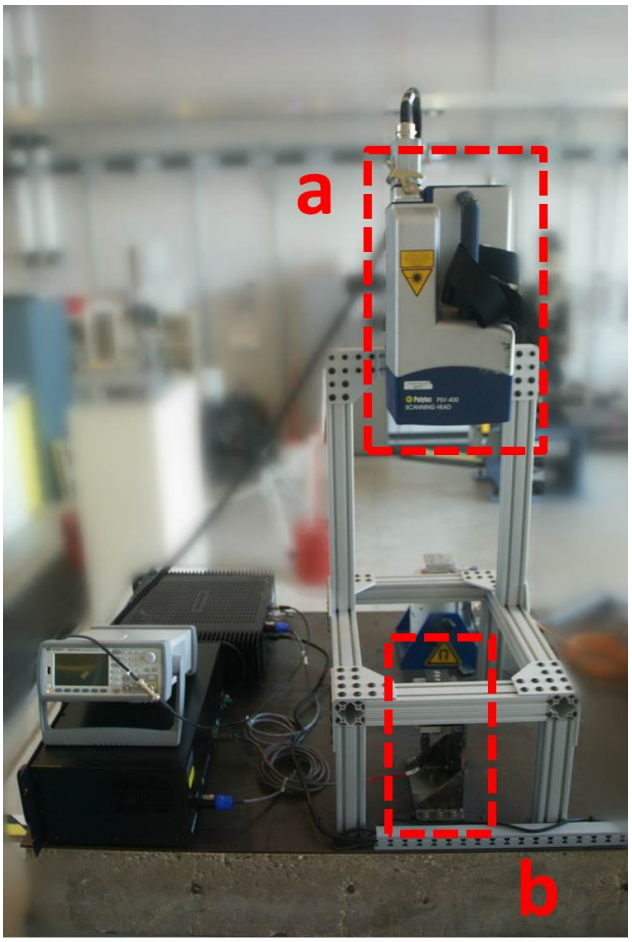

Figure 3.3. : Experimental setup with a (a) Polytec PSV-400 scanning laser Doppler vibrometer positioned above a cylindrical sample mounted to the (b) Meggitt shaker.

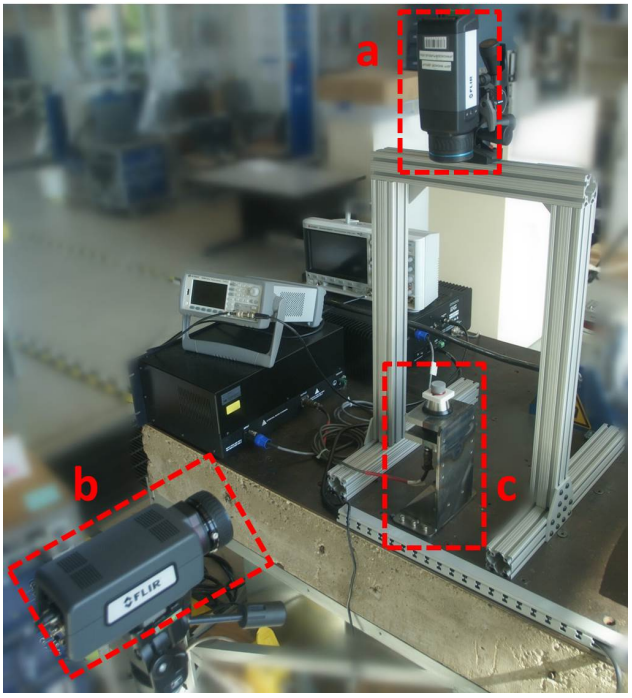

Figure 3.4. : Experimental setup with a (a) FLIR A325 infrared camera positioned above and a (b) FLIR A6507 infrared camera positioned to the side of a cylindrical sample mounted to the (c) Meggitt shaker.

A peak forcing amplitude of 1.25 V was used to obtain the thermal response of the cylinders. Each cylinder was excited at a resonant frequency for a 15 min time period, during which the frequency and forcing level were held constant. The aforementioned FLIR camera recorded the transient and steady-state thermal responses at the surface of the samples. Note that the emissivity of each sample was calibrated by determining the reflected apparent temperature of a perfect emitter and then calibrating the sample temperature to that of a known emissivity. The ambient temperature was also recorded during the test and then subtracted from the experimental temperature data in order to account for variations caused by the surrounding environment. The experimental set up for the thermal experiments is depicted in Figure 3.4.

3.3 Results

3.3.1 Mechanical Response

The mechanical response of each sample was found according to the procedure described above, utilizing the laser Doppler vibrometer to measure the velocity at a single point at the top/center of the cylinder. As a point of reference, a similar frequency response measurement was made on the shaker contact surface without the mounting baseplate or sample attachment pieces. These response functions show that there are significant resonances within the frequency range of interest.

Shaker Frequency Response

The frequency response for the shaker contact surface in response to a peak sinusoidal input of 500 mV is presented in Figure 3.5. The shaker head exhibits clear resonant behavior within the excitation range from 1 to 80 kHz, at approximately 18.5, 60, and 71 kHz. Operational deflection shapes, measured by the laser Doppler vibrometer in response to a 750 mV peak sinusoidal input to the shaker, were used to characterize these resonances. The operational deflection shapes are shown in Figure 3.6. The lowest resonance exhibited two peaks at 18.3 and 18.6 kHz, respectively, both characterized by a rocking motion, while both of the higher frequency resonances display a classic drumhead motion in response to mechanical vibration.

Particulate Composite Sample Frequency Response

As previously mentioned, particulate composite cylindrical samples were cast with a diameter of 2.54 cm and a height of 2.54 cm. Preliminary experiments were performed on full-height samples in an attempt to determine the frequency response; however, the waves traveling through the material were largely dissipated before reaching the top of the cylinder resulting in a response with a small signal-to-noise ratio.

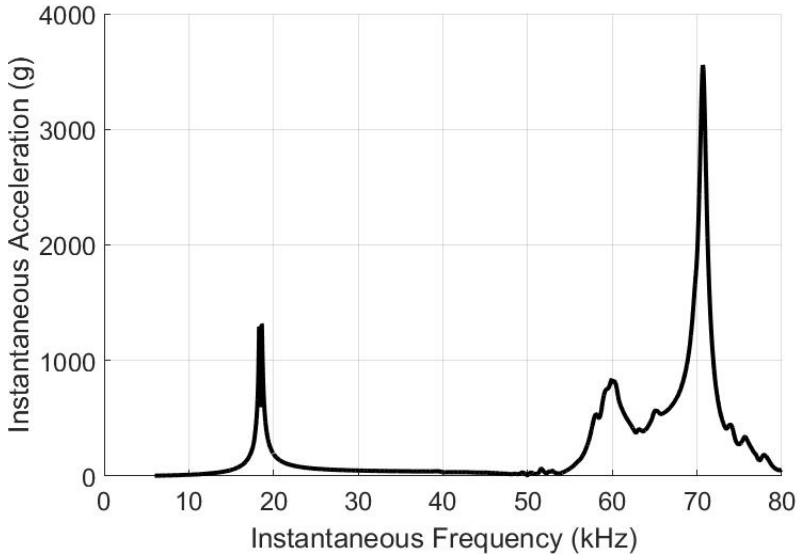

Figure 3.5. : Instantaneous acceleration versus frequency for the Meggitt shaker head.

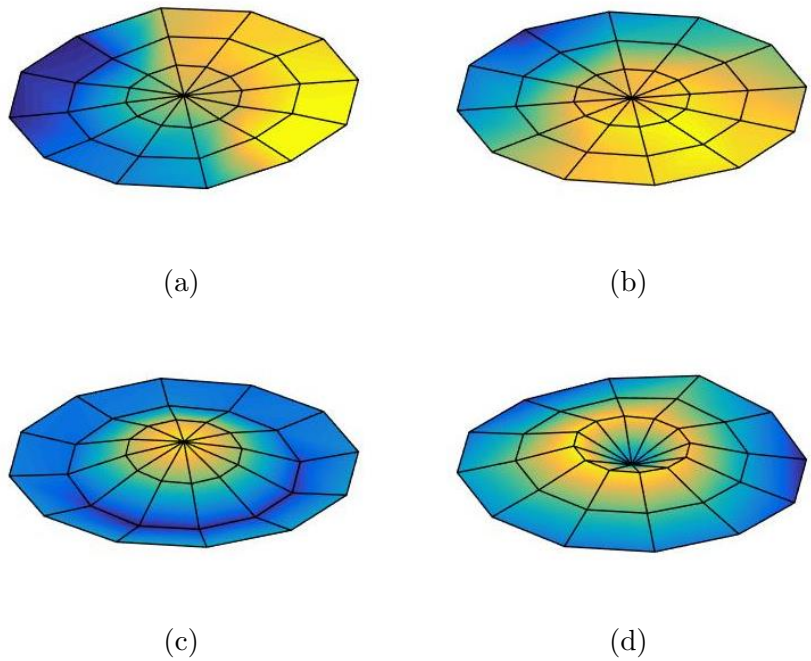

Figure 3.6. : Operational deflection shapes at (a) 18.3 kHz (b) 18.6 kHz (c) 60.2 kHz and (d) 70.7 kHz for the Meggitt shaker head.

In order to gain a better understanding of the observed response, the velocity at the center point of an 85-30 sample was measured in a similar manner in response to a 500 mV peak sinusoidal excitation at a single frequency for 10 ms. This was repeated at 15, 30, 45, 60, and 75 kHz to cover the large frequency range of the shaker. A spectrogram of the 10 ms response signal resulting from a 15 kHz input and a 75 kHz input are presented in Figures 3.7a and 3.7b, respectively. Spectrograms of the response for the 30, 45, and 60 kHz input signals are similar to that for the 75 kHz excitation where the amplitude of the excitation frequency does not stand out in the spectrum. The spectrograms visually indicate the signal strength at various frequencies present in a particular waveform—in this case, the velocity measurement. The color bar denotes the signal strength at each particular frequency and time, with red content corresponding to areas of high signal strength and blue content related to low signal strength. In Figure 3.7a, the horizontal red line indicates the signal is highly concentrated at 15 kHz as expected. The periodicity at frequencies above 40 kHz is most likely an artifact of the laser Doppler vibrometer. In contrast, Figure 3.7b exhibits red content ranging from 20 to 100 kHz indicating that a significant amount of noise was present in the response, suggesting the waves traveling through the material were dissipated before reaching the top of the cylinder. As a result, the final samples were cut to heights of 1.27 and 0.64 cm to enable an ample degree of wave propagation to the top of the sample. The spectrogram for a 1.42 cm height sample excited at 75 kHz is shown for reference in Figure 3.8. Although there is still noise present in the response, the forcing frequency can be clearly identified in the signal. The frequency response for a representative sample of each formulation at a height of 1.27 cm is presented in Figure 3.9. The corresponding frequency response functions for the 0.64 cm samples are included in Figure 3.10. Each of the twelve experimental samples exhibited multiple resonant frequencies across the 1 to 80 kHz range of interest. Data showing the repeatability of the frequency response measured here is included in Appendix B.

Due to the large number of resonances, the frequency range of interest was divided into four subranges: 1 to 20 kHz, 20 to 40 kHz, 40 to 60 kHz, and 60 to 80 kHz. The strongest resonance was determined by identifying the location of the largest peak amplitude of instantaneous acceleration within each subrange. The sample was then excited at this frequency

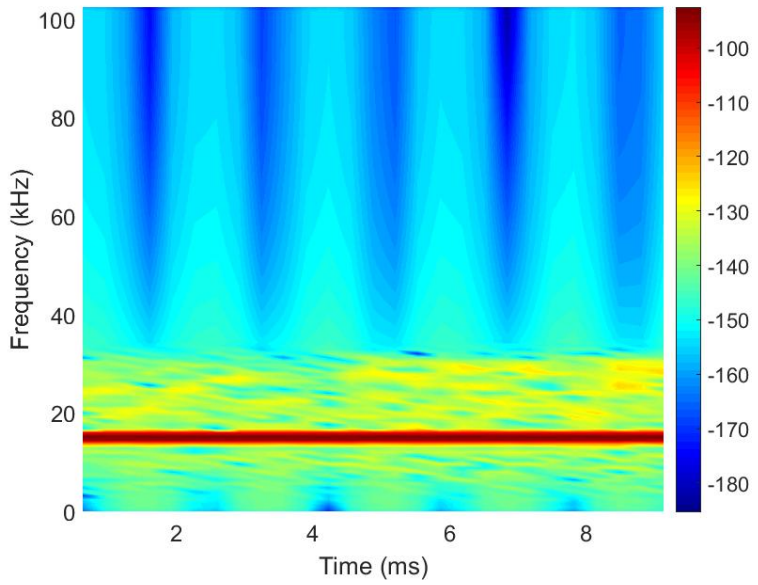

(a)

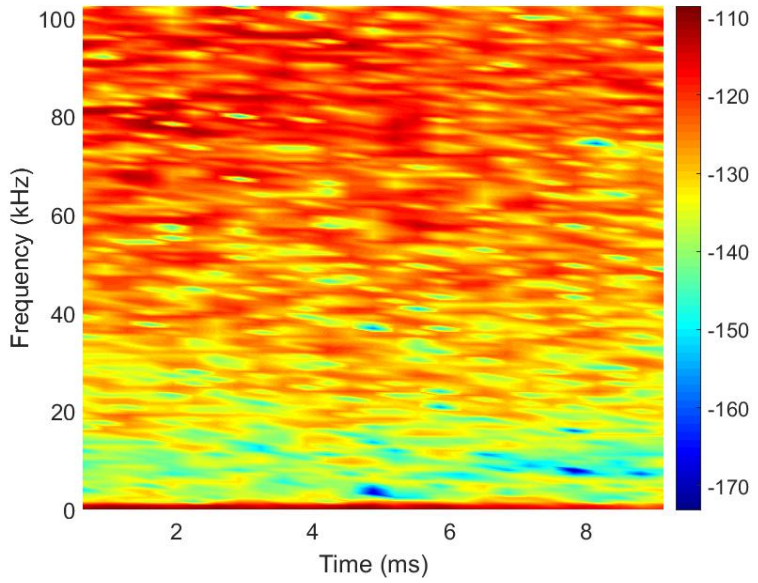

(b)

Figure 3.7. : Spectrogram of the velocity response at the center point on top of a 2.54 cm height 85-30 sample in response to sinusoidal mechanical excitation at (a) 15 kHz and (b) 75 kHz.

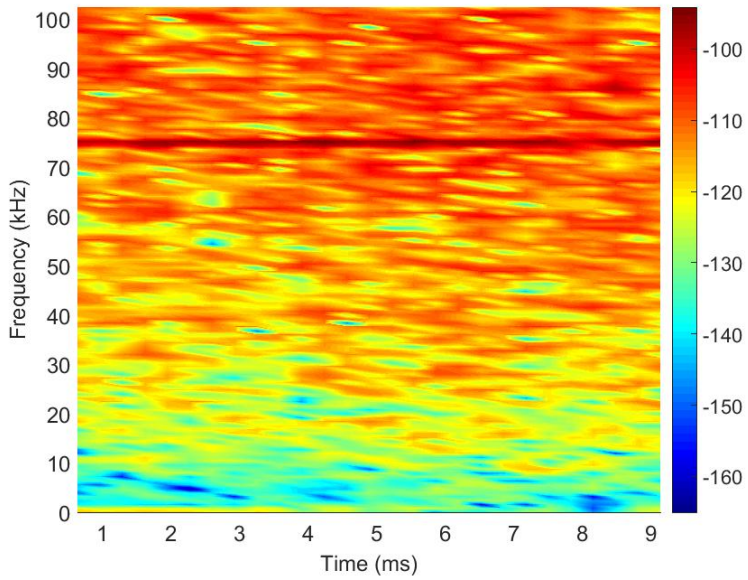

Figure 3.8. : Spectrogram of the velocity response at the center point on top of a 1.42 cm height 85-30 sample in response to sinusoidal mechanical excitation at 75 kHz.

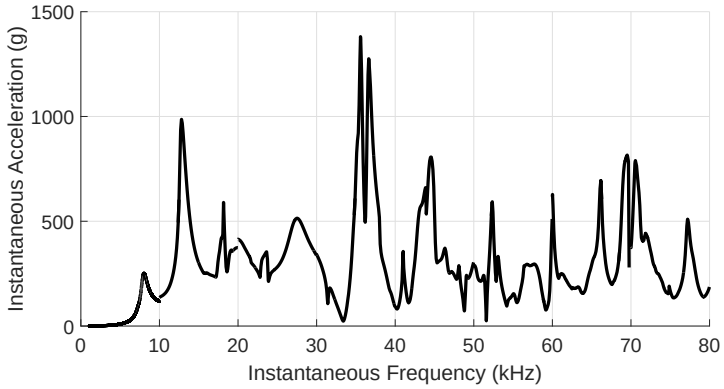

(a)

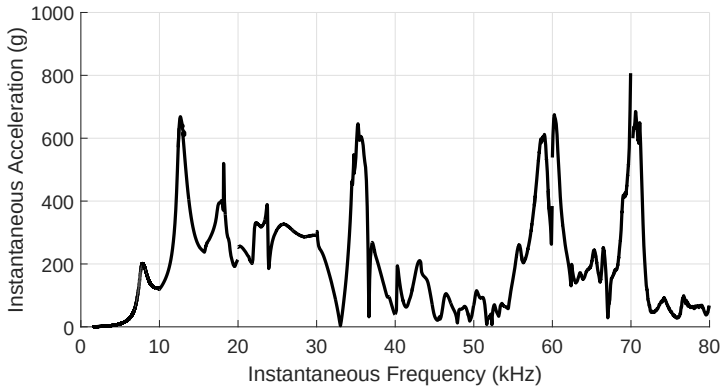

(b)

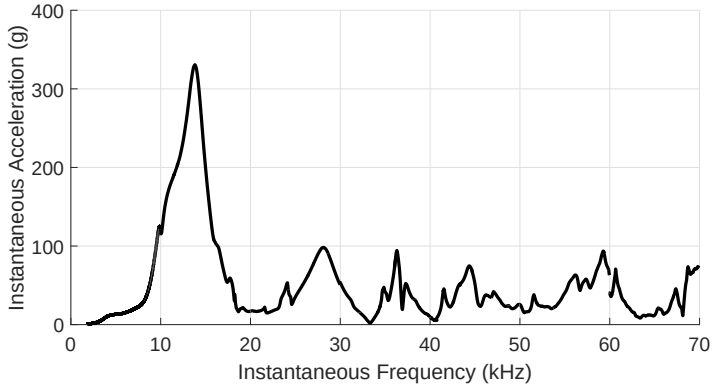

(c)

Figure 3.9. : Instantaneous acceleration versus frequency of 1.27 cm height samples prepared at 85% inert solids loading with (a) 0%, (b) 15%, and (c) 30% aluminum additive content.

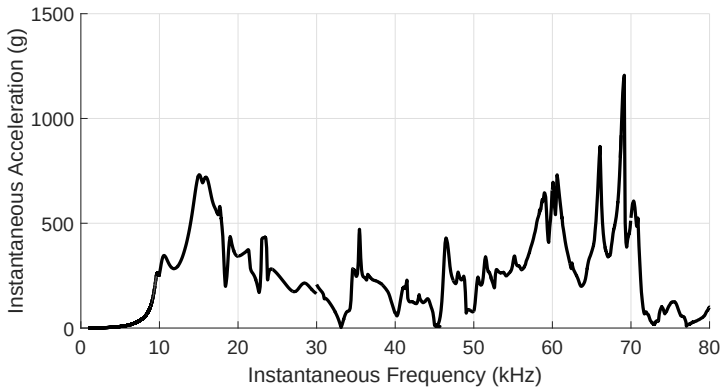

(a)

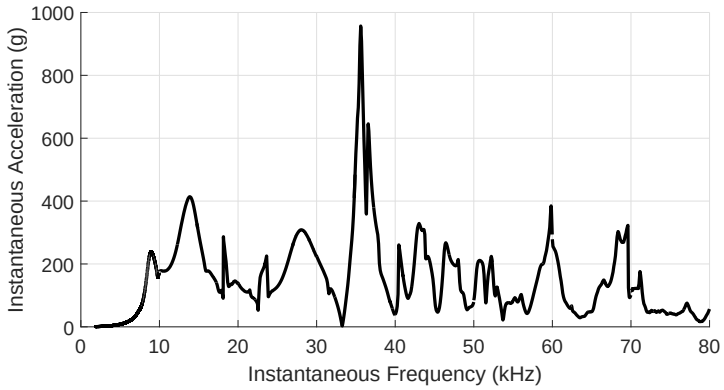

(b)

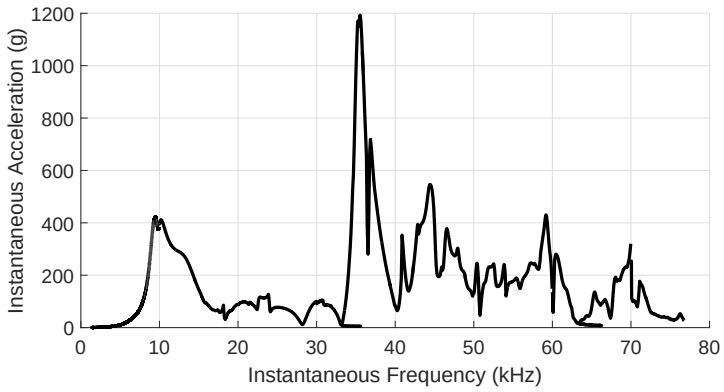

(c)

Figure 3.10. : Instantaneous acceleration versus frequency of 0.64 cm height samples prepared at 85% inert solids loading with (a) 0%, (b) 15%, and (c) 30% aluminum additive content.

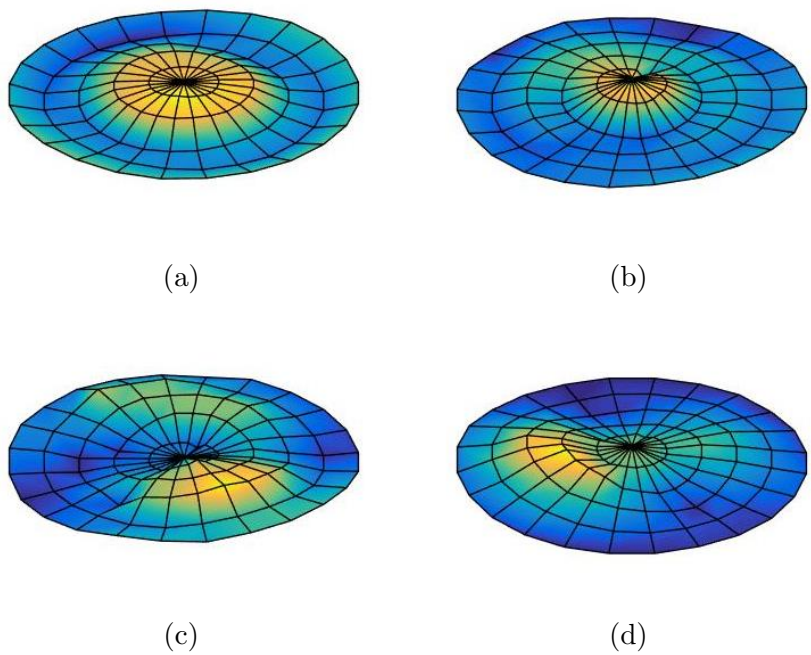

Figure 3.11. : Operational deflection shapes for a 1.27 cm height sample of 85% solids loading and 30% aluminum additive content at (a) 13.7 kHz (b) 28.3 kHz (c) 44.6 kHz and (d) 60.3 kHz.

and the operational deflection shape was measured using the laser Doppler vibrometer. For brevity, only two sets of operational deflection shapes are presented in Figures 3.11 and 3.12 for 1.27 cm and 0.64 cm height samples of 85% solids loading with 30% additive content; however, all of the samples exhibited qualitatively similar motion. The magnitude of instantaneous acceleration exhibited by the samples generally appeared to decrease as the amount of aluminum additive content increased, likely due to the change in microstructure and particle size distribution. Resonant frequencies in the first and second range of interest tended to exhibit drumhead-like motion, while frequencies above 40 kHz tended towards a rocking motion.

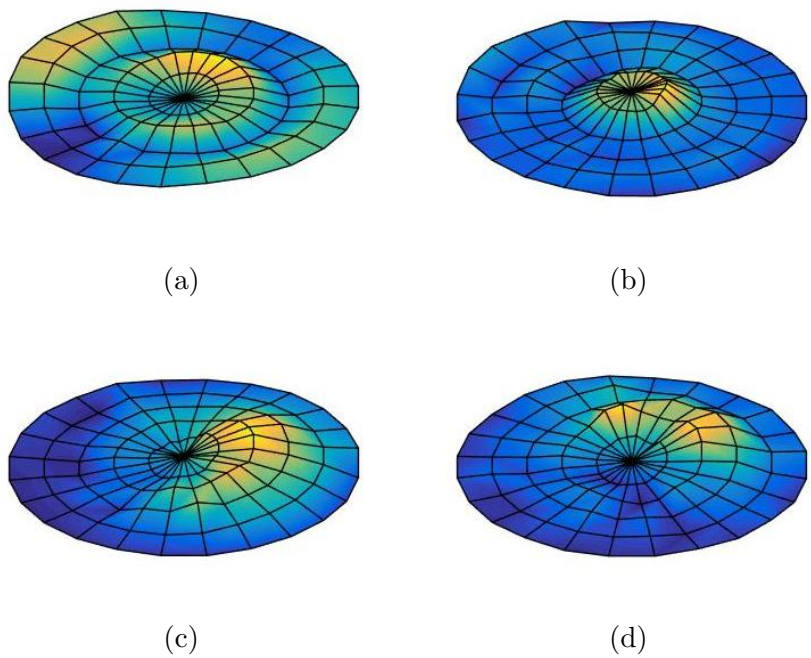

Figure 3.12. : Operational deflection shapes for a 0.64 cm height sample of 85% solids loading and 30% additive content at (a) 11.8 kHz (b) 35.16 kHz (c) 59.09 kHz and (d) 70.6 kHz.

3.3.2 Thermal Response

The thermal behavior of each sample was recorded in response to a 1.25 V peak sinusoidal input to the shaker at the maximum resonant peak within each of the four frequency subranges. Analysis of a single thermal experiment consists of four main temperature measurements, located at the top of the sample, the side of the sample, the side of the baseplate, and the ambient temperature of a reference object near the sample. The temperature of the baseplate was monitored in an attempt to identify the source of the heat generation throughout the 15 min experiment. Figure 3.13 depicts the maximum surface temperature at the top and side of the sample, as well as the baseplate temperature, for a 1.27 cm height sample of 85% solids loading with 15% aluminum additive content excited at 12.86 kHz and 70.58 kHz. The magnitude of temperature rise observed for this sample, on the order of 30°C, represents an approximate average surface temperature increase observed in this frequency range, with overall magnitudes varying from 10°C to 80°C. At frequencies in the lower subrange (1-20 kHz), the temperature rise of the sample far surpasses that of the baseplate, indicating the sample itself to be the major source of heat generation. As observed in Figure 3.14, the location of the maximum temperature increase occurs at the geometric center of the sample in this frequency subrange. In contrast, thermal experiments in the highest frequency subrange (60-80 kHz) exhibit baseplate temperatures greater than that of the sample. This suggests that the source of the temperature rise may be a combination of both heat generation within the particulate composite as well as conduction from the baseplate (which likely heats due to intermittent contact in the threaded fastener). Figure 3.15 illustrates the final thermal profile of the sample, exhibiting a monotonic decrease in temperature from the bottom to the top of the cylinder. Although presented graphically for a single sample, this trend was observed throughout the various sample geometries and formulations tested. The magnitude of temperature rise for all of the experiments performed in this study are included in Appendix A.

In an effort to reduce the observed conduction between the mounting components and the composite material, several additional samples were fabricated to include a thermal barrier between the bolt and the sample material. Glass mica ceramic and PEEK, a high

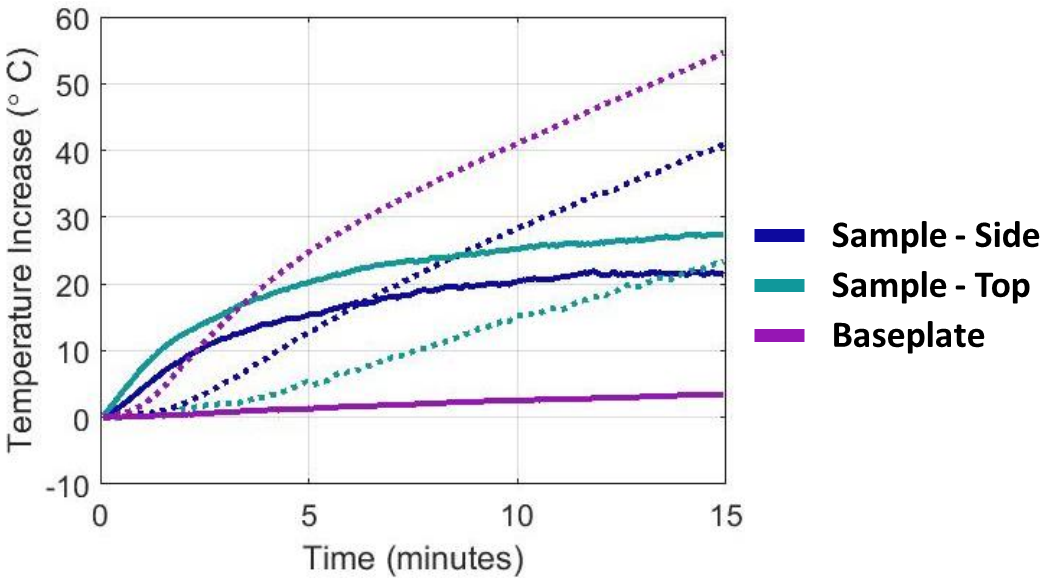

Figure 3.13. : Experimentally obtained cylinder maximum surface temperature versus time in response to harmonic excitation near a resonant frequency of the system for a sample with 85% solids loading and 15% additive content. The solid lines indicate the response at 12.86 kHz. The dotted lines indicate the response at 70.58 kHz.

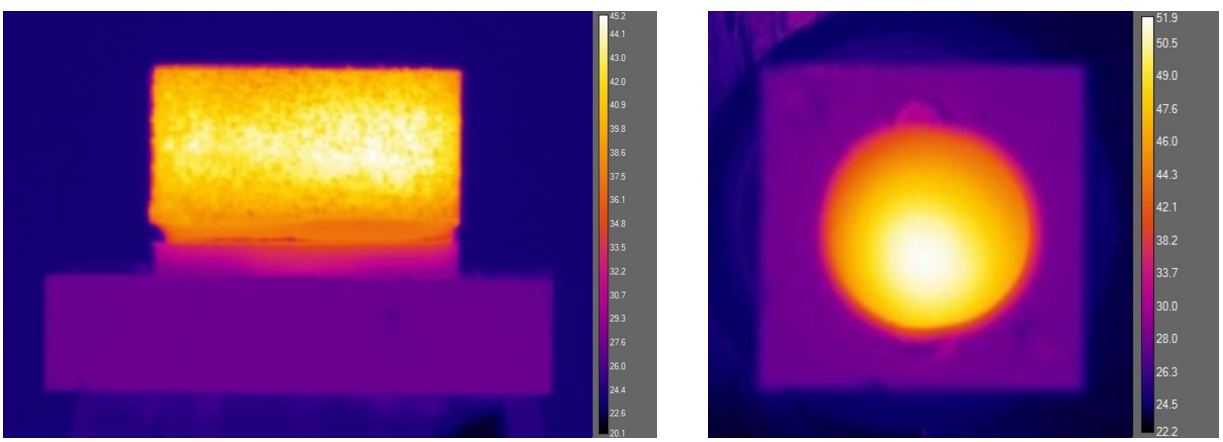

(a) (b)

Figure 3.14. : Experimentally obtained cylinder surface temperature profile after 15 min of harmonic excitation at 12.86 kHz for a sample with 85% solids loading and 15% additive content as viewed from the (a) side and the (b) top. Note that the surface temperature of the baseplate and shaker will differ slightly from those listed in the scale as the temperature bar is calibrated for the emissivity of the sample material.

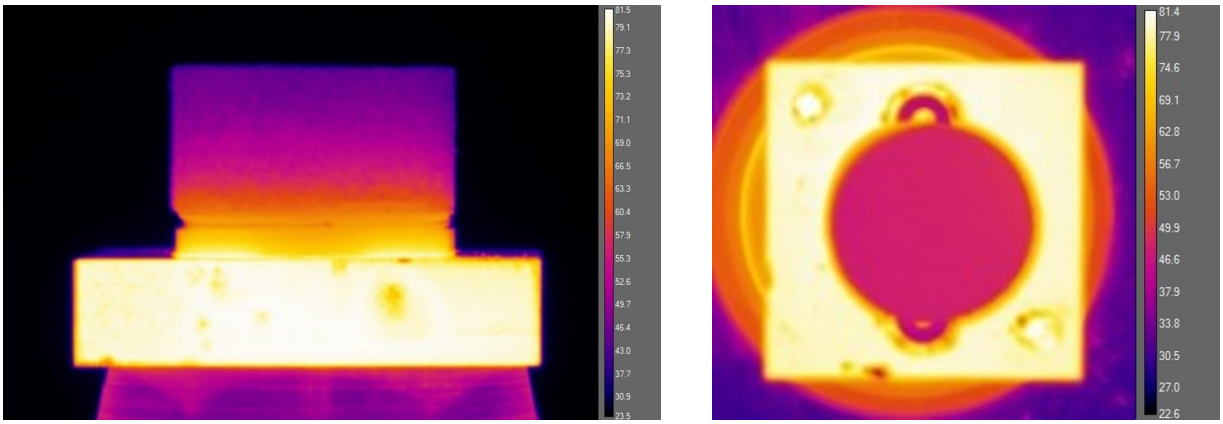

(a) (b)

Figure 3.15. : Experimentally obtained cylinder surface temperature profile after 15 min of harmonic excitation at 70.58 kHz for a sample with 85% solids loading and 15% additive content as viewed from the (a) side and the (b) top. Note that the surface temperature of the baseplate and shaker will differ slightly from those listed in the scale as the temperature bar is calibrated for the emissivity of the sample material.

density plastic, were chosen as the two thermal barriers. Each material was cut to 2.54 cm diameter discs at a thickness of 0.32 cm. One sample of each formulation was then epoxied to each of the two thermal barrier materials, attached to a bolt as before, and cut to a height of 1.27 cm. The mechanical response of these samples was determined in a similar manner to that outlined earlier in order to identify the major resonances within each of the four frequency subranges. The frequency response functions exhibit minor shifts in resonant frequencies due to the change in mass, but appear qualitatively similar to those presented above. Furthermore, the thermal behavior of these samples was recorded as before. The transient temperature profile for two samples of 85% solids loading with 30% additive is presented in Figure 3.16 for each of the thermal barrier materials at the resonance in the smallest frequency subrange (1-20 kHz). The samples attached to a PEEK thermal barrier appear to exhibit a greater temperature rise in this frequency range – a trend exhibited by each of the three different material formulations.

A comparison between the three different formulations for samples with no thermal barrier at a height of 1.27 cm excited in the first frequency subrange (1-20 kHz) is presented in Figure 3.17. Figure 3.17a and 3.17b represent the maximum transient surface temperature measured from the side and top of the cylinder sample, respectively. For a given sample height, formulations containing a weight percentage of aluminum additive content tended to exhibit greater temperature increases than corresponding samples with pure sucrose solids loading. This may be attributed to the increased thermal capacity of aluminum particles as compared to the sucrose particles. Interestingly, this trend within the formulations reverses for sinusoidal excitation in the highest frequency subrange (60-80 kHz). Overall, it appears that the thermal response is highly dependent on the type and relative amount of solid particles, as the varying particle sizes, thermal properties, and distribution of particles significantly change the microstructure of the material.

3.3.3 Temperature Increase Estimate

As shown experimentally in Figures 3.14 and 3.15, the sources of temperature rise within the particulate composite material varied depending on the frequency range of the input ex-

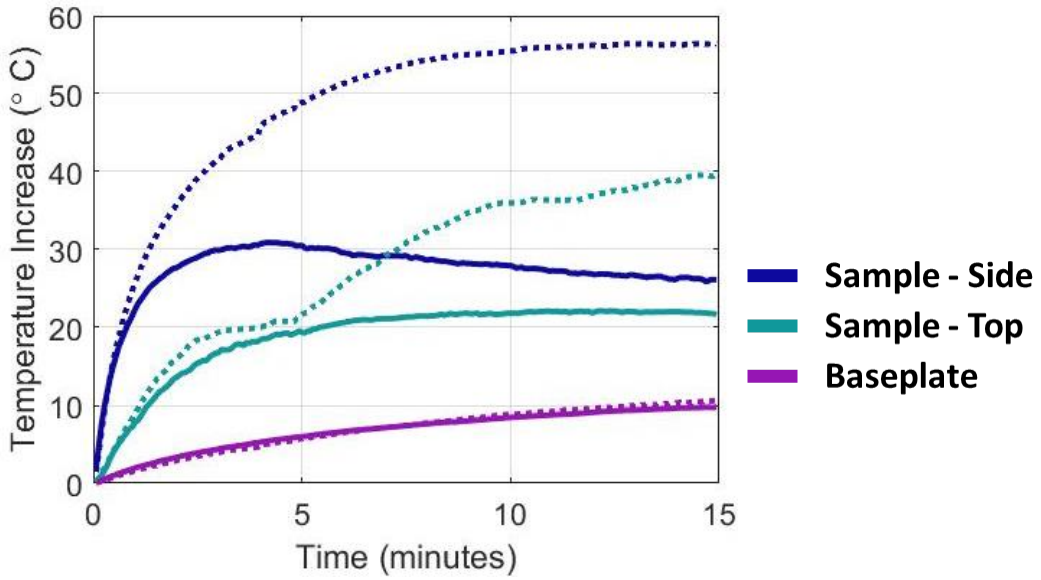

(a)

Figure 3.16. : Experimentally obtained cylinder maximum surface temperature versus time in response to harmonic excitation near a resonant frequency for two samples of 85% solids loading with 30% additive content. Solid lines indicate the response at 15.58 kHz with a glass mica ceramic barrier. Dotted lines represent the response at 15.70 kHz with a PEEK barrier.

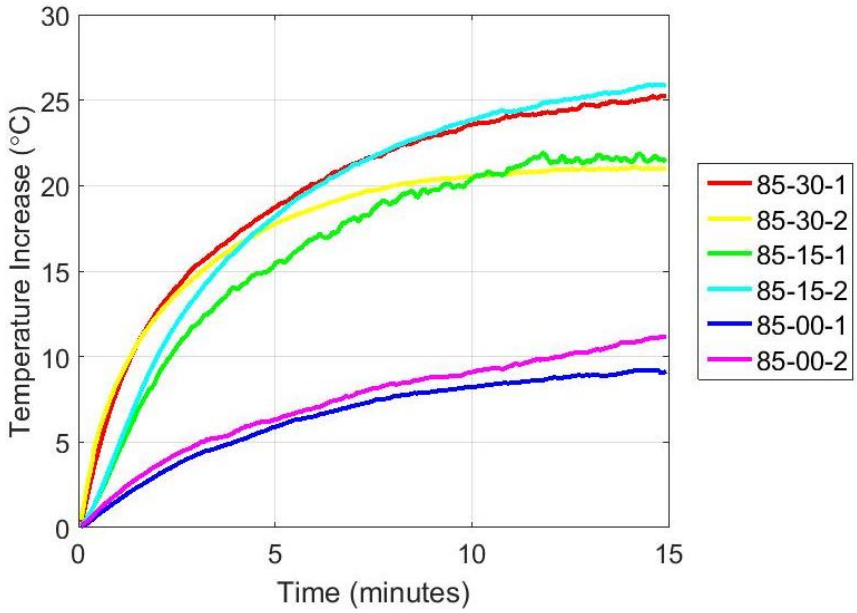

(a)

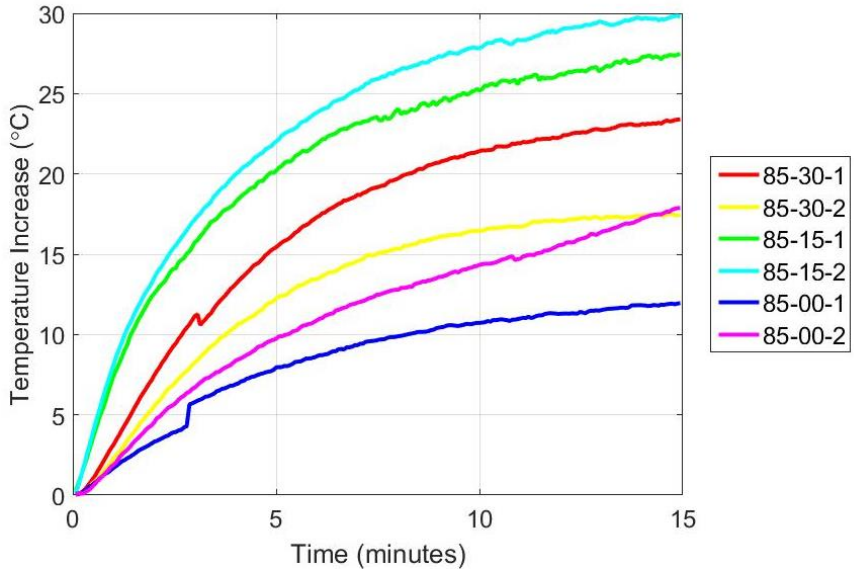

(b)

Figure 3.17. : Experimentally obtained maximum surface temperature versus time measured at the (a) side and (b) top of the cylindrical sample excited at the largest resonant frequency within the 1-20 kHz range. The legend indicates: solids loading - additive content - sample number.

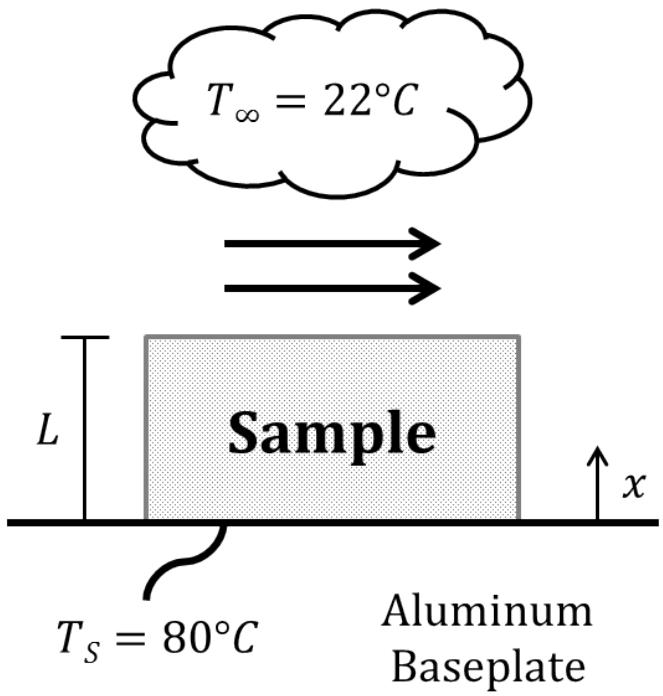

Figure 3.18. : One-dimensional heat transfer model of a vertical plane wall with applied boundary conditions.

citation. In the lowest frequency subrange (1-20 kHz), the maximum temperature increase occurred at the geometric center of the sample, indicating the sample itself to be the major source of heat generation. However, the thermal experiments in the highest frequency subrange (60-80 kHz) exhibited behavior that suggests heat transfer via conduction was occurring from the fixture components underneath into the sample material. With the aim of quantifying the conduction through the material, a simplified model was developed, as depicted in Figure 3.18, in which the sample was assumed to be suitably approximated by a one-dimensional, vertical plane wall. The 1.27 cm height of the sample was designated as the length of the wall, and the width dimension was assumed to be infinite. Assuming steady-state conditions with no heat generation, the appropriate form of the heat equation is given by [52]

$$\frac{d}{dx}\left(k\frac{dT}{dx}\right) = 0, \tag{3.1}$$

where k is the thermal conductivity of the sample, and $\frac{dT}{dx}$ is the temperature gradient with respect to position. Therefore, in the case of one-dimensional, steady-state conduction in a plane wall with no heat source, the heat flux is constant and independent of position. It follows, after two integration procedures, that the general solution for the temperature profile through the wall is given by

$$T(x) = C_1 x + C_2, \tag{3.2}$$

where C_1 and C_2 are integration constants obtained through the application of boundary conditions. The experimental setup was modeled by an aluminum baseplate at the bottom of the sample with ambient temperature air surrounding the remaining sides of the cylinder. In an attempt to approximate this, the bottom surface of the plane wall was modeled by a surface temperature of 80°C (a value taken from the experiment), and the top surface was exposed to a free convection condition with air at 22°C. These two conditions are represented in equation form as

$$T(x = 0) = T_S = 353.15 \text{ K}, \tag{3.3}$$

$$k\frac{dT}{dx} = h\left[T_\infty - T(x = L)\right]. \tag{3.4}$$

Substitution of Eq. 3.3 and 3.4 into Eq. 3.2 results in the final form of the temperature profile

$$T(x) = \left(\frac{T_\infty - T_S}{L + \frac{k}{h}}\right) x + T_S, \tag{3.5}$$

where T_S is the surface temperature specified above, T_∞ is the temperature of the ambient air, k is the thermal conductivity of the sample material, and h is the free convection coefficient for air. The thermal conductivity for a sample of 85% solids loading with 15% aluminum additive content was determined to be 0.491 W/m-K using the transient plane source technique [46]. Assuming a vertical plate immersed in ambient air flow, the free convection coefficient can be determined using empirical correlations for vertical plates [52]. This results in a coefficient equal to 8.75 W/m^2-K.

The temperature profile described by Eq. 3.5 using the one-dimensional plane wall approximation with experimental conditions is presented in Figure 3.19 as a function of axial position. As a comparison, experimental temperature data from the sample with 85% solids loading and 15% additive content presented in Figures 3.14 and 3.15 is shown versus axial position on the cylinder with $x = 0$ corresponding to the interface between the aluminum baseplate and the particulate composite energetic material. The one-dimensional plane wall temperature approximation, shown in yellow, roughly follows the experimental temperature profile exhibited in response to sinusoidal excitation at 70.58 kHz with the maximum temperature occurring at the baseplate. However, the experimental temperature profile in response to sinusoidal excitation at 12.86 kHz exhibits a parabolic shape along the axial direction with a baseplate temperature much lower than the sample itself. This comparison provides a preliminary verification of the conduction occurring from the base to the sample at higher frequency subranges, whereas the lower frequency subranges are exhibiting significant heat generation within the composite material coupled with little to no baseplate temperature increase.

3.4 Conclusions

The thermal and mechanical responses of particulate composite mock energetic cylinders, comprised of varying ratios of HTPB binder, sucrose particles, and aluminum powder, under contact excitation have been explored. Clear resonant behavior of the coupled shaker-cylinder system was observed across the entire frequency range of interest (1-80 kHz) for each of the three material formulations, and for each of the two cylinder heights of 1.27 cm and 0.64 cm. Resonant frequencies were separated into four frequency subranges, and the operational deflection shape for the dominant resonance within each subrange was identified through laser Doppler vibrometry. The majority of samples exhibited classic drum or rocking deflection shapes at the top surface when excited near dominant resonances.

The reported transient surface temperature patterns exhibit significant heat generation over the 15 min window of harmonic excitation, resulting in temperature increases on the order of 2-4°C/min, with several samples exceeding 100°C within the time frame of the

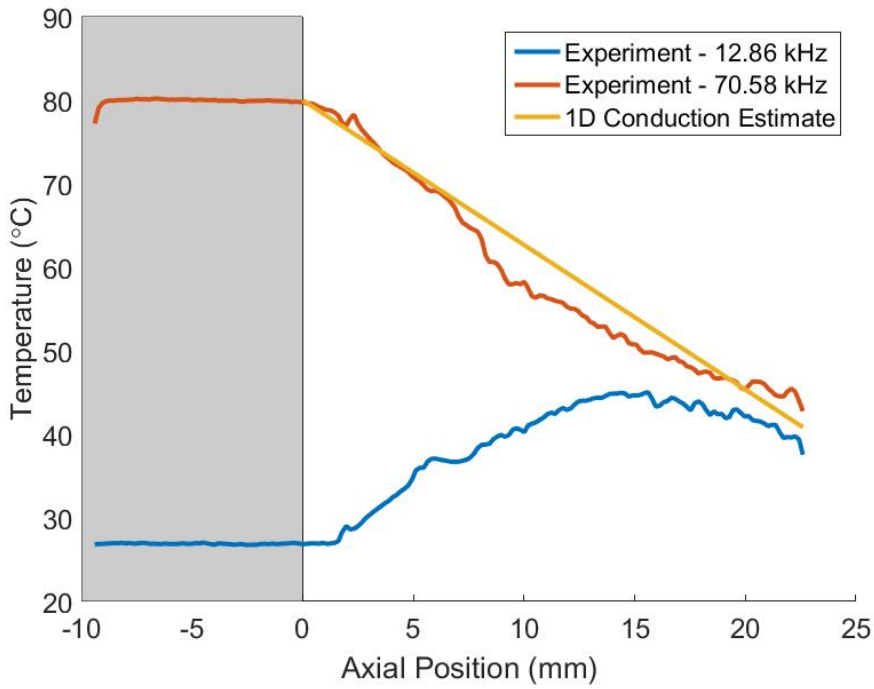

Figure 3.19. : Estimated surface temperature versus axial (vertical) position as a result of one-dimensional, steady-state conduction through a planar surface with material properties consistent with the 85% solids loading and 15% aluminum additive content formulation. Experimentally obtained maximum surface temperature profiles after 15 min of harmonic excitation at two frequencies for a sample with 85% solids loading and 15% additive content are included for comparison.

experiment. Near-resonant excitation at frequencies below 20 kHz exhibited a thermal response to suggest the heat generation was occurring within the sample itself, while excitation at frequencies of approximately 70 kHz provided a thermal profile consistent with conduction through the sample from the baseplate below. The data gathered throughout this study from experiments on various sample geometries and material formulations provides significant advances in our understanding of the thermomechanical behavior of particulate composite energetic materials at high frequencies. Significant increases in temperature can occur within the material under resonant vibratory excitation. Such information is extremely useful when developing protocols for the safe handling and transport of munition systems.

Future work will be directed towards identifying and quantifying the various sources of heat generation observed through these experiments, including viscous heating within the particulate composite material, particle/binder interactions, as well as conduction from the components of the sample fixture. The incorporation of the temperature-dependent material properties, in addition to the heating mechanisms described, will allow improved accuracy in the prediction and understanding of the thermal behavior for these samples. Efforts will also be made to determine the consequences of this heat generation, if observed in a live energetic particulate composite material.

4. HIGH–FREQUENCY RESONANT EXCITATION OF LIVE ENERGETIC MATERIALS

4.1 Introduction

Due to the increased heat generation exhibited by the mock energetic samples at high frequencies (1-80 kHz), it is of interest to verify the heat generation of the live energetic formulations in this frequency range. As such, experiments were performed in a similar manner to those outlined in the previous chapter with several modifications for safety purposes. Fully loaded composite samples were remotely subjected to harmonic base excitation while the thermal and mechanical response was measured using infrared thermography and laser Doppler vibrometry, respectively. This study is an attempt to expand upon the work presented for the low-frequency regime by providing significant advancement toward the characterization of these particulate composite energetic materials in response to contact mechanical excitation at high frequencies (greater than 1 kHz).

4.2 Experimental Techniques

4.2.1 Sample Preparation

The samples of live explosive material were prepared using RDX particles and spherical aluminum powder, held within a hydroxl-terminated polybutadiene (HTPB) binder as before. The RDX were characterized as Class I, with an average diameter of approximately 200 μm. The spherical aluminum powder was purchased from Valimet, Inc. and had an average particle diameter of 25 μm.

Cylinders were prepared according to the ratios of PBXN-109 propellant, given by Lochert *et al.* [51]. A summary of this formulation is given in Table 2.1. Note that all of the samples were prepared with identical solids loading and aluminum additive content.

Figure 4.1. : Representative cylinder sample of PBXN-109.

Fabrication of the live samples was performed as described in Section 3.2.1, utilizing proper safety precautions for handling RDX particles. In order to decrease the overall height of the live samples without having to cut energetic material on a lathe, cylindrical Teflon inserts with a diameter and height of 2.54 cm and 1.27 cm, respectively, were inserted into each of the cavities of the mold to cast cylinders with a final diameter of 2.54 cm and a height of 1.27 cm. The mass of each cylinder was measured as approximately 10 g.

After curing, the samples were epoxied to a PEEK thermal barrier and elevator bolt for placement into the test fixture. As before, the elevator bolts were painted a matte black to reduce radiation during thermal experiments. A representative cylinder is presented in Figure 4.1. Note that some inhomogeneities are clearly visible.

4.2.2 Experimental Setup

Similar to the mock energetic experiments, a Meggitt F7-1 piezoelectric shaker mounted to a marble isolation table was used to mechanically excite the cylinders at moderate excitation levels. The elevator bolts epoxied on the bottom of the cylinders were fastened to a baseplate mounted atop the shaker head. Similar to the elevator bolts, the baseplate was painted matte black to reduce radiation. A Keysight 33509B Waveform Generator provided the sinusoidal input signal to the Wilcoxon Research® PA8HF power amplifier with a maximum input signal of 1.5 V_{rms}. In order to allow remote control of the experiment, the

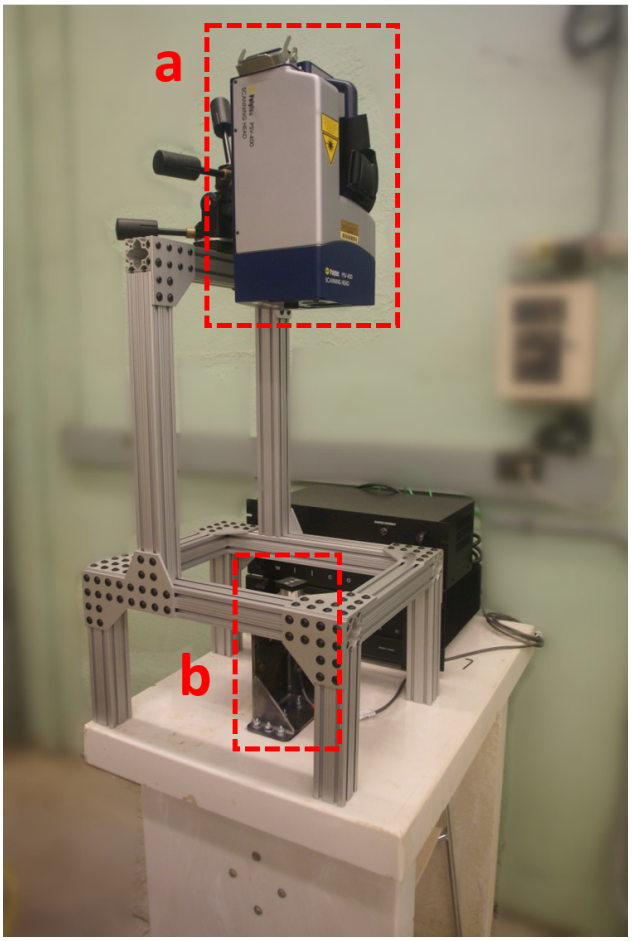

Figure 4.2. : Experimental setup with a (a) Polytec PSV-400 scanning laser Doppler vibrometer positioned above a cylindrical sample mounted to the (b) Meggitt shaker.

waveform generator was situated at the exterior control with a cable pass-through providing connection to the amplifier and remaining components on the interior of the test cell. The signal was then routed to the Wilcoxon Research® N8HFS impedance matching network and through to the shaker head. The shaker is characterized by a frequency range of 1 to 80 kHz with a maximum force output of 50 N. The thermal response was recording using a FLIR A6507 thermal camera at the side of the sample with an accuracy of $\pm$ 2°C or $\pm$ 2%. A Polytec PSV-400 scanning laser Doppler vibrometer was used to record the frequency response of each cylinder. The experimental set up for the mechanical experiments is presented in Figure 4.2.

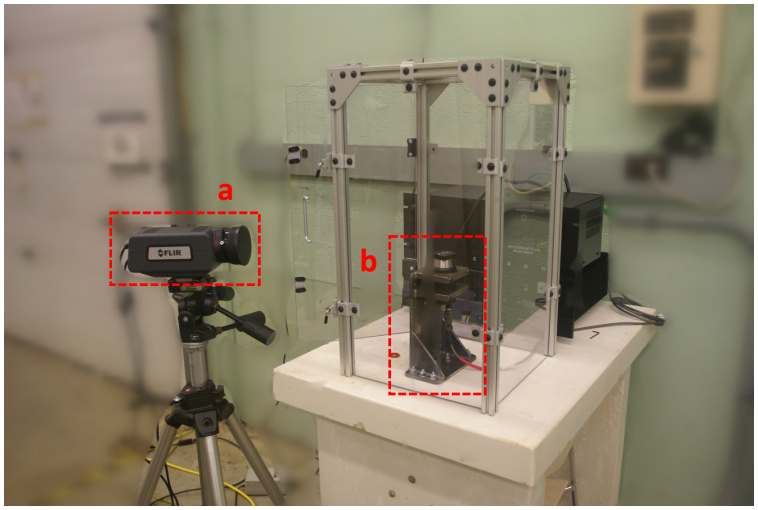

Figure 4.3. : Experimental setup with a (a) FLIR A6507 infrared camera positioned to the side of a cylindrical sample mounted to the (b) Meggitt shaker.

Frequency and thermal responses were obtained in a similar manner to the mock energetic samples, described in Section 3.2.2. As a safety precaution, a polycarbonate enclosure surrounding the shaker and sample was added to protect against the effects of potential deflagration of the sample during testing. The space constraint imposed by this enclosure limited the FLIR thermal measurement to a single side view, as opposed to top and side views that were gathered for the mock energetic cylinders. The experimental set up for the thermal experiments is presented in Figure 4.3.

4.3 Results and Discussion

4.3.1 Mechanical Response

In previous experiments with mock energetic material, the resonance identified in the lowest frequency subrange (1-20 kHz) exhibited the greatest heat generation within the sample with minimal conduction from fixture components, thus the live energetic material experiments focused primarily in this range. The frequency response for two samples of PBXN-109 with a height of 1.27 cm is presented in Figure 4.4. Swept sinusoidal input was

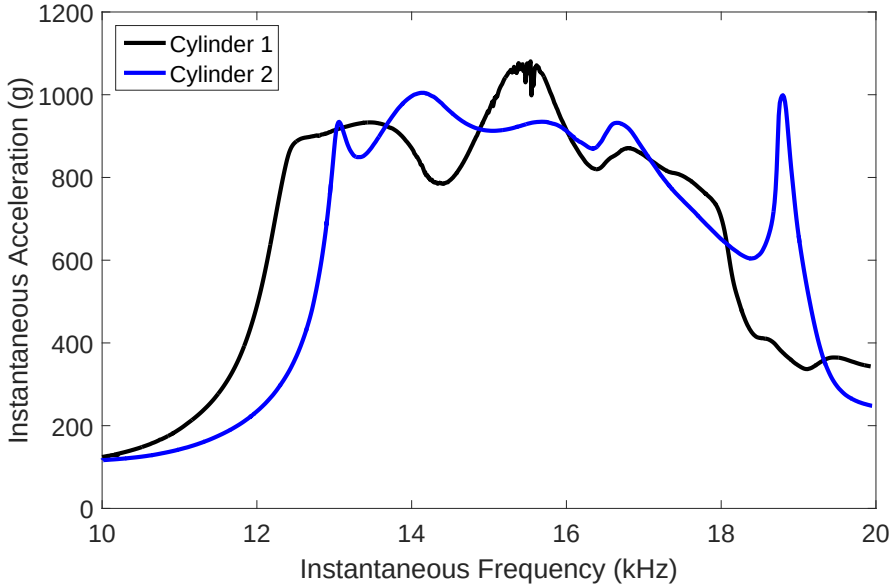

Figure 4.4. : Instantaneous acceleration versus frequency for two 1.27 cm height PBXN-109 samples.

limited to 10 to 20 kHz as each of the mock energetic samples exhibited a significant resonance in this range, and the largest resonance was identified near 15 kHz for each cylinder.

4.3.2 Thermal Response

The thermal behavior of each sample was recorded in response to a sinusoidal input at the aforementioned resonant peak identified within the 1-20 kHz frequency subrange. Analysis of a single thermal experiment consists of three main temperature measurements, located at the side of the sample, the side of the baseplate, and the ambient temperature of a reference object near the sample. The baseplate temperature was monitored in an attempt to identify the source of heat generation throughout the 30 min experiment. The maximum surface temperature at the side of the sample is shown in Figure 4.5 for two 1.27 cm height samples excited at 15.53 kHz (Cylinder 1) and 14.14 kHz (Cylinder 2). In each case, the temperature of the sample far surpassed that of the fixture components, indicating a strong heat generation within the sample itself. The temperature variation at the side of the

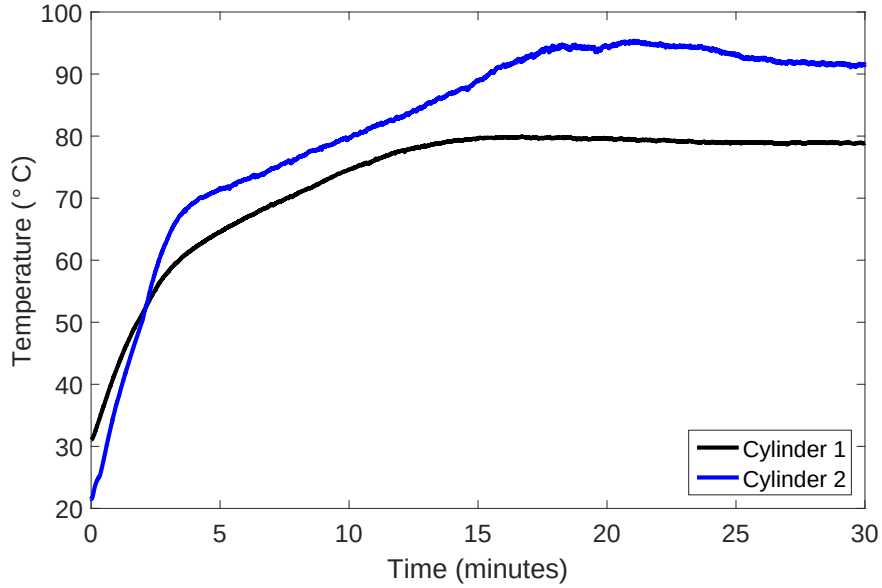

Figure 4.5. : Experimentally obtained maximum side surface temperature versus time in response to harmonic excitation with 1.5 V peak input to the shaker near a resonant frequency for two cylindrical samples of PBXN-109 in the 10-20 kHz frequency range.

sample exhibited by two nominally identical samples both provided evidence of the potential influence of microscale behavior resulting from interactions between the particle and the binder, porosity in the composite material, or damage occurring during the experiments.

After a qualitative comparison of the samples pre- and post-test (verified by a shore A hardness tester), it was noted that the samples exhibit significant softening as the temperature increases with an order of magnitude decrease in hardness; thus shifting the resonant frequency over the course of the 30 min experimental window. In an effort to observe this, an experiment, referred to herein as a frequency-tracking experiment, was performed as follows:

- The frequency response of the sample was determined using the laser Doppler vibrometer (LDV) in the range from 10 to 20 kHz with a sinusoidal input amplitude to the shaker of 500 mV peak. This is denoted as '0 min' in Figure 4.6a.

- The FLIR thermal camera was used to capture the temperature response of the sample throughout a 42 min experimental window, in which a 7 min scheme was repeated 6

times. For 5 min, the input was held constant at the peak frequency identified in the '0 min' frequency response and a peak amplitude of 1.5 V. The remaining 2 min was used to perform a frequency sweep lasting approximately 90 s across the 10 to 20 kHz range at a peak amplitude of 500 mV.

- After the 42 min experiment, the frequency response at each time interval was determined, and the peak frequency within the 10 to 20 kHz range was identified and plotted versus time. This data was used to identify a linear fit, with the slope indicating the sweeping rate to be used in the following thermal experiment.

- The sample was excited for 30 min at a constant peak sinusoidal input amplitude of 1.5 V with a swept frequency corresponding to the slope determined in the previous step.

The procedure outlined above was replicated on two virgin samples of inert PBXN-109, prior to experimentation on live material. The initial experiment, designated as Cylinder 3, ended abruptly due to a minor shaker issue in which the amplifier switched off at the end of the '19 min' frequency response scan. The frequency responses obtained prior to this issue are included below in Figure 4.6a, and the thermal response associated with this 25 min experiment is presented in Figure 4.6b.

As a result of the minor shaker malfunction, fewer data points were identified for the peak frequency versus time plot as shown in Figure 4.7. However, the linear fit was determined using the four data points obtained with a resulting slope of -32 Hz/min for Cylinder 3.

The following thermal experiment for this sample acounted for the 32 Hz/min drop in peak frequency over the 30 min excitation window. The resulting maximum side temperature of Cylinder 3 is shown below in Figure 4.8a. At approximately 20 min, the maximum side temperature appeared to exhibit a dramatic decrease. Upon removal of the sample from the fixture, it was observed that the epoxy connecting the PEEK thermal barrier to the bolt was completely detached as shown in Figure 4.8b—most likely occurring near the point in time at which the temperature began to drop. Prior to the epoxy detachment, however, the temperature was steadily increasing. This supports the hypothesis that the peak frequency can be tracked as the softening occurs within the sample.

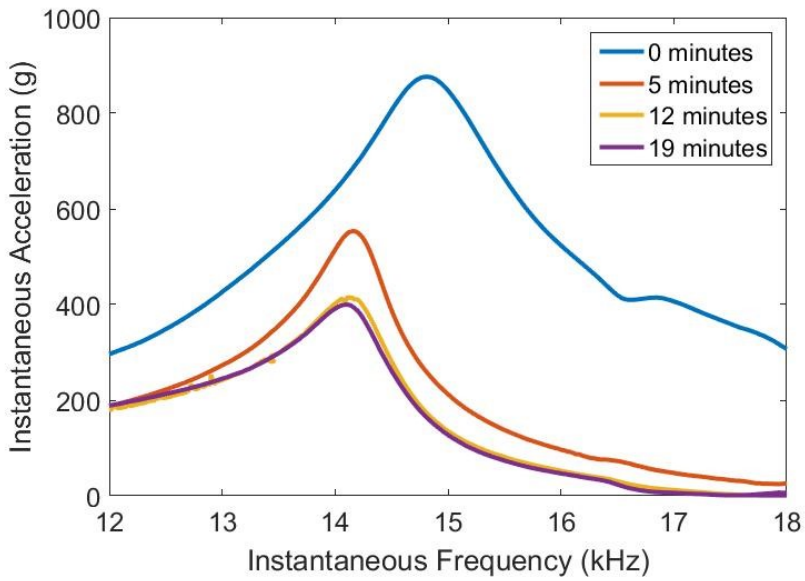

(a)

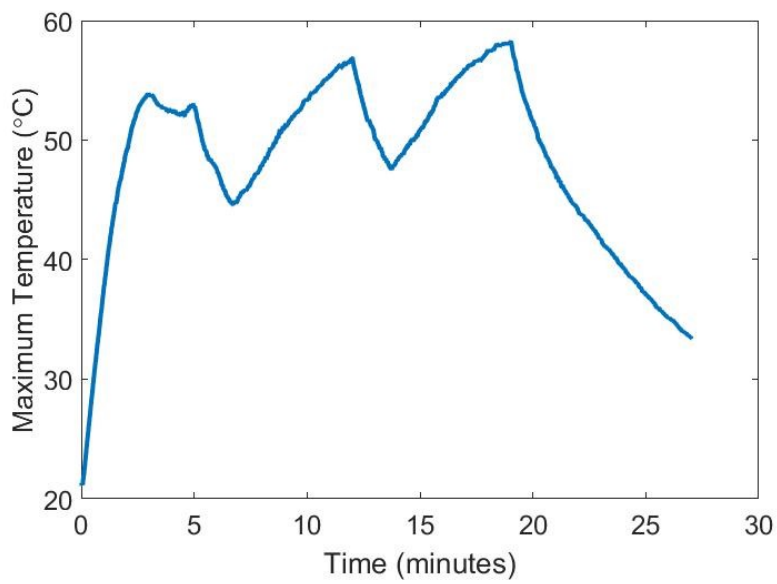

(b)

Figure 4.6. : Experimentally obtained (a) instantaneous acceleration versus frequency of the 1.27 cm height inert PBXN-109 Cylinder 3 at intermittent time intervals with (b) corresponding maximum side surface temperature versus time in response to near-resonant harmonic excitation at 14.81 kHz.

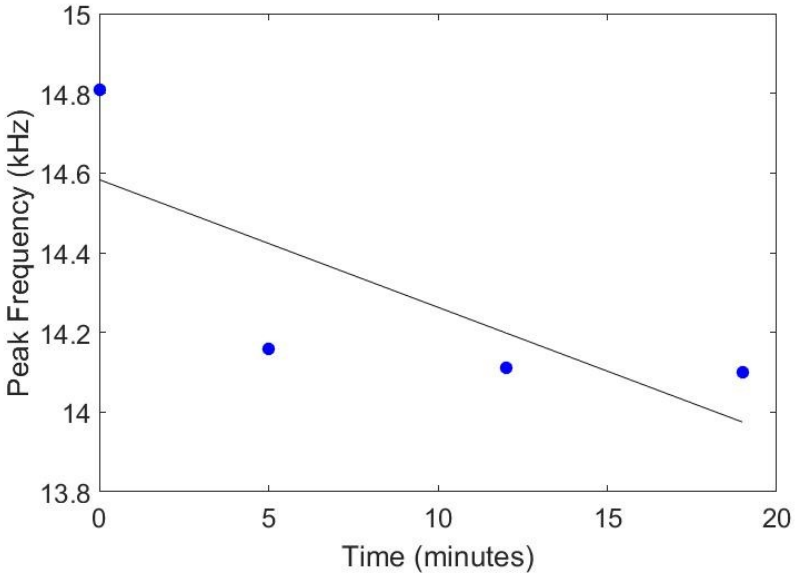

Figure 4.7. : Experimentally obtained peak frequency versus time for Cylinder 3 (1.27 cm height inert PBXN-109) in response to near-resonant contact excitation at 14.81 kHz.

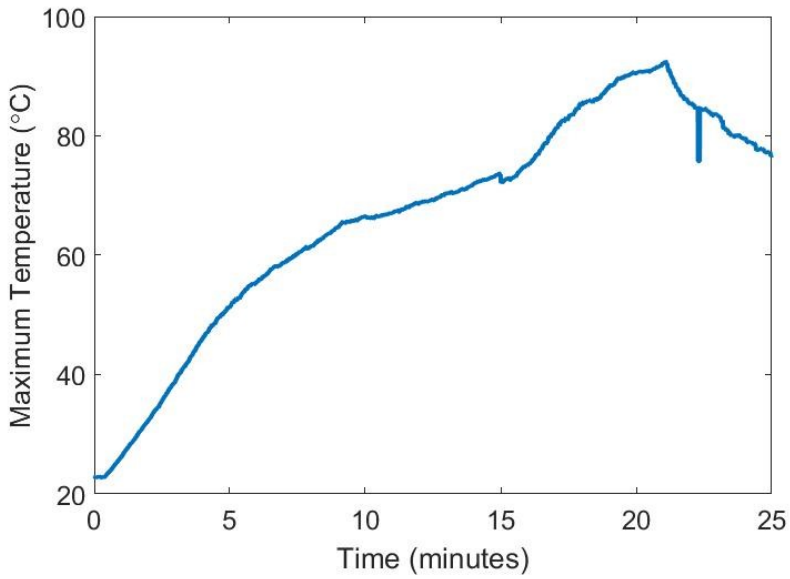

(a)

(b)

Figure 4.8. : Experimentally obtained (a) maximum side surface temperature versus time in response to harmonic excitation at 1.5 V peak input to the shaker swept near a resonant frequency and (b) post-test image for Cylinder 3 of inert PBXN-109.

As a point of comparison, the entire experimental procedure outlined above was repeated on a second sample, referred to as Cylinder 4. The frequency response curves and thermal results from the initial 40 min experiment are presented in Figure 4.9. Each of the frequency responses exhibit a clear resonance that shifts down and to the left as time progresses due to the softening. The peak frequencies were identified and plotted versus time in Figure 4.10.

The linear fit displayed in Figure 4.10 for the peak frequency versus time data is characterized by a slope of -30.7 Hz/min. That value was used to determine the sweep rate for the following 30 min experiment. The maximum temperature results and post-experiment images of Cylinder 4 are shown in Figure 4.11. In this case, the sample reached a maximum surface temperature of 122.3°C. Approximately 20-25 min into the experiment, a resin was observed to melt, boil, and drop out near the bottom of the sample as shown in Figure 4.11b. This material is potentially a combination of either epoxy or binder material from the interior of the sample. In addition, the sample detached between the PEEK thermal barrier and bolt, likely causing the rapid temperature decrease at the end of the experiment.

The inert PBXN-109 samples analyzed using the frequency-tracking experimental method each exhibited maximum surface temperatures greater than the corresponding experiments in response to constant sinusoidal excitation. The slowly swept sinusoidal input was able to account for the downward shift in resonant frequency due to material softening with temperature. However, the temperature profiles each displayed several slope variations throughout the experimental window. Due to limitations with the piezoelectric shaker, the voltage input had to be varied from a constant sinusoidal signal to a swept sinusoidal signal to determine the frequency response at intermittent time intervals. During each interval in which the frequency response was recorded, the temperature of the sample decreased by approximately 10-20°C before pivoting upward again while time continued to increase. When applying the linear fit of the peak resonant frequency with respect to time, the fluctuation of temperature was not taken into account when determining the sweep rate for the final thermal experiment. Ideally, barring equipment limitations on force output, a banded signal with an upper limit at the initial resonant frequency of the system would more precisely account for the shift in resonance.

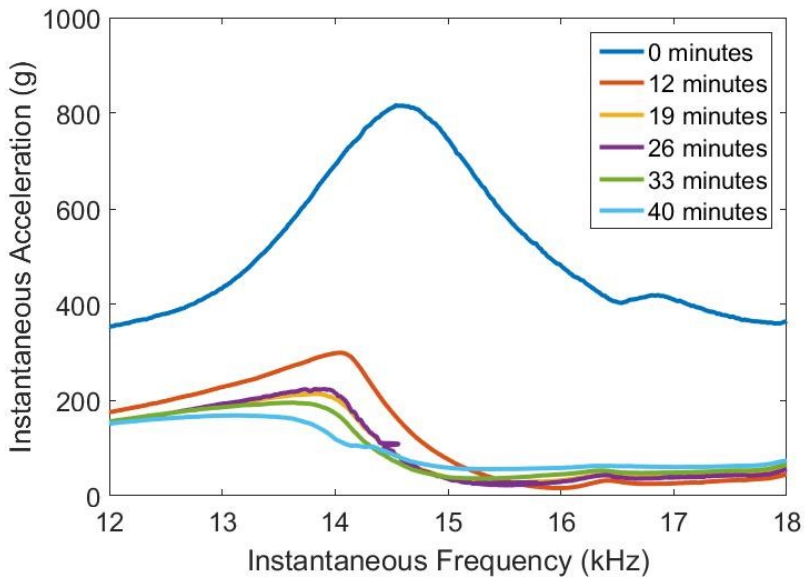

(a)

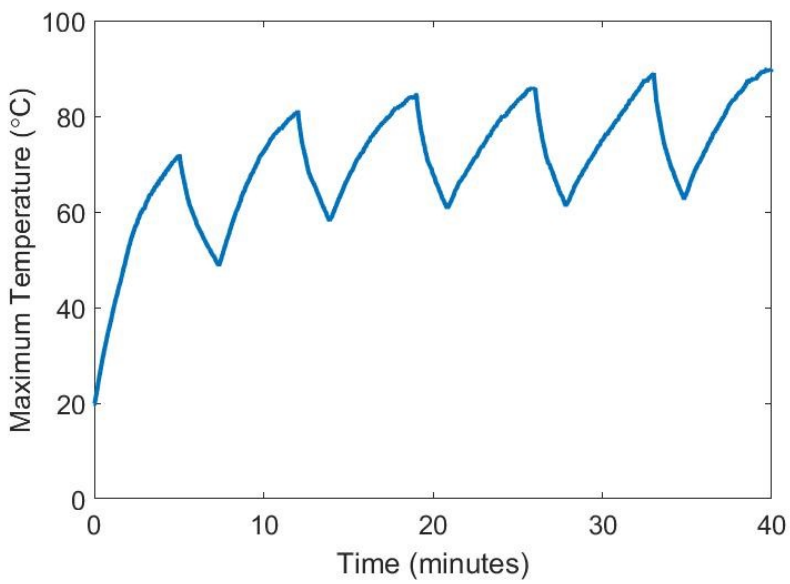

(b)

Figure 4.9. : Experimentally obtained (a) instantaneous acceleration versus frequency of the 1.27 cm height inert PBXN-109 Cylinder 4 at intermittent time intervals with (b) corresponding maximum surface temperature versus time in response to near-resonant harmonic excitation at 14.54 kHz.

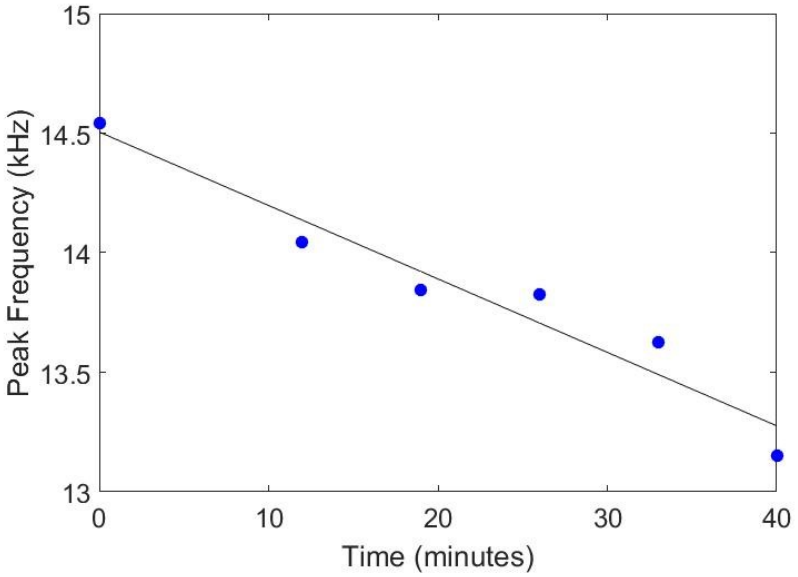

Figure 4.10. : Experimentally obtained peak frequency versus time for Cylinder 4 (1.27 cm height inert PBXN-109) in response to contact excitation at 14.81 kHz.

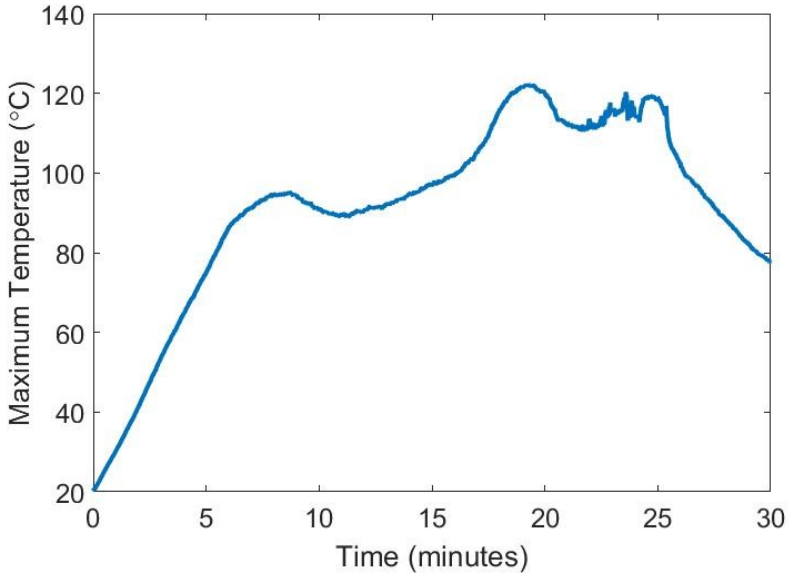

(a)

(b)

Figure 4.11. : Experimentally obtained (a) maximum side surface temperature versus time in response to harmonic excitation at 1.5 V peak input to the shaker swept near a resonant frequency and (b) post-test image for Cylinder 4 of inert PBXN-109.

4.4 Conclusions

The thermal and mechanical responses of particulate composite energetic cylinders, comprised of HTPB binder, RDX particles, and spherical aluminum powder, under contact excitation have been presented. Clear resonant behavior was observed in the frequency range of interest (10-20 kHz), consistent with thermal behavior observed in comparable inert samples. The reported transient surface temperature patterns exhibit significant heat generation over the 30 min window of harmonic excitation, resulting in temperature increases on the order of 3-4°C/min. Temperature rises of this magnitude may present significant challenges when incorporating polymer-bonded energetic materials into a variety of munitions systems. In order to determine the proper mitigation method for this type of behavior, the full extent of this phenomena must be explored for this formulation, as well as others that may be characterized by increased vibration sensitivity.

To account for the significant material softening exhibited in response to the large temperature variations in the reported experiments, a method was presented to account for the resonant frequency shift in the material as the temperature increases. Previously, single frequency response functions were recorded prior to the experiment in which thermal response was monitored via an infrared thermal camera. In contrast, in the frequency-tracking experiment, frequency response curves were recorded at intermittent time intervals, the resonant frequencies were plotted versus relative experimental time, and a linear fit was applied to identify a sweep rate. The thermal behavior was then monitored in response to slowly swept sinusoidal excitation, resulting in significant surface temperature increases on the order of 100°C. Thus, the experimental method incorporating resonant frequency tracking provided increased thermal response in the samples of PBXN-109 and provided confirmation of the material softening observed qualitatively in previous experiments.

The results presented here verify the potential for significant temperature increases in particulate composite energetic materials, both inert and live, in response to mechanical vibration at frequencies in the range of 10 to 20 kHz. Thus, a unique challenge is presented with regard to the safe handling of munition systems when subjected to vibratory loads as the temperature rises may be exacerbated by confinement or insulation, leading to a high

potential for unintended deflagration. Precise understanding of the thermal and mechanical behavior of these materials in the application environment is imperative to maintain safety and performance.

5. HIGH–FREQUENCY RESONANT EXCITATION OF ENERGETIC MATERIALS AT ELEVATED AMBIENT TEMPERATURES

5.1 Introduction

Significant characterization has been performed for mock and live composite energetic materials at ambient environmental conditions; however, the mechanical and thermal response of these materials at elevated temperatures is of interest, as this may be pertinent in particular applications. In a preliminary slow cook-off test, a wire was embedded at the center of two samples of fully loaded PBXN-109 cast to 2.54 cm diameter and 1.64 cm height. A voltage was applied across the wire to initiate deflagration. The first sample was initiated from room temperature, approximately 23°C, while the second sample was heated to approximately 50°C before initiation. A several-second time lag prior to deflagration was observed in the first experiment, whereas the preheated sample began to burn almost instantly as the voltage was applied. This suggests an increased sensitivity of the energetic material when preheated. In an effort to characterize this phenomenon in response to contact excitation, an enclosure was constructed to seal the sample around the Meggitt F7-1 piezoelectric shaker in the existing experimental setup outlined in Chapter 3. A detailed description of this experimental enclosure, as well as preliminary results to verify functionality of the system is outlined here.

5.2 Experimental Techniques

5.2.1 Sample Preparation

The four samples of inert material used in these verification experiments were prepared using sucrose particles as a mock material substituting for RDX crystals. Sucrose particles were sieved to a diameter range of 106 to 355 μm to closely resemble the published particle distribution of PBXN-109. Spherical aluminum powder and hydroxyl-terminated polybuta-

diene binder (HTPB) were added in ratios consistent with PBXN-109 as before, given by Lochert *et al.* [51]. Note that all of the samples were prepared with identical solids loading and aluminum additive content.

Fabrication of the samples was performed as outlined in Section 3.2.1, with each cylinder cast to a final diameter of 2.54 cm and a height of 1.27 cm. The mass of each sample was approximately 10-12 g. After curing, the samples were epoxied to a PEEK thermal barrier and elevator bolt for placement into the test fixture. The elevator bolts were previously painted a matte black to reduce radiation during thermal experiments.

5.2.2 Experimental Setup

As described in Section 3.2.2, a Meggitt F7-1 piezoelectric shaker was used to mechanically excite the cylinders at various excitation levels. The elevator bolts epoxied on the bottom of the cylinders were fastened to a baseplate mounted atop the shaker head. Similar to the elevator bolts, the baseplate was painted matte black to reduce radiation. A Keysight 33509B Waveform Generator provided the sinusoidal input signal to the Wilcoxon Research® PA8HF power amplifier with a maximum input signal of 1.25 V_{rms}. The signal was then routed to the Wilcoxon Research® N8HFS impedance matching network and through to the shaker head. The shaker is characterized by a frequency range of 1 to 80 kHz with a maximum force output of 50 N. The thermal response was recorded using a FLIR A6507 thermal camera at the side of the sample with an accuracy of $\pm$ 2°C or $\pm$ 2%. A Polytec PSV-400 scanning laser Doppler vibrometer was used to record the frequency response of each cylinder.

The elevated ambient temperature condition was achieved through the construction of a custom enclosure with an internal volume of approximately 2400 cm^3, which is shown in Figure 5.1. The front panel held a FLIR inspection window to allow infrared transmission from the sample, and the top panel held a piece of coated anti-reflective (AR) glass that was transparent to the laser wavelength associated with the laser Doppler vibrometer (LDV). In order to avoid complete confinement in the case of a sample deflagration, the tempered AR glass panel was loosely held within the small indent of the polycarbonate enclosure to

provide a blow-out panel. Mounted at the back of the enclosure was an OMEGA™ FCH-FGC10262R compact fan heater with a nominal power output of 60 W, a volumetric flow rate of 13.6 m^3/hr, and an operating temperature range of -10 to 70°C. A thermocouple (Type K) was integrated into the heated space of the enclosure to provide the temperature feedback to the control system, and the flame-retardant foam at the bottom insulates around the shaker.

The gray box to the right in Figure 5.1a housed the temperature controller and power supply responsible for monitoring the air temperature within the enclosure throughout the entire experiment. The OMEGA™ CN16PT-330 Platinum Series PID controller utilized a single-pole, double-throw mechanical relay, along with the thermomcouple input mentioned above, to monitor and adjust the air temperature inside the enclosure at a maximum sampling frequency of 20 Hz. The accuracy of the thermocouple was verified prior to experimentation using the FLIR A6507 thermal camera. In order to allow experimental analysis for both inert and live energetic formulations, the controller was monitored remotely from a laptop outside of the experimental test cell for the entirety of the data collection.

5.3 Results and Discussion

With the aim of verifying the functionality of the elevated temperature enclosure, four samples of inert PBXN-109 were analyzed in the experimental setup described above. Two cylinders were analyzed at an enclosure air temperature of 22°C, while the remaining two were analyzed under air temperatures of 60°C. Based on the previous experiments, a significant amount of material softening was expected during these experiments due to the high temperatures. To account for this, the experiments were performed utilizing the frequency-tracking method outlined in Section 4.3.2 in which the peak resonant frequency was scanned intermittently during the initial thermal response with constant sinusoidal excitation. This was then followed by a thermal experiment in response to a constant-amplitude, slowly sweeping sinusoidal excitation at a sweep rate corresponding to the shift in peak frequency identified by the frequency responses in the initial test.

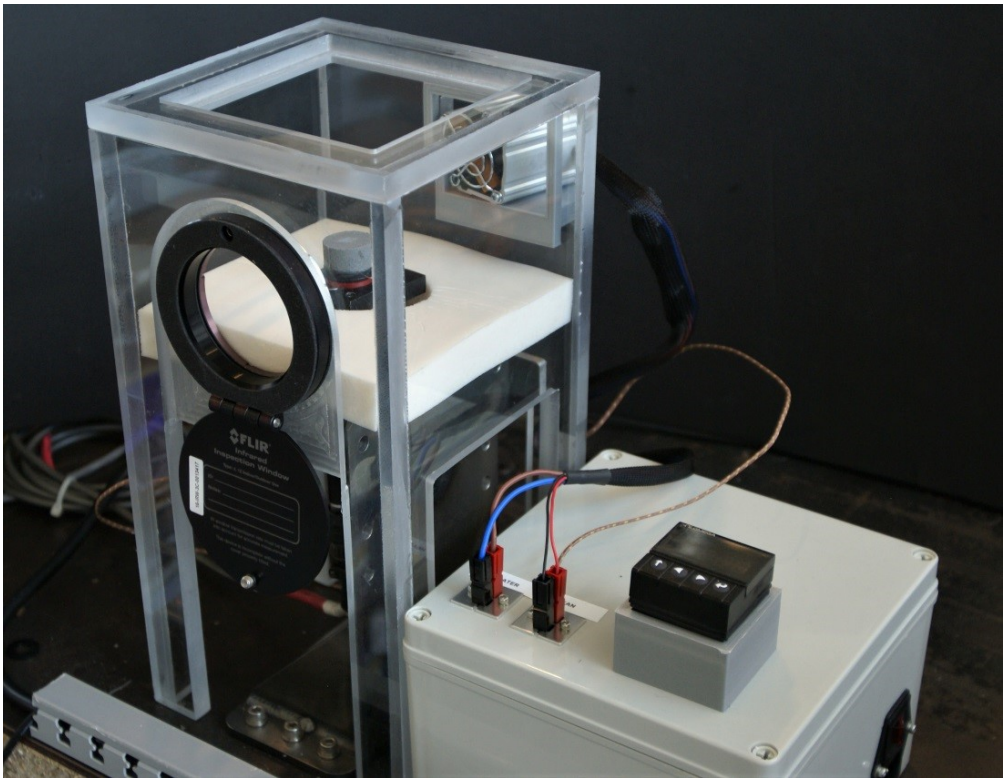

(a)

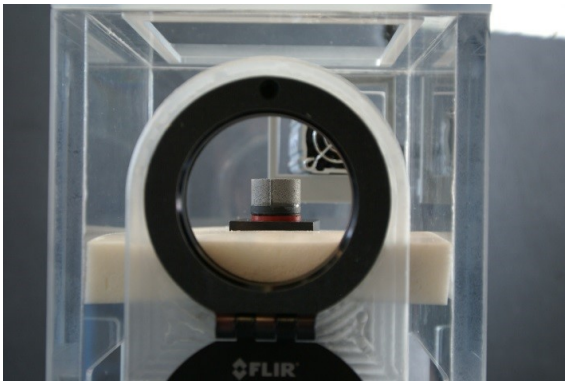

(b)

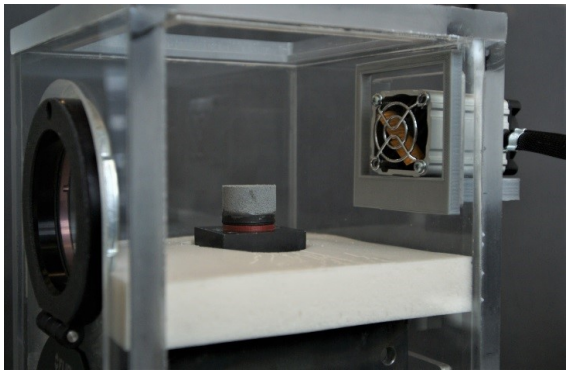

(c)

Figure 5.1. : Custom experimental enclosure used to provide elevated temperature environments up to 70°C surrounding the Meggitt F7-1 shaker as viewed (a) isometrically, (b) from the front, and (c) from the right side.

5.3.1 Mechanical Response

The frequency response functions and corresponding thermal response for the initial experiment with the elevated temperature enclosure maintained at 60°C is shown in Figure 5.2. For comparison, similar plots for one of the nominally-identical samples analyzed in the enclosure at 22°C are included in Figure 5.3. In contrast to the sample at 22°C inside the enclosure, the sample exposed to the 60°C environment exhibited resonant peaks that did not consistently soften as time progressed in the experiment. The resonant peak in Figure 5.2a appears to initially soften with the large temperature variation in the first 10 min of the experiment, followed by a slight hardening, before settling near a specific value. This behavior is consistent with the maximum temperature profile in that the initial 20 min were characterized by a temperature increase of approximately 20°C, while the final 20 min produced a gradual 5°C temperature rise. As observed in previous experiments, larger increases in temperature tend to produce more significant peak frequency shifts. Also of note, the resonant peak in the sample analyzed at 22°C, shown in Figure 5.3a, appeared to settle rather quickly as compared to the previous frequency-tracking experiments. As with the sample at elevated ambient conditions, the sample experienced a drastic temperature rise in the initial 10-20 min followed by a slow decline with each successive frequency scan. This may be potentially be attributed to the added air convection produced by the fan heater in the elevated temperature enclosure setup.

5.3.2 Thermal Response

Similarly to the previous frequency-tracking experiments, a second thermal experiment was performed after the linear sweep rate was determined for each sample of inert PBXN-109 using the intermittent frequency response functions presented above. The peak frequency at each time interval was plotted against the relative time in the corresponding initial thermal experiment. A linear fit was then applied to these data points to obtain a sweep rate in units of Hz/min. As with previous samples analyzed at room temperature, each of the four samples exhibited sweep rates in the range of -30 Hz/min. By utilizing a slowly swept sinusoidal excitation, as opposed to the constant sine wave analyzed previously, the shift

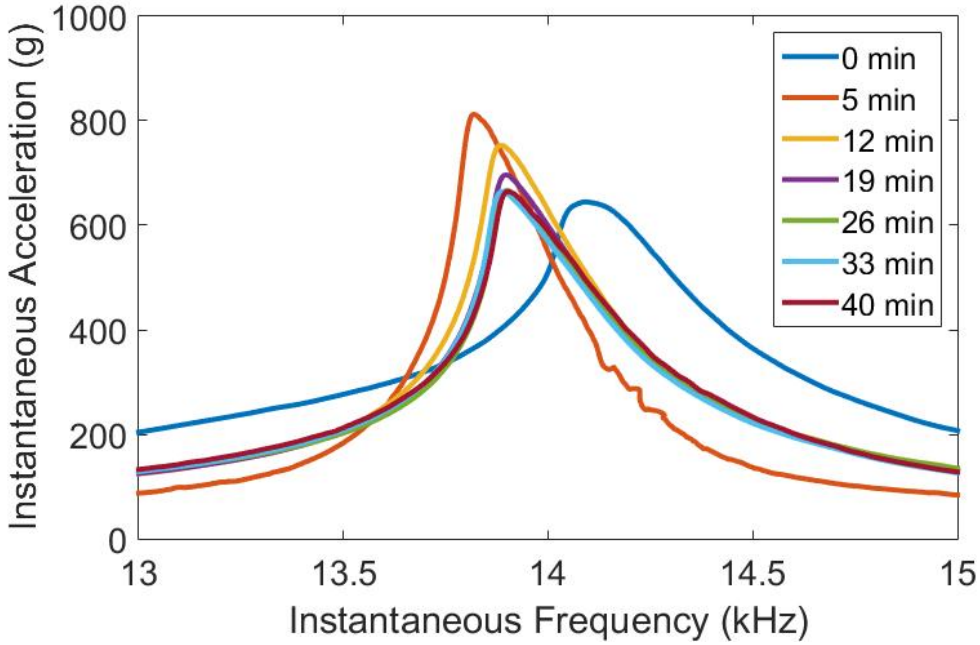

(a)

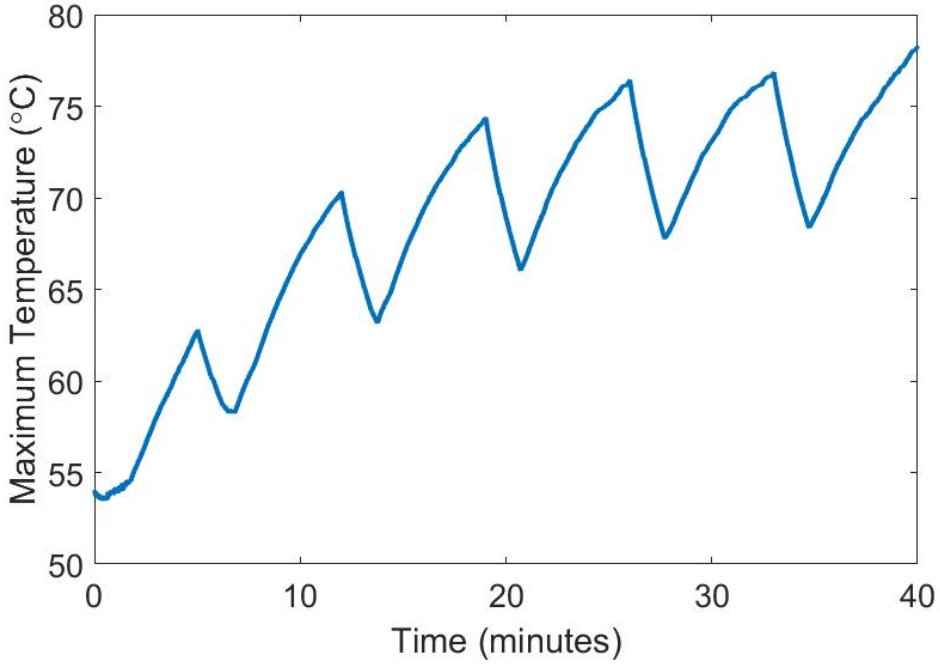

(b)

Figure 5.2. : Experimentally obtained (a) instantaneous acceleration versus frequency of 1.27 cm height inert PBXN-109 cylinder contained in a 60°C enclosure at intermittent time intervals with (b) corresponding maximum surface temperature versus time in response to near-resonant harmonic excitation at 14.09 kHz.

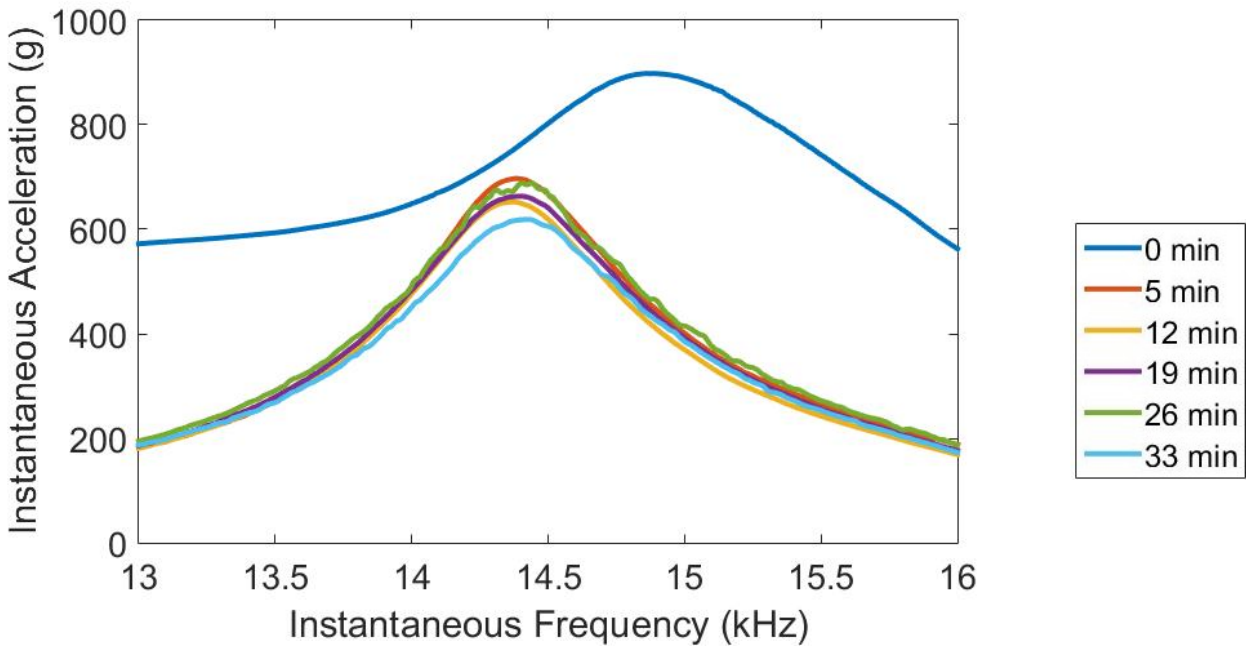

(a)

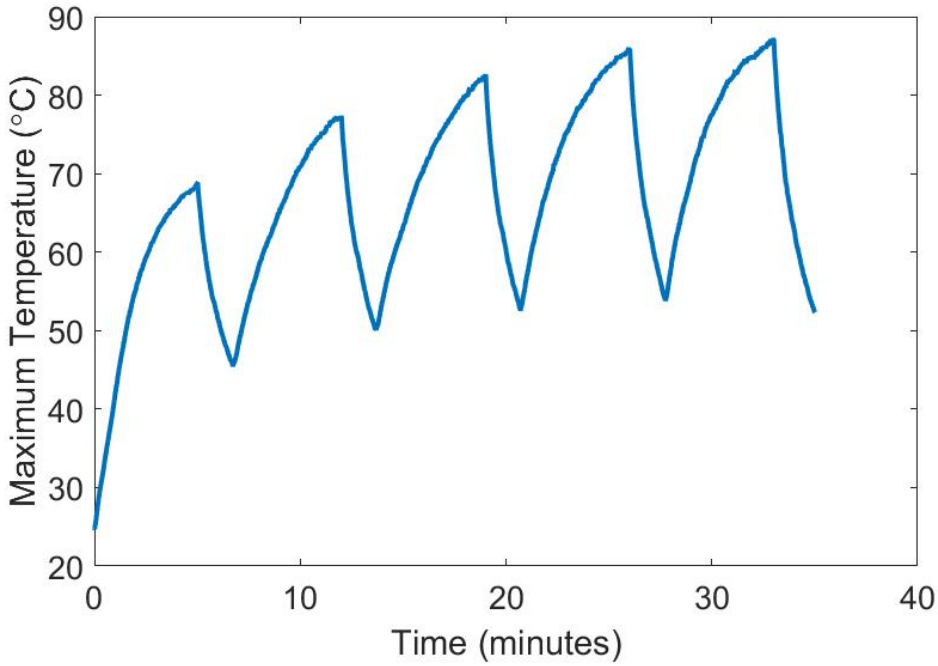

(b)

Figure 5.3. : Experimentally obtained (a) instantaneous acceleration versus frequency of 1.27 cm height inert PBXN-109 cylinder contained in a 22°C enclosure at intermittent time intervals with (b) corresponding maximum surface temperature versus time in response to near-resonant harmonic excitation at 14.86 kHz.

exhibited by the resonant peak may potentially be accounted for and consequently exploited to a greater extent.

The maximum surface temperature for each of the four inert, cylindrical PBXN-109 samples is presented in Figure 5.4. The first sample analyzed at an environmental air temperature of 22°C exhibited several interesting characteristics; the surface temperature dropped by approximately 10°C after 10 min of slowly swept sinusoidal excitation before pivoting to a positive slope for the final 15 min of the experiment to reach a maximum surface temperature of almost 120°C. In addition, the epoxy used to adhere the sample to the elevator bolt did not maintain its integrity, resulting in the sample detaching from the mounting fixture in the final minutes of the experiment as evident by the sharp temperature decrease at 30 min. The slope deviation mentioned previously after 10 min of excitation may have been due to a glass transition in the epoxy, prior to its failure near the end of the experiment. The manufacturer specifications estimate the glass transition of the cured epoxy to be approximately 60°C. The second sample analyzed while exposed to a room temperature environment displayed a similar slope discontinuity at approximately 10 min after reaching a maximum surface temperature of 75°C. However, as opposed to the rebound observed previously, the temperature steadily declined for the remainder of the sinusoidal excitation. There was no detachment observed between the sample and the elevator bolt, although the decrease in temperature may suggest a potential degradation in the strength of the epoxy or damage sustained by the sample material itself.

The samples analyzed at elevated environmental temperatures of 60°C, displayed in purple and yellow in Figure 5.4, each exhibit a much smoother temperature rise than the room temperature counterparts. A wide, shallow peak in temperature was observed in the first sample exposed to elevated temperature environments, while the second sample exhibited a steady, gradual increase in temperature as a result of the slowly swept sinusoidal excitation. The slope discontinuity may be due to an epoxy or sample material degradation as observed in the ambient experiments, however, a larger sample set analyzed at elevated environmental conditions is required to provide strong conclusions in this regard.

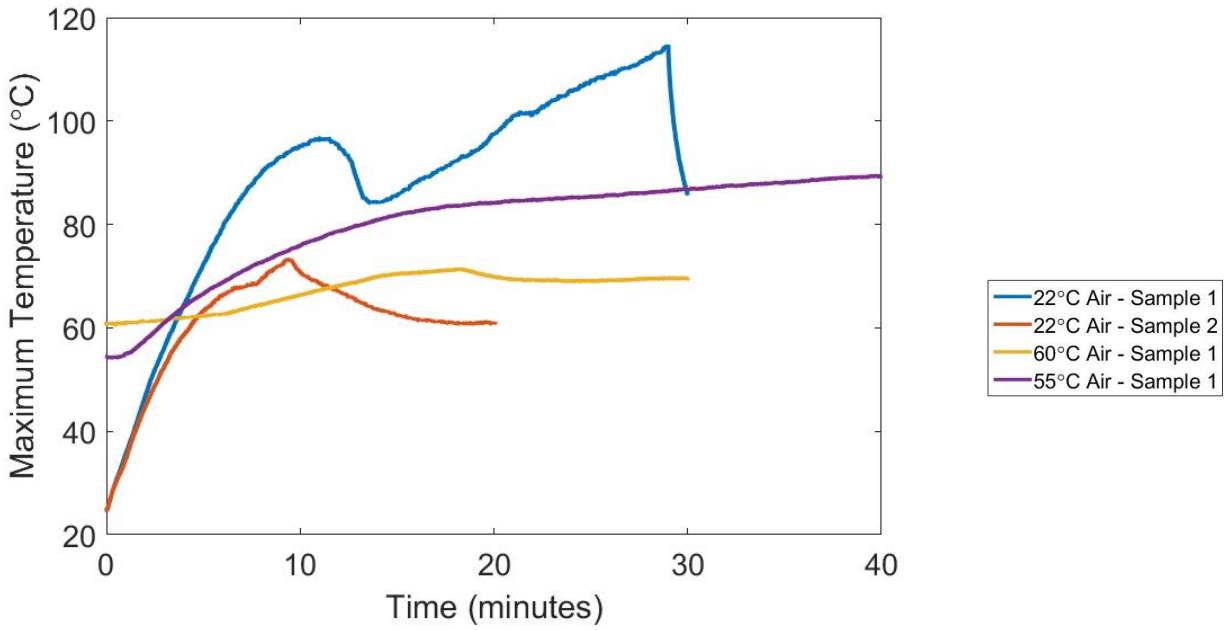

(a)

Figure 5.4. : Experimentally obtained cylinder maximum surface temperature versus time in response to harmonic excitation swept near a resonant frequency for 4 cylindrical samples of inert PBXN-109 surrounded by varying environmental air temperature conditions.

5.4 Conclusions

As stated previously, the results presented in this chapter represent a preliminary investigation designed to verify the functionality of the elevated temperature enclosure. The custom enclosure was designed and constructed using polycarbonate panels with specialty glass panels transparent to the infrared and laser wavelengths associated with the FLIR thermal camera and laser Doppler vibrometer, respectively. The bottom of the enclosure was formed from a piece of flame-retardant foam to insulate the shaker from the elevated air temperatures. A PID controller was connected to a compact fan heater and thermocouple to provide a closed-loop control system that continuously monitored the air temperature near the sample throughout the experiments with a maximum attainable temperature of approximately 65°C.

Initial experiments utilizing the elevated temperature enclosure compared the results of four inert PBXN-109 cylindrical samples: two analyzed at an environmental air temperature of 22°C, and two at 60°C. Frequency responses were recorded at distinct time intervals and were used to determine the resonant frequency due to swept sinusoidal excitation. The thermal response of each sample was measured using a FLIR infrared thermal camera. Due to the expected softening of the material with the significant temperature variation, the frequency-tracking experiment was performed to account for the resonant frequency shift in the material as the temperature increased. The samples analyzed at room temperature inside the enclosure each exhibited steep initial temperature increases, a slope discontinuity in the maximum surface temperature, and degradation in the strength of the epoxy used to adhere the cylinders to the elevator bolts for mounting into the experimental fixture. The samples analyzed at environmental air temperatures of 60°C displayed maximum surface temperature profiles with a steady, gradual increase across the 30-40 min experimental window. The maximum surface temperature achieved in this investigation of approximately 120°C was observed in a sample exposed to an environment of 22°C air, however, a larger sample set is needed in order to draw strong conclusions regarding the effect of the elevated temperature environment on the thermomechanical behavior of these composite energetic

materials. Future work in this area is intended to achieve this, as well as exacerbate the effect even further by increasing the enclosure temperature upwards of 100°C.

6. HEAT GENERATION OF ENERGETIC MATERIALS UNDER HIGH–FREQUENCY RESONANT EXCITATION

6.1 Introduction

As a complement to the experimental results presented herein, a heat dissipation model was of interest to theoretically validate the observed material behavior. Ideally, the analysis seeks to estimate the volumetric heat generation of a specific energetic material and consequently predict temperature profiles of a material in response to high–frequency resonant excitation. In practice, this presents several challenges as the sample form factor is not conventional and the material behavior is not well predicted in this frequency range.

The energetic material can be modeled as a lumped mass, characterized by an effective mass, stiffness, and damping. Prior work has been performed utilizing this method at low–frequency excitations with surrogate energetic materials by Paripovic [53], wherein the material was modeled as a nonlinear spring, damper, and viscoelastic element during uniaxial compression tests. The elastic behavior was described using the general equation of motion

$$m\ddot{x} + c(\dot{x} - \dot{y}) + k(x - y) + v(\dot{x} - \dot{y}, x - y) = 0, \tag{6.1}$$

assuming harmonic base excitation.

A material is classified as viscoelastic if it simultaneously behaves as an elastic solid and viscous fluid. Paripovic investigated the effect of a hereditary model using a convolution of a relaxation kernel and driving function. The relaxation kernel used was a finite sum of exponential functions, with the number of functions determined by the model order analyzed. The variety of model combinations analyzed provided the ability to predict the response about a specified operating point, and consequently determine stress-strain behavior for the material of interest. Woods utilized a similar modeling approach when describing the behavior of surrogate composite energetic materials at low frequencies, with the addition

of several assumptions [54]. If the analysis is restricted solely to steady-state behavior in response to harmonic loading, stress and strain can be assumed to vary harmonically at the forcing frequency of the system. Incorporating hysteric damping to the model, it follows that the energy dissipated in the material over one loading cycle is estimated by the area enclosed by the hysteresis loop of the stress-strain plot. Assuming that the time scale over which the temperature variation occurs is much slower than the mechanical loading and the energy dissipation is purely output as heat, the time-averaged volumetric heat generation can be determined as follows.

$$r_{avg} = \pi_0(\eta\omega) \tag{6.2}$$

where η is the material loss factor, ω is the frequency of excitation, and π_0 is the strain energy density given by

$$\pi_0 = \frac{E'\epsilon_0^2}{2(1-\nu^2)} \tag{6.3}$$

where E' is the real part of the dynamic modulus, ν is Poisson's ratio, and ϵ_0 is the strain magnitude. Combining the heat generation rate with an appropriate heat transfer equation yields a prediction for the temperature distribution of the composite sample in response to harmonic base excitation. This technique was proven effective at predicting the elastic behavior of the polymer as a homogeneous material at low frequencies (less than 1000 Hz) in which strain rates were much lower. However, it did not account for high–frequency wave propagation and the particle/binder interactions that occurred between the solid crystals and the polymer matrix that have been shown to be significant as the frequency range is increased.

Alternatively, the composite energetic material can also be modeled as a representative volume or random media. The utilization of a representative volume element (RVE) to predict mechanical properties of heterogeneous materials is an established method for various fiber composites. By definition, the RVE must completely capture the composite mixture as a whole and significant research has been performed in an effort to identify the specific RVE size necessary to satisfy this requirement [55, 56]. The approach hinges on the idea that a single array or unit cell of the composite can be characterized at the microscale, statistically

represented as a homogeneous material, and related to the average stresses and strains at the macroscale. Overall, the method is well characterized in the literature for a variety of composite structures. Sun *et al.* explored the mechanical properties of unidirectional fiber–reinforced composites, emphasizing the importance of considering periodicity and symmetry when selecting appropriate boundary conditions that accurately depict the deformed shape of the material [57]. Using a similar approach, Gusev predicted the overall elastic constants of a periodic elastic composite characterized by nonoverlapping identical spheres [58]. Finally, Yeong *et al.* proposed a technique to allow a three–dimensional reconstruction of the microstructure using information obtained from a two-dimensional micrograph or image, applicable to general multiphase and anisotropic media [59]. This method of analysis was considered for the material of interest for this work, however, the variability in the material formulation, complexity of the modeling procedure, and required increase in computational power presented significant drawbacks.

In an attempt to capture the unique qualities of the material described above, including the viscoelastic behavior and frequency–dependent properties, the following sections outline a potential model to characterize the heat dissipation of composite energetic materials in response to high–frequency mechanical excitation.

6.2 Analytical Approach and Discussion

The system of interest is comprised of a particulate composite cylindrical sample of inert or live energetic material. The sample is subjected to longitudinal mechanical vibration at the base via a piezoelectric shaker with a frequency range of 1 to 80 kHz. The thermal behavior in response to sinusoidal excitation has been measured experimentally using infrared thermography, eliciting maximum surface temperatures on the order of 90 to 120°C. The response of the sample in regards to mechanical and thermal behavior will be approximated using the following one-dimensional analysis.

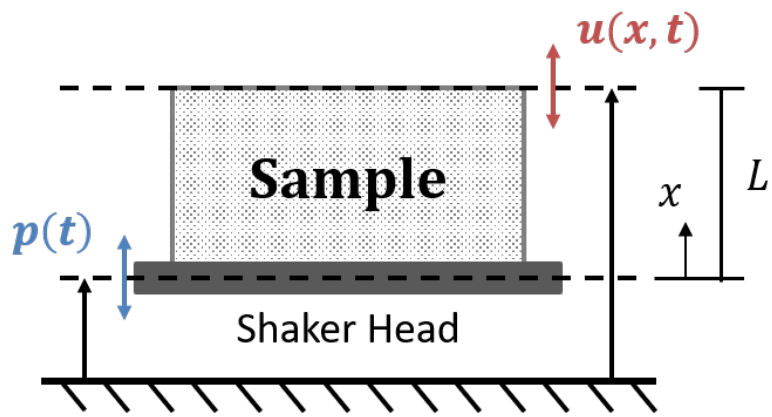

Figure 6.1. : One-dimensional longitudinal vibration of a prismatic bar with harmonic base motion.

6.2.1 Mechanical Response

To approximate the mechanical response of the composite energetic material to harmonic excitation, the sample is assumed to behave as a prismatic bar subjected to base motion, $p(t)$ in the longitudinal direction. A schematic of the system of interest in shown in Figure 6.1. Neglecting displacements in the transverse directions, the longitudinal vibration of the bar is described by the equation of motion [60]

$$\rho A \frac{\partial^2 u(x,t)}{\partial t^2} + c\frac{\partial}{\partial t}\left[u(x,t) - p(t)\right] - EA\frac{\partial^2}{\partial x^2}\left[u(x,t) - p(t)\right] = 0, \tag{6.4}$$

where $u(x,t)$ is the absolute displacement of the bar as illustrated in the schematic in Figure 6.1, $p(t)$ is the harmonic base motion, and ρ, A, c, and E are the material density, cross-sectional area, material damping coefficient, and elastic modulus, respectively. At this point, it is beneficial to define the relative displacement of the bar as

$$v(x,t) = u(x,t) - p(t). \tag{6.5}$$

Differentiating Eq. 6.5 gives

$$\frac{\partial u(x,t)}{\partial t} = \frac{\partial v(x,t)}{\partial t} + \frac{\partial p(t)}{\partial t} \tag{6.6}$$

$$\frac{\partial^2 u(x,t)}{\partial t^2} = \frac{\partial^2 v(x,t)}{\partial t^2} + \frac{\partial^2 p(t)}{\partial t^2} \tag{6.7}$$

$$\frac{\partial^2 u(x,t)}{\partial x^2} = \frac{\partial^2 v(x,t)}{\partial x^2} \tag{6.8}$$

Substituting the derivatives into Eq. 6.4 and dividing through by ρA results in the following equation of motion governing the longitudinal vibration of the bar relative to the base motion:

$$\frac{\partial^2 v}{\partial t^2} + \frac{c}{\rho A}\frac{\partial v}{\partial t} - s^2\frac{\partial^2 v}{\partial x^2} = -\frac{\partial^2 p}{\partial t^2}, \tag{6.9}$$

where c is the damping coefficient of the material and s is the material wave speed defined as

$$c = \alpha M + \beta K, \tag{6.10}$$

$$s = \sqrt{\frac{E}{\rho}}. \tag{6.11}$$

The damping coefficient used in this analysis, given in Eq. 6.10, represents Rayleigh or proportional damping in which α and β represent the mass (M) and stiffness (K) proportional damping coefficients, respectively. The coefficients can be combined to determine a damping ratio over a range of frequencies for implementation into a modal analysis as

$$\zeta = \frac{1}{2}\left(\frac{\alpha}{2\pi f} + \beta 2\pi f\right) \tag{6.12}$$

where the frequency f is measured in Hz. To determine α and β, two prescribed damping ratios, ζ_1 and ζ_2, at corresponding frequencies, f_1 and f_2, are identified to span the frequency range of interest. In this case, the initial set of values is chosen based upon the results for the PBXN-109 plate samples described in Chapter 2 with a loss factor of 0.58 at a frequency of 50 Hz for plates of 85% solids loading with 30% aluminum additive content. The loss factor characteristic of viscoelastic materials is commonly estimated as twice the damping

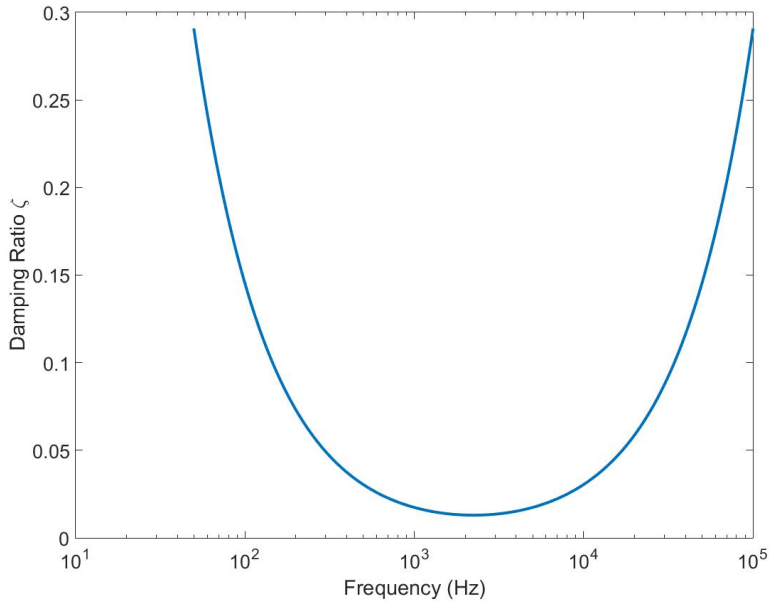

Figure 6.2. : Equivalent damping ratio as a function of frequency with $\zeta_1 = \zeta_2 = 0.29$, $f_1 = 50$ Hz, and $f_2 = 100,000$ Hz.

ratio, therefore, ζ_1 is defined as 0.29 at $f_1 = 50$ Hz. The second set of values is chosen such that the response is not overdamped across the frequency range of interest. For reference, a sample damping curve is shown in Figure 6.2. The effect of these parameters on the response will be explored later. The proportional damping coefficients are then calculated using the equations:

$$\alpha = 4\pi f_1 f_2 \frac{\zeta_1 f_2 - \zeta_2 f_1}{f_2^2 - f_1^2}, \tag{6.13}$$

$$\beta = \frac{\zeta_2 f_2 - \zeta_1 f_1}{\pi \left(f_2^2 - f_1^2\right)}. \tag{6.14}$$

Using the separation of variables method, the solution form of Eq. 6.9 is assumed to be

$$v(x,t) = \sum_{n=1}^{m} U_n(x) T_n(t), \tag{6.15}$$

where m is the total number of modes used to capture the desired frequency range of interest, $U_n(x)$ is the normal mode shape corresponding to the natural frequency ω_n, and $T_n(t)$

indicates the response of the bar with respect to time. Substitution of Eq. 6.15 into Eq. 6.9 yields

$$\sum_{n=1}^{m} U_n(x)\ddot{T}_n(t) + \frac{c}{\rho A}\sum_{n=1}^{m} U_n(x)\dot{T}_n(t) - s^2\sum_{n=1}^{m} U_n''(x)T_n(t) = -\frac{\partial^2 p}{\partial t^2}, \tag{6.16}$$

where $(\dot{\ })$ denotes a derivative with respect to time and $(\ )'$ denotes a derivative with respect to position. For a fixed-free bar, the normal mode shape functions $U_n(x)$ and corresponding natural frequencies ω_n are given by [60]

$$U_n(x) = C_n \sin\frac{(2n+1)\,\pi x}{2L}, \tag{6.17}$$

$$\omega_n = \frac{(2n+1)\,\pi s}{2L}, \quad n = 0, 1, 2, ... \tag{6.18}$$

Utilizing the relation $U_n''(x) = -\frac{\omega_n^2}{s^2}U_n(x)$, Eq. 6.16 can be simplified to yield

$$\sum_{n=1}^{m} U_n(x)\ddot{T}_n(t) + \frac{c}{\rho A}\sum_{n=1}^{m} U_n(x)\dot{T}_n(t) + \omega_n^2\sum_{n=1}^{m} U_n(x)T_n(t) = -\frac{\partial^2 p}{\partial t^2}. \tag{6.19}$$

Multiplying Eq. 6.19 by an arbitrary mode shape $U_p(x)$ and integrating over the length of the bar results in the following equation:

$$\sum_{n=1}^{m} \ddot{T}_n(t)\int_0^L U_n(x)U_p(x)dx + \frac{c}{\rho A}\sum_{n=1}^{m} \dot{T}_n(t)\int_0^L U_n(x)U_p(x)dx$$
$$+\,\omega_n^2\sum_{n=1}^{m} T_n(t)\int_0^L U_n(x)U_p(x)dx = -\int_0^L \frac{\partial^2 p}{\partial t^2}U_p(x)dx. \tag{6.20}$$

Provided the mode shapes are normalized using the condition

$$\int_0^L U_n^2(x) = 1, \tag{6.21}$$

the equation of motion can be simplified significantly. Due to the orthogonality of the mode shapes, the three integrals on the left-hand side of the equation are nonzero only at $n = p$, at which the integral is equal to 1. Therefore, the equation above simplifies to

$$\ddot{T}_n(t) + 2\zeta_n\omega_n\dot{T}_n(t) + \omega_n^2 T_n(t) = -\int_0^L \frac{\partial^2 p}{\partial t^2} U_n(x)dx \tag{6.22}$$

One can define the modal participation factor, γ_n, as

$$\gamma_n = \int_0^L U_n(x)dx. \tag{6.23}$$

This provides a measure of the strength with which each mode contributes to the overall response of the bar in the longitudinal direction. Taking the Fourier Transform of both sides of Eq. 6.22 yields

$$\int_{-\infty}^{\infty} \ddot{T}_n(t)e^{j\omega t}dt + 2\zeta_n\omega_n \int_{-\infty}^{\infty} \dot{T}_n(t)e^{j\omega t}dt + \omega_n^2 \int_{-\infty}^{\infty} T_n(t)e^{j\omega t}dt = -\gamma_n \int_{-\infty}^{\infty} \ddot{p}(t)e^{j\omega t}dt. \tag{6.24}$$

Using the definition of the Fourier Tranform, the following can be stated:

$$\int_{-\infty}^{\infty} \ddot{T}_n(t)e^{j\omega t}dt = -\omega^2 \int_{-\infty}^{\infty} T_n(t)e^{j\omega t}dt, \tag{6.25}$$

$$\int_{-\infty}^{\infty} \dot{T}_n(t)e^{j\omega t}dt = j\omega \int_{-\infty}^{\infty} T_n(t)e^{j\omega t}dt. \tag{6.26}$$

In addition, let the following Fourier Transforms be defined as

$$\hat{T}_n(\omega) = \int_{-\infty}^{\infty} T_n(t)e^{j\omega t}dt, \tag{6.27}$$

$$\ddot{P}(\omega) = \int_{-\infty}^{\infty} \ddot{p}(t)e^{j\omega t}dt, \tag{6.28}$$

$$P(\omega) = \int_{-\infty}^{\infty} p(t)e^{j\omega t}dt, \tag{6.29}$$

where $\ddot{P}(\omega)$ is the Fourier Transform of the base acceleration and $P(\omega)$ is the Fourier Transform of the base displacement. The magnitude of each of these is determined by scanning the

velocity in time at the baseplate (with a sample attached) using laser Doppler vibrometry, and performing the necessary signal processing to obtain displacement and acceleration in terms of frequency. Substituting the above definitions into Eq. 6.24 provides the following equations for the Fourier Transform of the relative and absolute displacement of the sample at position x and forcing frequency ω in rad/s.

$$\hat{T}_n(\omega) = \frac{\gamma_n \ddot{P}(\omega)}{(\omega_n^2 - \omega^2) + j2\zeta_n\omega_n\omega} \tag{6.30}$$

$$V(x,\omega) = \sum_{n=1}^{m} U_n(x)\hat{T}_n(\omega) \tag{6.31}$$

$$U(x,\omega) = V(x,\omega) + P(\omega) \tag{6.32}$$

In addition to the length of the rod, the system described above requires two material properties as input values: (1) the elastic modulus E, estimated as 135 MPa by Paripovic for inert PBXN-109 with 85% solids loading and 30% aluminum additive content [53], and (2) density, taken as the average of the inert 85-30 samples described in Chapter 3. Using these values, the first two natural frequencies of the sample are found to be 6449 Hz and 19346 Hz from Eq. 6.18. In prior work, the frequency range from 1 to 20 kHz exhibited the greatest heat generation within the sample, therefore, these peaks are of primary interest. The remaining parameters of the system include the number of modes m, damping coefficient ζ_2, and corresponding frequency f_2 at the upper end of the frequency range. Table 6.1 was constructed to determine how each of these parameters affects the frequency and amplitude of the first two resonances of interest.

The top rows of Table 6.1 monitor the first and second resonance as the number of modes m is decreased from 100 to 20. Utilizing fewer modes in the overall summation for the displacement decreases the computation time, thus providing a more efficient analysis. The frequency and amplitude at each resonance remains the same for 100 and 20 modes, thus the summation of 20 modes appears sufficient for analysis within the frequency range of interest up to 20 kHz. The middle rows of Table 6.1 determine the effect of increasing the upper frequency limit of the damping ratio, defined as f_2. As f_2 increases from 100,000 Hz

Table 6.1. : Parameter variation for longitudinal vibration analysis

Number of Modes	ζ_1	f_1	ζ_2	f_2	1st Resonance		2nd Resonance	
m		(Hz)		(Hz)	$f_{m=1}$ (Hz)	$\lvert U(L,f)\rvert$ (μm)	$f_{m=2}$ (Hz)	$\lvert U(L,f)\rvert$ (μm)
100	0.29	50	0.29	100,000	6445	702	19518	9.75
60	0.29	50	0.29	100,000	6445	702	19518	9.75
30	0.29	50	0.29	100,000	6445	702	19518	9.75
20	0.29	50	0.29	100,000	6445	702	19518	9.75
20	0.29	50	0.29	200,000	6447	1270	19385	19.0
20	0.29	50	0.29	300,000	6448	1730	19363	28.1
20	0.29	50	0.29	400,000	6448	2120	19356	36.9
20	0.29	50	0.29	500,000	6448	2460	19352	45.5
20	0.29	50	0.20	100,000	6447	972	19422	13.9
20	0.29	50	0.15	100,000	6447	1230	19388	18.4
20	0.29	50	0.10	100,000	6448	1690	19364	27.2
20	0.29	50	0.05	100,000	6448	2690	19351	52.4

to 500,000 Hz, the displacement amplitude at $x = L$ appears to increase for each resonance while the frequency at which it occurs remains relatively constant. This suggests a decrease in damping provided at these frequencies. The bottom rows of Table 6.1 observe the effect of varying the damping ratio defined at the upper frequency limit, defined as ζ_2. In this case, the displacement amplitude at $x = L$ increases at both the first and second resonant frequencies as ζ_2 decreases. The second resonant frequency does exhibit minor change due to the variation in ζ_2 with an overall decrease of almost 100 Hz.

6.2.2 Thermal Response

For comparison to the experimental data, the mechanical response determined above can be used to estimate the mechanical energy generation within the sample and predict the axial temperature distribution over time. The stress and strain at any position x in the sample can be determined in the frequency domain using the following equations

$$\epsilon(x, \omega) = \frac{\partial}{\partial x} \left[V(x, \omega) \right], \tag{6.33}$$

$$\sigma(x, \omega) = E^* \epsilon(x, \omega), \tag{6.34}$$

where E^* represents the complex modulus of elasticity determined using the loss factor of the material and ω is the forcing frequency of the system in rad/s. The complex nature of the modulus results in the phase lag between stress and strain that is characteristic of viscoelastic materials when subjected to harmonic motion. To couple the thermal and mechanical behavior of this composite material under sinusoidal base excitation, the energy balance of the system must first be determined. According to the First Law of Thermodynamics, the energy-balance for a continuous solid of unit volume is defined as

$$W = Q + \Delta U, \tag{6.35}$$

in which W refers to the external mechanical energy, Q refers to the heat transfer with the surroundings, and ΔU is the internal energy variation of the system. As observed in the experimental data of the previous chapter, the cyclic deformation process typically

results in transient temperature profiles characterized by a rapid temperature increase in the first several minutes, followed by a relatively stable region of constant temperature [61, 62]. During the initial linear phase of temperature increase, the process can be assumed to be adiabatic due to the significant contribution of the internal energy of the system [39]. As part of a hybrid method for determining the fraction of plastic work that is converted to heat in annealed 302 stainless steel, Zehnder *et al.* investigated the constraints on the adiabatic assumption and concluded that a Fourier number less than or equal to 0.1 is acceptable for assuming an adiabatic deformation process [63]. The Fourier number is determined by

$$F_o = \frac{\alpha t}{L^2}, \tag{6.36}$$

where α is the thermal diffusivity of the material, t is the time scale of the experiment, and L is the length of the sample. For the material and geometric values of this work, the analytical temperature profile will be produced for a time scale of 60 s. This should capture the initial rapid temperature increase exhibited in the experimental data while still maintaining consistency with the adiabatic assumption.

Under this assumption, the heat transfer term Q in Eq. 6.35 drops out and the energy-balance for the system simplifies to

$$\dot{W} = \rho c \dot{\theta} + \dot{E}, \tag{6.37}$$

in which $\dot{W}$ is defined as the rate of mechanical energy, ρ and c are the density and specific heat of the material, respectively, $\dot{\theta}$ is the rate of change of temperature with respect to time, and $\dot{E}$ is the rate of stored energy within the material. At this point, it is common to introduce a parameter β that defines the fraction of mechanical energy dissipated as heat [38, 39, 63]; thus, $1 - \beta$ defines the fraction of mechanical energy that is stored within the material. Mathematically, this relationship is described as

$$\beta \dot{W} = \rho c \dot{\theta}. \tag{6.38}$$

The rate of mechanical energy due to material deformation $\dot{W}$ can be determined from its definition:

$$\dot{W} = \sigma\dot{\epsilon}, \tag{6.39}$$

where σ is the stress determined from the predicted strain of the sample in Eq. 6.34, and $\dot{\epsilon}$ is the strain rate determined as the time derivative with respect to t of the strain found from Eq. 6.33. In a physical sense, the $\dot{W}$ term is defined as the time rate of change of the area inside the stress-strain hystersis loop of the material undergoing cyclic deformation.

As mentioned previously, the mechanical response described in the previous section identified the first two natural frequencies of the sample in response to longitudinal vibration as 6449 Hz and 19346 Hz. Consequently, the displacement plot of the sample in the frequency domain exhibits two main resonances at the damped natural frequencies. It is at forcing frequencies near these the two resonances that the largest magnitude of heat generation would be expected, thus the thermal analysis will focus largely on forcing frequencies in that range. The complex magnitude of stress and strain at the first resonance (approximately 6445 Hz) as determined from Eqs. 6.34 and 6.33, respectively, is shown in Figure 6.3. As expected, the strain lags the stress by a finite phase angle, characteristic to the cyclic deformation of viscoelastic materials. Using these values, the rate of mechanical energy generation per unit length can be calculated from Eq. 6.39 for a frequency range of 5 to 8 kHz as shown in Figure 6.4. The axial profile of the mechanical energy generation exhibits significant local maxima near the base of the sample ($x \approx 0.001$ m) and just above the vertical center ($x \approx \frac{2L}{3}$ m), and resembles that of the axial stress and strain, as expected.

For comparison, similar plots for the complex magnitude of stress and strain at the second resonance (approximately 19518 Hz) are shown in Figure 6.5. Note that the magnitude is significantly decreased at this resonance, as expected due to the drastic difference in peak amplitude exhibited in the displacement frequency response. In addition, the mechanical energy generation per unit length is plotted in Figure 6.6 at a range of forcing frequencies from 18 to 21 kHz. The maximum amplitude of the mechanical energy generation at this resonance is approximately 5.5 W/m, as compared to the 9000 W/m predicted at the first resonance of the sample. This is consistent with the expectations as the fundamental mode of vibration is typically characterized by the largest contribution to the overall response.

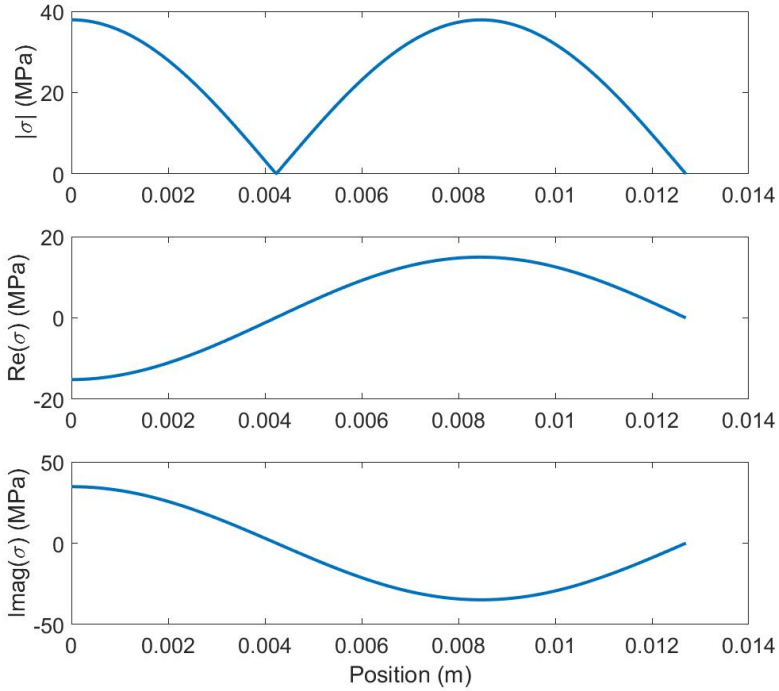

(a)

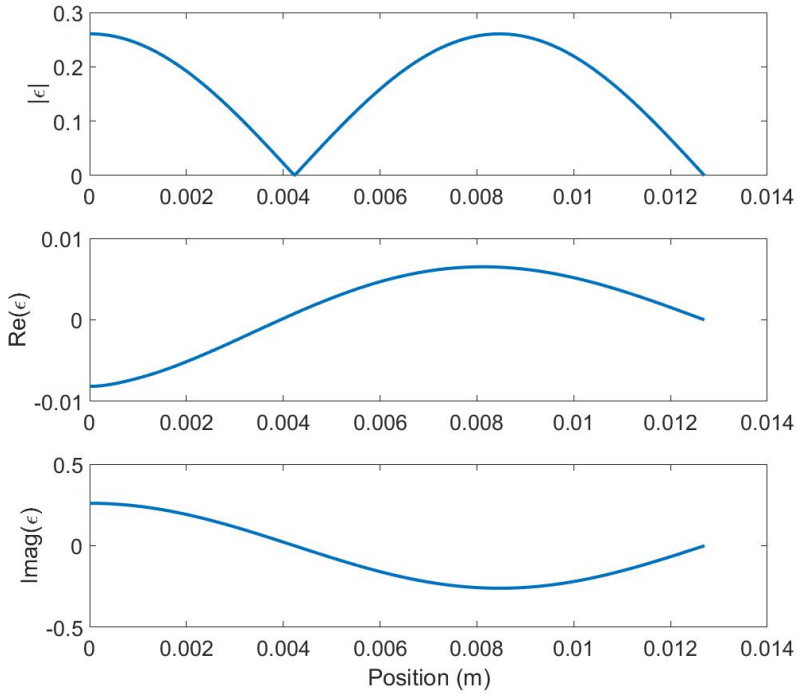

(b)

Figure 6.3. : Analytical (a) stress and (b) strain in the frequency domain as a function of axial position along the length of the cylinder for a resonant forcing frequency of 6445 Hz.

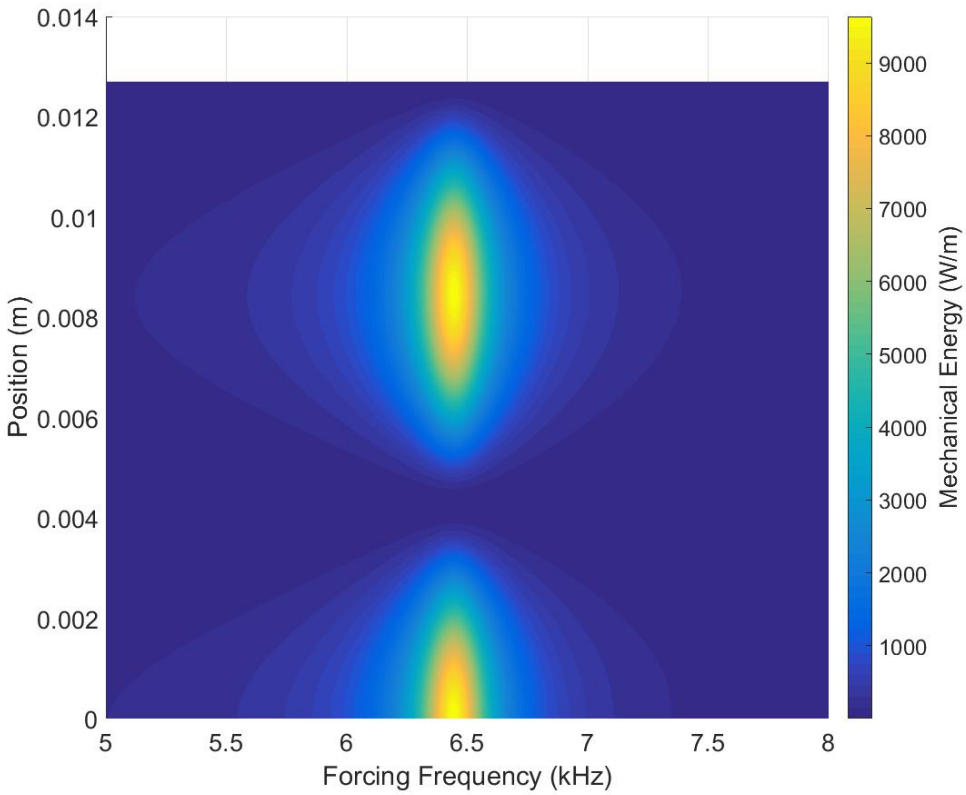

Figure 6.4. : Rate of mechanical energy generation per unit length as a function of axial position along the length of the cylinder and forcing frequency from 5 to 8 kHz.

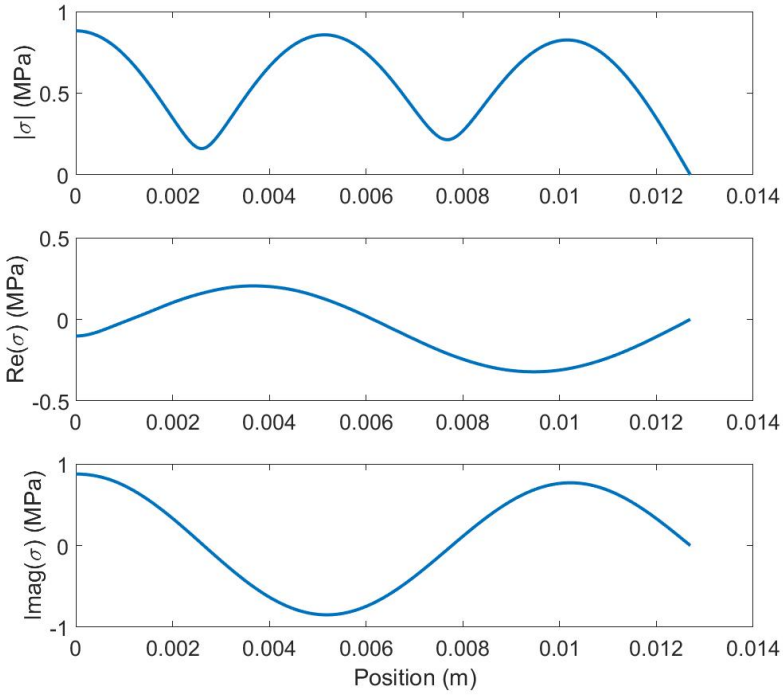

(a)

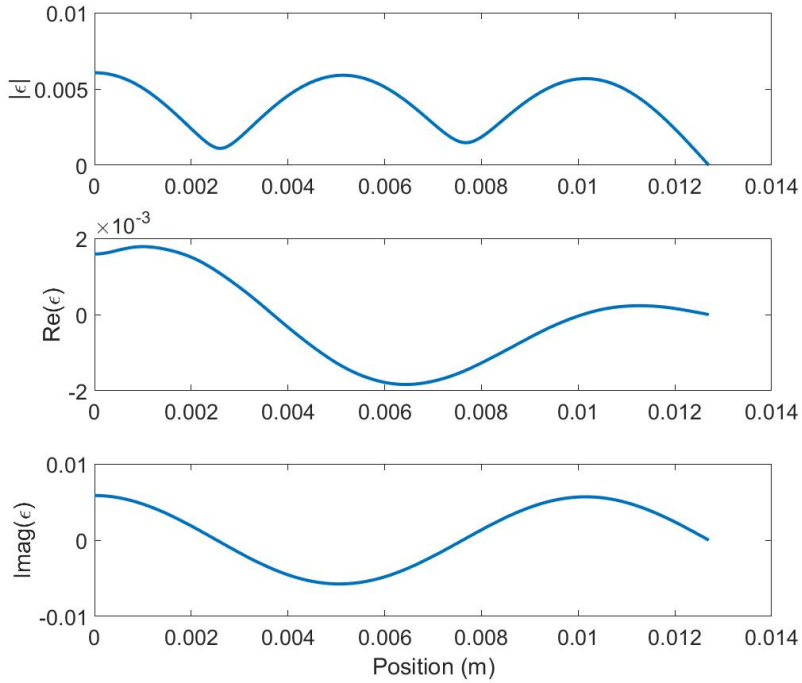

(b)

Figure 6.5. : Analytical (a) stress and (b) strain in the frequency domain as a function of axial position along the length of the cylinder for a resonant forcing frequency of 19518 Hz.

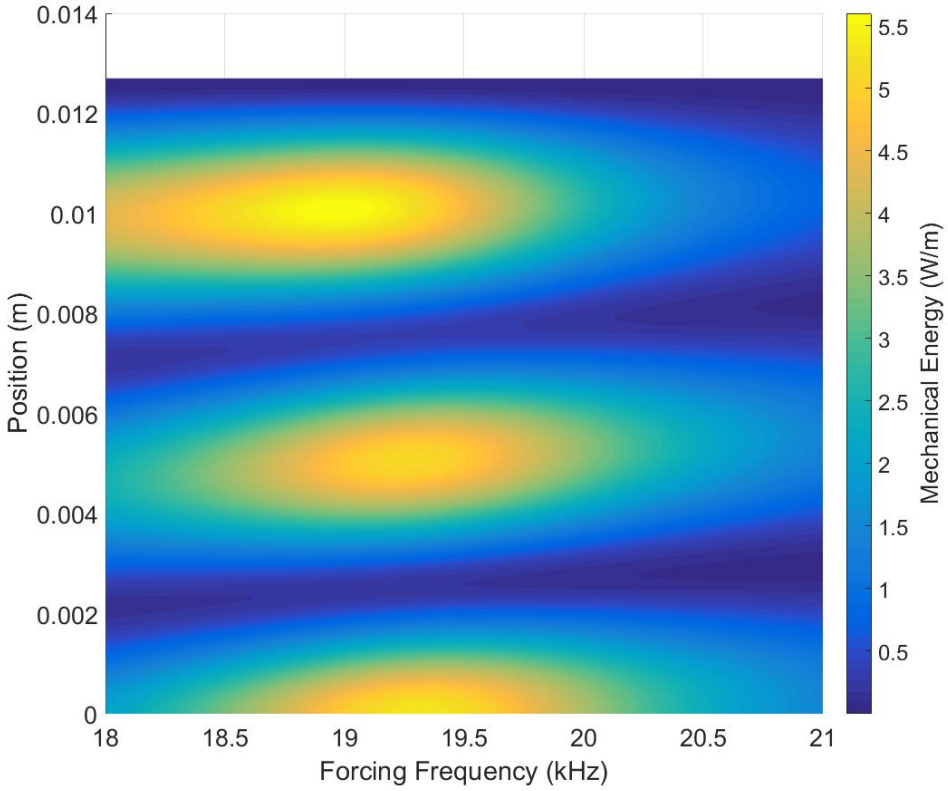

Figure 6.6. : Rate of mechanical energy generation per unit length as a function of axial position along the length of the cylinder and forcing frequency from 18 to 21 kHz.

To facilitate a direct comparison to the experimental temperature results, the rate of mechanical energy generation per unit length can be used in conjunction with a heat transfer model to predict a temperature profile as a function of axial position x and time t. As before, the system will be analyzed along the length of the cylinder assuming no heat transfer in the transverse direction; thus the one-dimensional heat transfer equation is defined as

$$\frac{\partial \theta}{\partial t} = \alpha \frac{\partial^2 \theta}{\partial x^2} + \frac{q}{\rho c}, \tag{6.40}$$

in which θ represents temperature, α is the thermal diffusivity of the sample, ρ is the density of the sample, c is the specific heat, and q is the rate of heat dissipation or generation in Watts per unit volume. The energy generation q in Eq. 6.40 must account for the various sources of heat generation or dissipation in the physical system. In this case, the analysis will consider the following:

- heat generation in the material due to mechanical deformation,
- heat dissipation to the surroundings due to convection, and
- heat dissipation to the surroundings due to radiation.

The combination of these heat mechanisms result in an energy generation in units of W/m^3 equal to

$$q = \frac{\beta}{A}\dot{W} - \frac{P}{A}\left[h(\theta - \theta_\infty) + \hat{\sigma}\hat{\epsilon}(\theta^4 - \theta_\infty^4)\right], \tag{6.41}$$

where β provides the fraction of mechanical energy converted to heat as defined in Eq. 6.38, $\dot{W}$ represents the rate of mechanical energy generation due to deformation as predicted above, P and A are the perimeter and cross-sectional area of the sample, h is the coefficient of convection in W/(m^2-K), θ_∞ is the ambient temperature of the surroundings in Kelvin, $\hat{\sigma}$ is the Stefan-Boltzmann constant equal to 5.67×10^{-8} W/(m^2-K^4), and $\hat{\epsilon}$ is the emissivity of the sample surface. The coefficient of convection in this system was estimated using an empirical expression for a vertical flat plate exposed to air at room temperature. For simplicity, the temperature profile at the first and second resonance will be determined using numerical integration; however, note that this analysis may be carried out at any

forcing frequency of interest. The axial position and time variables can be discretized into N and B finite subintervals, respectively, as

$$x_n = n\Delta x, \quad n = 0, 1, 2..., \ N, \tag{6.42}$$

$$t_i = i\Delta t, \quad i = 0, 1, 2..., \ B, \tag{6.43}$$

in which the length of the rod $L = N\Delta x$, and the time interval $T = B\Delta t$. The size of the subintervals for each variable can be determined by choosing an initial estimate for N and B and increasing by integer values until the solution to the heat equation does not change. Using this process, the axial position subinterval Δx was chosen as 0.1 mm and the time subinterval Δt was chosen as 0.6 ms. A forward difference approximation for the first-order derivatives and a central difference approximation for the second-order derivatives evaluated at i and n, respectively, provides

$$\frac{\partial \theta}{\partial t} = \frac{\theta_n^{i+1} - \theta_n^i}{\Delta t}, \tag{6.44}$$

$$\frac{\partial^2 \theta}{\partial x^2} = \frac{\theta_{n+1}^i - 2\theta_n^i + \theta_{n-1}^i}{(\Delta x)^2}. \tag{6.45}$$

Substituting the difference approximations into Eq. 6.40 results in the following discretization for the heat equation:

$$\theta_n^{i+1} = \alpha \Delta t \left[\frac{\theta_{n+1}^i - 2\theta_n^i + \theta_{n-1}^i}{(\Delta x)^2} \right] + \frac{q}{\rho c} \Delta t + \theta_n^i. \tag{6.46}$$

The one–dimensional transient heat equation of interest is first-order with respect to time and second-order with respect to position; thus, a single initial condition and two boundary conditions are needed to provide a solution. For simplicity, the initial condition can be prescribed as a simple sinusoidal distribution equal to

$$\theta(x, 0) = \sin \pi x. \tag{6.47}$$

At the endpoints of the rod, boundary conditions are chosen to approximate the physical system. The base of the sample ($x = 0$) is rigidly fixed to the aluminum baseplate which

maintains a constant ambient temperature for the time interval of interest, thus the temperature profile is constrained to a constant surface temperature of 23°C or 296.15 K. The boundary condition at the end of the sample ($x = L$) is specified to be adiabatic to align with the mechanical energy assumptions discussed previously. In equation form, the boundary conditions are expressed as follows:

$$\theta(0, t) = 296.15 \text{ K}, \tag{6.48}$$

$$-k\frac{\partial\theta(L, t)}{\partial x} = 0. \tag{6.49}$$

Finally, the material properties necessary to provide a solution to the one-dimensional heat transfer equation are summarized in Table 6.2. The results presented herein utilize the properties for inert PBXN-109 with 85% solids loading and 30% additive content. Transient thermal properties for diffusivity and conductivity for the inert formulation of 85% solids and 30% aluminum were determined using the transient plane source technique [46]. The specific heat was estimated using values published in literature for hydroxyl-terminated polybutadiene (HTPB) composite propellants [64, 65]. The density was calculated as the average measured density of the inert cylindrical samples comprised of 85% solids loading and 30% aluminum described in Chapter 3, and the emissivity of the sample was calibrated during the experiments by determining the reflected apparent temperature of a perfect emitter and then calibrating the sample temperature to that of a known emissivity.

The axial temperature profile of the sample in response to 60 s of numerically-simulated sinusoidal excitation at the first resonance of 6445 Hz is shown in Figure 6.7. Recall from Eq. 6.38, β was defined as the fraction of the mechanical energy dissipated as heat with the remainder of the energy termed as stored energy in the material; therefore, a β value of 1.0 indicates that 100% of the mechanical energy was dissipated as heat. There is significant difficulty in measuring the value of β experimentally as it is a material property that is both strain and strain-rate dependent; however, numerous methods have been proposed in literature primarily for metals and a few polymer composite materials [36,39]. To observe the effect of β on the overall thermal response, the axial temperature profile has been plotted at five values of β from 1.0 to 0.6 in Figure 6.7. Comparison of these values with the

Table 6.2. : Thermophysical properties for inert PBXN-109 formulation with 85% solids loading and 30% aluminum additive content

Material Property	Value
Thermal Diffusivity, α	0.348 m^2/s
Thermal Conductivity, k	0.652 W/(m-K)
Specific Heat, c	1500 J/(kg-K)
Density, ρ	1258 kg/m^3
Emissivity, $\hat{\epsilon}$	0.97

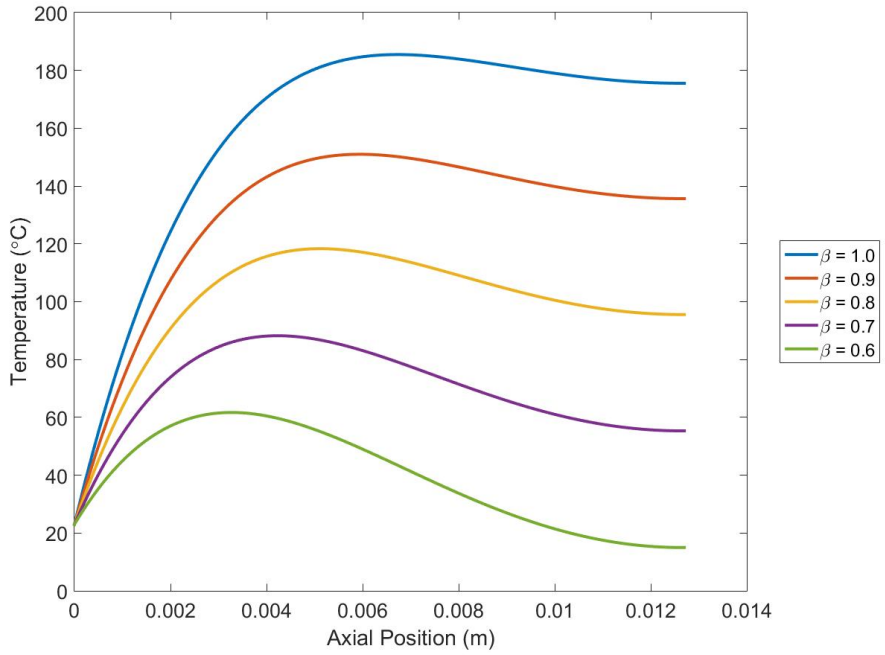

Figure 6.7. : Numerically obtained transient temperature profile as a function of axial position in the cylinder after 60 s of sinusoidal excitation at the first resonant frequency of 6445 Hz.

maximum surface temperature measured experimentally allows conjecture as to the fraction of mechanical energy converted to heat in the experimental data, potentially on the order of 0.7-0.9. Also of note, the shape of the temperature profile correlates well with that exhibited in the experiments, with the largest temperature increase occurring near the vertical center of the sample as viewed from the side of the cylinder.

For comparison, a similar solution of temperature versus axial position in the sample in response to 60 s of numerically-simulated sinusoidal excitation at the second resonance of 19518 Hz was determined; however, the resulting temperature values were deemed unrealistic. Note that the rate of mechanical energy $\dot{W}$ for the second resonance is significantly smaller than that for the first resonance, thus the response is dominated by the losses to the environment. As such, the effect of β in this case is negligible on the temperature profile, and the adiabatic assumption described previously is no longer applicable. The temperature behavior determined for this resonance was not accurate as the physical system is most likely

not consistent with the assumptions made for the solution of the heat equation. In the experimental data, a similar trend was observed in that the first resonance analyzed in the 1-20 kHz frequency range consistently produced the greatest temperature increase in the sample on the order of 100°C with the subsequent resonances resulting in temperature variations on the order of 10°C. Furthermore, the higher resonances did not tend to exhibit the rapid temperature increase within the first several minutes; thus, the adiabatic assumption for this temperature solution most likely does not hold as true as in the case of the first resonance.

The analytical thermal response of this material to harmonic base excitation provides sufficient correlation at the predicted first resonance of the sample to experimental analysis in the lowest frequency subrange of 1-20 kHz. Although it is not an all-encompassing model, the proposed theory can serve as an approximation for the heat generation and transient temperature profile for particulate composite inert and fully-loaded energetic materials.

6.3 Conclusions

To supplement the experimental results presented in previous chapters, the mechanical and thermal response of particulate composite energetic cylinders under contact harmonic excitation was analytically determined at a range of frequencies up to 20 kHz. The cylinder was modeled as a one-dimensional rod subjected to axial base excitation, allowing the determination of the longitudinal displacement as a function of axial position and forcing frequency. Rayleigh damping was incorporated to model the damping behavior of the material with proportional coefficients as a function of frequency. The predicted first and second resonance of the sample fell within the 1-20 kHz frequency range of interest as the forcing frequencies in this range resulted in the greatest magnitude of temperature increase in experimental data.

Using the longitudinal displacement to calculate stress, strain, and strain rate, the rate of mechanical energy expended per unit length of the material was estimated at two forcing frequencies equal to the first and second resonance of the sample. The first resonance resulted in mechanical energy rates on the order of 9000 W/m, while the rate at the second resonance provided rates closer to 6 W/m. These values correspond to the trends observed

experimentally in that the first resonance in the range of 1-20 kHz produced temperature increases on the order of 100°C with subsequent temperature variations at higher frequencies on the order of 10°C. In addition, a parameter β was defined under adiabatic conditions to estimate the fraction of the mechanical energy converted to heat generation, with the remainder of the energy classified as energy stored within the material. This value is difficult to measure experimentally due to its strong dependence on material properties, strain, and strain rate.

The thermal response of the sample to harmonic excitation was numerically estimated with a one-dimensional heat transfer equation with energy generation. From experimental data, the transient temperature profiles were observed to exhibit a trend of a drastic temperature increase in the first several minutes of deformation, followed by a relatively isothermal stabilization stage. As proposed in literature, the initial rapid temperature increase characteristic of cyclic mechanical deformation was regarded as adiabatic for short time intervals. Under these assumptions, the axial temperature profile of the cylinder after 60 s of harmonic excitation was simulated at each of the first two predicted resonant frequencies of the sample. The energy generation term accounted for heat generation within the material, heat dissipation to the environment due to convection, and heat dissipation to the environment due to radiation. The numerically obtained axial temperature profile provided a maximum temperature of approximately 180°C near the vertical center of the cylinder under the assumption that all of the mechanical energy was dissipated as heat ($\beta = 1$). Maximum temperature values predicted at β equal to 0.7 and 0.8 ranged from 80°C to 120°C, suggesting this may be an estimate for the fraction of mechanical energy that was dissipated as heat in the experimental analysis. In contrast, the axial temperature profile obtained in response to harmonic excitation at the second resonant frequency produced unrealistic temperature values, most likely due to the significantly lower heat generation estimate and the loss of adiabatic conditions in the heat transfer analysis.

Overall, the model presented herein provided an analytical estimate of the heat generation and transient temperature profile for particulate composite energetic cylinders, and displayed thermal and mechanical behavior consistent with experimental data at the predicted first resonant frequency.

7. CONCLUSIONS AND FUTURE RECOMMENDATIONS

7.1 Summary and Conclusions

The research methods described in this document utilized contact harmonic excitation at a broad range of frequencies in an effort to characterize the thermal behavior of particulate composite polymer-bonded energetic materials. A thorough understanding of the thermo-mechanical response and heat generation mechanisms of energetic materials is crucial when designing, fabricating, and handling munitions systems that must safely withstand a variety of environmental conditions. To this end, the unique contributions of the present work are summarized below.

7.1.1 Low–Frequency Excitation

At frequencies below 1000 Hz, the bulk composite samples exhibited behavior consistent with classic mechanics and vibrations theory. An insulated boundary condition, as is often present in a real-world scenario, provided greater temperature increases within the sample, and a simple viscoelastic damping model provided approximate upper bounds for the temperature increase that coincided well with experimental results. An increased amplitude of excitation caused a relatively linear increase in temperature rise observed over one hour, with no temperature increase exceeding 5°C/hr. However, the material itself began to break down due to cracks and imperfections as the acceleration increased beyond approximately 5 g, presenting challenges as this may contribute to unpredicted behavior or de-bonding from structural housings in the field. Finally, samples characterized by the addition of intentional stress concentrations, such as cracks, holes, and geometric alterations, appeared to behave similarly to the bulk pristine composite in regard to frequency response and operational deflection shape near the experimentally-observed first resonant frequency. Local heat generation surrounding each stress concentration may result in increased temperatures and

potential propagation of defects, such as cracks, in this frequency range due to long duration excitations.

7.1.2 High–Frequency Excitation

Heat generation rates increased significantly as the frequency of excitation exceeded 1000 Hz. A designed experiment aimed at quantifying the temperature increase achievable in a frequency range of 1 to 80 kHz for a variety of mock energetic sample formulations and geometries was presented in Chapter 3. The size of the sample did not appear to provide a major indicator of the potential heat generation, while formulation variation with respect to aluminum additive content resulted in approximate trends as samples of pure mock crystals generally exhibited greater temperature increases. The extension of this high frequency study to the fully-loaded energetic composite was described in Chapter 4, as an experimental method to account for the resonant frequency shift associated with large temperature changes in the material was introduced. As expected, the cylindrical samples of PBXN-109 – an energetic material formulation comprised of HTPB, RDX crystals, and aluminum powder – exhibited temperature rises on the order of 3-4°C/min. By utilizing a slowly swept sinusoidal excitation, the maximum temperature achieved increased significantly, with a maximum observed surface temperature of 122°C. The drastic temperature rise was accompanied by a melted resin protruding from the side of the sample – likely a combination of HTPB binder and/or epoxy. From this study, it was suggested that particle / binder interactions within this particular formulation provide the more dominant source of heat generation in this frequency range, as opposed to the viscous heating characteristic of the lower frequency studies. This interaction is largely under-characterized and not well understood for energetic materials as of yet, but the temperature data gathered herein provides significant advancement towards the thermal characterization of particulate composite energetic materials required to safely, design, handle, and transport munitions systems. The design, fabrication, and functional verification of a custom enclosure to analyze the mechanical and thermal response of inert and fully loaded energetic materials under elevated environmental air temperatures up to 65°C was presented in Chapter 5. In preliminary experiments, a small sample set of inert

PBXN-109 cylinders were analyzed within the enclosure at temperatures of 22°C and 60°C. A maximum surface temperature of 120°C was observed in a sample exposed to air at 22°C. However, a larger sample set is required to draw strong conclusions regarding the effect of the elevated temperature environment on the thermomechanical behavior of these composite energetic materials. A method of analytically determining the heat dissipation evident in the experimental results for comparison to the observed material behavior was described in Chapter 6. The cylindrical sample was modeled as a one-dimensional rod subjected to harmonic base excitation, and the resulting mechanical response was used to estimate the rate of mechanical energy expended per unit length at the predicted resonant frequencies. The thermal response was numerically integrated using a one-dimensional heat transfer equation accounting for energy generation in the form of internal heat generation, and convective/radiative losses to the surrounding environment. Axial temperature profiles predicted at the first resonant frequency provided maximum temperatures at the vertical center of the cylinder on the order of 120°C, consistent with experimental results.

7.2 Future Work

The conclusions presented above for the overall contributions of this work describe distinct thermal and mechanical behavior in two frequency regimes. Contact excitation in the low–frequency regime results in heating rates on the order of 2-4°C/hr, as compared to the high frequency regime in which heating rates exceeded 3-4°C/min. Although the high–frequency regime proved to elicit greater response in regard to heating rate, there is future work in each distinct range that would aid in the further characterization of these particulate composite energetic materials with regard to their thermal and mechanical response. A few recommendations for work in the future are listed below.

7.2.1 Low–Frequency Regime

- *Material Aging*: As is common with polymer materials, particulate composite energetic materials exhibit significant aging effects over time as the material stiffness increases, thus altering the mechanical behavior. In real-world applications, munition systems

can be kept in service for years, therefore, the behavior over time must be accounted for.

- *Induced Damage*: It is well known that thermal cycling due to vibratory loading induces damage in the material. This may prove to be interesting at low frequencies, as munitions may be transported on long-duration flights which can result in issues with de-bonding within the system. It would be interesting to determine the effects of the thermal cycling in this frequency regime.

7.2.2 High–Frequency Regime

- *Extreme Temperature Environments*: In certain applications, the energetic materials may experience extreme temperature environments in excess of 100°C. To maintain safe handling and sound system design, it would be of interest to characterize the thermal and mechanical behavior of polymer–bonded energetic materials at these temperatures beyond the preliminary experiments presented in Chapter 5.

- *Material Softening Behavior*: The present research developed an experimental technique referred to as a frequency–tracking experiment to monitor and account for the material softening and subsequent shift in resonant frequency while undergoing high–frequency mechanical excitation. It would be of interest to modify the experimental setup to allow a random vibration input to the piezoelectric shaker, as this would allow the user to excite a range of frequencies near the initial resonance. This method would also allow an additional benefit, as the random excitation allows the determination of a transfer function in the frequency domain; such a function would aid in separating the coupled dynamics of the sample and the piezoelectric shaker and potentially provide useful insight with regard to modeling the energetic material sample in isolation.

- *Plasticity and Thermal Modeling*: A robust, three-dimensional model to predict thermal and mechanical behavior would be of interest to investigate potential new formulations at high frequencies.

- *High–Frequency Material Properties*: The majority of material properties available for composite energetic materials were not determined in the frequency range investigated herein. In order to provide a successful prediction of material behavior, a systematic technique for determining the properties at frequencies up to 20 kHz would be beneficial.

- *Induced Damage*: Similar to the low–frequency regime, the effect of thermal cycling and induced damage may prove interesting as the damage mechanisms are most likely more complex in the higher frequency range.

- *Particle–Binder Interface*: The body of work currently established for the thermomechanics of energetic materials suggests that the particle-binder interface is of great consequence in terms of heating rates and mechanical properties. Investigation into the mechanisms of this effect, as well as characterization of the interface with regard to strength, should be of interest in the energetic material community.

REFERENCES

REFERENCES

[1] J.O. Mares, J.K. Miller, N.D. Sharp, D.S. Moore, D.E. Adams, L.J. Groven, J.F. Rhoads, and S.F. Son. Thermal and mechancial response of PBX 9501 under contact excitation. *Journal of Applied Physics*, 113(8):084904, 2013.

[2] J.K. Miller, D.C. Woods, J.F. Rhoads. Thermal and mechanical response of particulate composite plates under inertial excitation. *Journal of Applied Physics*, 116(24):244904, 2014.

[3] A.E.D.M. van der Heijden, Y.L.M. Creyghton, E. Marino, R.H.B. Bouma, G.J.H.G. Scholtes, W. Duvalois. Energetic materials: crystallization, characterization and insensitive plastic bonded explosives. *Propellants, Explosives, Pyrotechnics*, 33(1):25–32, 2008.

[4] Z.A. Roberts, J.O. Mares, J.K. Miller, I.E. Gunduz, S.F. Son, J.F. Rhoads. Phase changes in embedded HMX in response to periodic mechanical excitation. *Challenges in Mechanics of Time Dependent Materials*, 2:79–86, 2017.

[5] J. Paripovic, P. Davies. A model identification technique to characterize the low frequency behaviour of surrogate explosive materials. *Journal of Physics: Conference Series*, 744(1):012124, 2016.

[6] R. Arefinia, A. Shojaei. On the viscosity of composite suspensions of aluminum and ammonium perchlorate particles dispersed in hydroxyl terminated polybutadiene—new empirical model. *Journal of Colloid and Interface Science*, 299(2):962–971, 2006.

[7] S.Y. Fu, X.Q. Feng, B. Lauke, and Y.W. Mai. Effects of particle size, particle/matrix interface adhesion and particle loading on mechanical properties of particulate–polymer composites. *Composites Part B: Engineering*, 39(6):933–961, 2008.

[8] K. Wakashima and H. Tsukamoto. Mean-field micromechanics model and its application to the analysis of thermomechanical behaviour of composite materials. *Materials Science and Engineering: A*, 146(1):291–316, 1991.

[9] T.B. Lewis and L.E. Nielsen. Dynamic mechanical properties of particulate-filled composites. *Journal of Applied Polymer Science*, 14(6):1449–1471, 1970.

[10] S.B. Ratner, V.I. Korobov. Self-heating of plastics during cyclic deformation. *Polymer Mechanics*, 1(3):63–68, 1965.

[11] F. Dinzart, A. Molinari, R. Herbach. Thermomechanical response of a viscoelastic beam under cyclic bending; self-heating and thermal failure. *Archives of Mechanics*, 60(1):59–85, 2008.

[12] A.D. Dimarogonas, N.B. Syrimbeis. Thermal signatures of vibrating rectangular plates. *Journal of Sound and Vibration*, 157(3):467–476, 1992.

[13] R.F. Gibson. Modal vibration repsonse measurements for characterization of composite materials and structures. *Composites Science and Technology*, 60(15):2769–2780, 2000.

[14] E.C. Botelho, A.N. Campos, E. de Barros, L.C. Pardini, M.C. Rezende. Damping behavior of continuous fiber/metal composite materials by the free vibration method. *Composites Part B: Engineering*, 37(2-3):255–263, 2006.

[15] A. Katunin, M. Fidali. Self-heating of polymeric laminated composite plates under the resonant vibrations: Theoretical and experimental study. *Polymer Composites*, 33(1):138–146, 2012.

[16] C.M. Cady, W.R. Blumenthal, G.T. Gray III, D.J. Idar. Mechanical properties of plastic-bonded explosive binder materials as a function of strain-rate and temperature. *Polymer Engineering and Science*, 46(6):812–819, 2006.

[17] A. Tokmakoff, M.D. Fayer, Dana D. Dlott. Chemical reaction initiation and hot-spot formation in shocked energetic molecular materials. *Journal of Physical Chemistry*, 97(9):1901–1913, 1993.

[18] R. Behnke, M. Kaliske, M. Klüppel. Thermo-mechanical analysis of cyclically loaded particle-reinforced elastomer components: experiment and finite element simulation. *Rubber Chemistry and Technology*, 89(1):154–176, 2016.

[19] A.M. Walid, G.Z. Liang. Different methods for developing relaxation modulus master curves of AP-HTPB solid propellant. *Chinese Journal of Energetic Materials*, 25(10):810–816, 2017.

[20] N.P. Loginov, S.M. Muratov, and N.K. Nazarov. Initiation of explosion and kinetics of explosive decomposition under vibration. *Combustion, Explosion, and Shock Waves*, 12(3):367–370, 1976.

[21] N.P. Loginov. Structural and physicochemical changes in RDX under vibration. *Combustion, Explosion and Shock Waves*, 33(5):598–604, 1997.

[22] M.A. Biot. Linear thermodynamics and the mechanics of solids. *Proceedings of the Third U.S. National Congress of Applied Mechanics*, 1–18, 1958.

[23] J. Rantala, D. Wu, and G. Busse. Amplitude-modulated lock-in vibrothermography for NDE of polymer and composites. *Research in Nondestructive Evaluation*, 7(4):215–228, 1996.

[24] L.H. Tenek, E.G. Henneke II, and M.D. Gunzburger. Vibration of delaminated composite plates and some applications to non-destructive testing. *Composite Structures*, 23(3):253–262, 1993.

[25] J. Renshaw, J.C. Chen, S.D. Holland, and R.B. Thompson. The sources of heat generation in vibrothermography. *NDT & E Int.*. 44(8):736–739, 2011.

[26] V. Vavilov, D. Nesteruk. Comparative analysis of optical and ultrasonic stimulation of flaws in composite materials. *Russian Journal of Nondestructive Testing*, 46(2):736–739, 2011.

[27] R.B. Mignogna, R.E. Green Jr., J.C. Duke Jr., E.G. Henneke II, K.L. Reifsnider. Thermographic investigation of high-power ultrasonic heating in materials. *Ultrasonics*, 19(4):159–163, 1981.

[28] O.P. Chervinko. Calculating the critical parameters characterizing the thermal instability of a viscoelastic prism with a stress concentrator under harmonic compression. *International Journal of Applied Mechanics*, 40(8):916–922, 2004.

[29] O.P. Chervinko, I.K. Senchenkov, N.N. Yakimenko. Vibrations and self-heating of a viscoelastic prism with a cylindrical inclusion. *International Journal of Applied Mechanics*, 43(6):647–653, 2007.

[30] W. Luo, T. Yang, Z. Li, L. Yuan. Experimental studies on the temperature fluctuations in deformed thermoplastics with defects. *International Journal of Solids and Structures*, 37(6):887–897, 2000.

[31] J.O. Mares, J.K. Miller, I.E. Gunduz, J.F. Rhoads, and S.F. Son. Heat generation in an elastic binder system with embedded discrete energetic particles due to high-frequency, periodic mechanical excitation. *Journal of Applied Physics*, 116(20):204902, 2014.

[32] N.D. Parab, Z.A. Roberts, M.H. Harr, J.O. Mares, A.D. Casey, I.E. Gunduz, M. Hudspeth, B. Claus, T. Sun, K. Fezzaa, S.F. Son, W.W. Chen. High speed X-ray phase contrast imaging of energetic composites under dynamic compression. *Applied Physics Letters*, 109(13):131903, 2016.

[33] M.W. Chen, S. You, K.S. Suslick, D.D. Dlott. Hot spot in energetic materials generated by infrared and ultrasound, detected by thermal image microscopy. *Review of Scientific Instruments*, 85(2):023705, 2014.

[34] S. You, M.W. Chen, D.D. Dlott, K.K. Suslick. Ultrasonic hammer produces hot spots in solids. *Nature Communications*, 6:6581, 2015.

[35] D.C. Woods, J.K. Miller, and J.F. Rhoads. On the thermomechanical response of HTPB-based composite beams under near-resonant excitation. *Journal of Vibration and Acoustics*, 137(5):054502, 2015.

[36] P. Knysh, Y.P. Korkolis. Determination of the fraction of plastic work converted into heat in metals. *Mechanics of Materials*, 86:71–80, 2015.

[37] D. Macdougall. Determination of the plastic work converted to heat using radiometry. *Experimental Mechanics*, 40(3):298–306, 2000.

[38] R. Kapoor, S. Nemat-Nasser. Determination of temperature rise during high strain rate deformation. *Mechanics of Materials*, 27(1):1–12, 1998.

[39] X. Tong, X. Chen, J. Xu, C. Sun, W. Liang. Excitation of thermal dissipation of solid propellants during the fatigue process. *Materials & Design*, 128:47–55, 2017.

[40] L. Mullins. Softening of rubber by deformation. *Rubber Chemistry and Technology*, 42(1):339–362, 1969.

[41] R.W. Ogden, D.G. Roxburgh. A pseudo-elastic model for the Mullins effect in filled rubber. *Proceedings of the Royal Society of London, Series A: Mathematical, Physical and Engineering Sciences*, 455(1988):2861–2877, 1999.

[42] R. Schapery, D. Cantey. Thermomechanical response studies of solid propellants subjected to cyclic and random loading. *American Institute of Aeronautics and Astronautics Journal*, 4(2):255–264, 1966.

[43] R. Schapery. Effect of cyclic loading on the temperature in viscoelastic media with variable properties. *American Institute of Aeronautics and Astronautics Journal*, 2(5):827–835, 1964.

[44] R. Schapery. Thermomechanical behavior of viscoelastic media with variable properties subjected to cyclic loading. *Journal of Applied Mechanics*, 32(3):611–619, 1965.

[45] R. Farris, R. Schapery. Development of solid rocket propellant nonlinear viscoelastic constitutive theory, Volume 1. *Aerojet Solid Propulsion Company*, Text, 1973.

[46] S. Flueckiger, Y. Zheng, T. Pourpoint. Transient plane source method for thermal property measurements of metal hydrides. *ASME 2008 Heat Transfer Summer Conference*, 1:9–13, 2008.

[47] J.E. Field, N.K. Bourne, S.J.P Palmer, S.M. Walley, J. Sharma, B.C. Beard. Hot-spot ignition mechanisms for explosives and propellants. *Philosophical Transactions of the Royal Society of London A: Mathematical, Physical and Engineering Sciences*, 339:269–283, 1992.

[48] W. Holmes, R.S. Francis, M.D. Fayer. Crack propagation induced heating in crystalline energetic materials. *The Journal of Chemical Physics*, 110(7):3576–3583, 1999.

[49] A. Tokmakoff, M.D. Fayer, D.D. Dlott. Chemical reaction initiation and hot-spot formation in shocked energetic molecular materials. *The Journal of Physical Chemistry*, 97(9):1901–1913, 1993.

[50] S. Chen, X. Hong, J.R. Hill, D.D. Dlott. Ultrafast energy transfer in high explosives: Vibrational cooling. *The Journal of Physical Chemistry*, 99(13):4525–4530, 1995.

[51] I.J. Lochert, R.M. Dexter, and B.L. Hamshere. Evaluation of Australian RDX in PBXN-109. *Technical Report, Australian Government DSTO*, 2002.

[52] T.L. Bergman, A.S. Lavine, F.P.Incropera, and D.P. Dewitt. Fundamentals of Heat and Mass Transfer. John Wiley & Sons, (2011).

[53] J. Paripovic. Identification of the low frequency dynamic behavior of surrogate explosive materials. *ProQuest*, 2018.

[54] D.C. Woods. On the use of mechanical and acoustical excitations for selective heat generation in polymer-bonded energetic materials. *ProQuest*, 2016.

[55] T. Kanit, S. Forest, I. Galliet, V. Mounoury, D. Jeulin. Determination of the size of the representative volume element for random composites: statistical and numerical approach. *International Journal of Solids and Structures*, 40(13-14):3647–3679, 2003.

[56] W.J. Drugan, J.R. Willis. A micromechanics-based nonlocal constitutive equation and estimates of representative volume element size for elastic composites. *Journal of the Mechanics and Physics of Solids*, 44(4):497–524, 1996.

[57] C.T. Sun, R.S. Vaidya. Prediction of composite properties from a representative volume element. *Composites Science and Technology*, 56(2):171–179, 1996.

[58] A.A. Gusev. Representative volume element size for elastic composites: a numerical study. *Journal of the Mechanics and Physics of Solids*, 45(9):1449–1459, 1997.

[59] C.L.Y. Yeong, S. Torquato. Reconstructing random media. *Physical Review E*, 57(1):495–506, 1998.

[60] S.S. Rao. Vibration of continuous systems. *Wiley Online Library*, Text, 2007.

[61] M. Liakat, M.M. Khonsari. On the anelasticity and fatigue fracture entropy in high-cycle metal fatigue. *Materials & Design*, 82:18–27, 2015.

[62] R. Munier, C. Doudard, S. Calloch, B. Weber. Determination of high cycle fatigue properties of a wide range of steel sheet grades from self-heating measurements. *International Journal of Fatigue*, 63:46–61, 2014.

[63] A.T. Zehnder, E. Babinsky, T. Palmer. Hybrid method for determining the fraction of plastic work converted to heat. *Experimental Mechanics*, 38(4):295–302, 1998.

[64] T.L. Jackson, J. Buckmaster. Heterogeneous propellant combustion *American Institute of Aeronautics and Astronautics Journal*, 40(6):1122–1130, 2002.

[65] W. Cai, P. Thakre, V. Yang. A model of AP/HTPB composite propellant combustion in rocket-motor environments. *Combustion Science and Technology*, 180(12):2143–2169, 2008.

APPENDIX

A. HIGH-FREQUENCY MOCK ENERGETIC THERMAL EXPERIMENT DATA

Results from the thermal experiments performed with no thermal barriers are presented in Table A.1. Twelve experiments were conducted twice to verify repeatability. The majority of the samples exhibited similar behavior in the first and second experiments; however, discrepancies between first and second experiment may be attributed to measurement error in the thermal cameras; environmental changes within the test space, as the experiments were performed on different days; or aging effects of the composite material itself. Note that a resonance of the piezoelectric shaker was identified at approximately 60 kHz, resulting in a shaker shutdown within the 15 min test window. The experiments affected by this are marked with an asterisk.

The temperature increases for samples with the glass mica ceramic and PEEK thermal barriers are provided in Table A.2. Each of the six samples in this set exhibited a dominant frequency in the largest subrange at, or around, 60 kHz, therefore, those experiments were omitted due to the aforementioned shaker resonance. In one experiment, the temperature exceeded the calibrated range of the FLIR A6507 thermal camera at the side resulting in an incorrect transient ambient temperature measurement. Therefore, the temperature increases reported with a plus sign indicate a magnitude obtained by simply subtracting a static room temperature value from the absolute temperature.

Table A.1. : Temperature increase for samples of various height and formulation in response to harmonic excitation at the dominant resonant frequency within four subranges (1-20, 20-40, 40-60, and 60-80 kHz).

1.27 cm Sample Height													
	Sample Formulation	85-00				85-15				85-30			
	Sample Number	1		2		1		2		1		2	
1-20 kHz	Frequency (kHz)	11.41		12.81		12.68		12.53		13.66		13.60	
	Side Avg Temp Increase (°C)	7.7		9.5		18.2		21.2		20.3	10.3	15.3	
	Side Max Temp Increase (°C)	9.2		11.2		21.9		25.9		25.2	13.0	21.1	
	Top Avg Temp Increase (°C)	10.3		13.4		23.3		26.1		21.1	12.1	15.9	
	Top Max Temp Increase (°C)	12.0		17.9		27.5		29.8		23.4	12.8	17.5	
	Baseplate Temp Increase (°C)	1.5		1.9		3.4		3.7		7.8	4.0	6.2	
20-40 kHz	Frequency (kHz)	35.45		35.59		35.26		35.53		28.27		27.85	
	Side Avg Temp Increase (°C)	0.6	1.3	0.4		1.1		0.7		0.1		0.3	0.5
	Side Max Temp Increase (°C)	0.6	1.6	0.5		1.1		0.9		0.2		0.2	0.6
	Top Avg Temp Increase (°C)	1.4	1.1	1.4		1.2		1.0		1.4		0.7	0.8
	Top Max Temp Increase (°C)	1.5	1.2	1.3		1.3		0.9		1.3		0.8	0.7
	Baseplate Temp Increase (°C)	0.5	0.8	0.7		0.9		1.1		0.6		0.6	1.0
40-60 kHz	Frequency (kHz)	59.34		44.54		58.77		58.58		44.60		44.30	
	Side Avg Temp Increase (°C)	13.2*		7.6	3.3	18.1*	17.4*	16.9*		4.2		6.6	
	Side Max Temp Increase (°C)	22.0*		9.3	3.8	28.6*	26.5*	26.1*		6.9		10.4	
	Top Avg Temp Increase (°C)	8.6*		6.9	3.0	14.7*	14.5*	14.2*		4.2		7.6	
	Top Max Temp Increase (°C)	10.1*		6.6	2.3	20.8*	16.8*	16.0*		4.8		8.1	
	Baseplate Temp Increase (°C)	28.6*		8.5	2.6	38.1*	36.4*	36.9*		9.2		10.6	
60-80 kHz	Frequency (kHz)	69.68		69.52		70.58		60.16		60.33		60.21	
	Side Avg Temp Increase (°C)	29.1	29.7	32.0		26.5	26.6	6.6*		9.4*		6.8*	
	Side Max Temp Increase (°C)	47.2	45.5	50.9		40.9	39.9	12.1*		16.4*		12.8*	
	Top Avg Temp Increase (°C)	20.7	21.6	23.5		22.4	22.2	4.6*		8.4*		5.6*	
	Top Max Temp Increase (°C)	31.0	30.6	34.1		23.3	22.6	5.3*		8.8*		6.2*	
	Baseplate Temp Increase (°C)	60.5	54.8	62.3		54.3	51.3	19.1*		21.1*		17.3*	
0.635 cm Sample Height													
	Sample Formulation	85-00				85-15				85-30			
	Sample Number	3		4		3		4		3		4	
1-20 kHz	Frequency (kHz)	14.14		15.09		18.15		13.88		9.48		11.83	
	Side Avg Temp Increase (°C)	52.8	52.1	11.2		1.2		11.3	8.7	6.6		14.0	
	Side Max Temp Increase (°C)	63.7	62.1	15.8		1.3		13.8	10.5	7.7		16.7	
	Top Avg Temp Increase (°C)	57.2	61.7	9.8		2.0		13.7	10.0	9.2		19.2	
	Top Max Temp Increase (°C)	64.5	77.2	10.6		2.2		16.2	11.6	9.8		21.6	
	Baseplate Temp Increase (°C)	14.2	24.6	17.8		0.8		4.1	4.0	1.8		4.4	
20-40 kHz	Frequency (kHz)	35.43		35.45		35.61		35.61		35.54		35.16	
	Side Avg Temp Increase (°C)	0.5		0.4		1.1	1.4	1.3		1.1		0.9	
	Side Max Temp Increase (°C)	0.5		0.4		1.1	1.4	1.4		1.4		1.0	
	Top Avg Temp Increase (°C)	0.9		0.3		1.3	1.8	2.6		1.6		1.5	
	Top Max Temp Increase (°C)	0.9		0.3		1.4	1.2	2.6		1.6		1.5	
	Baseplate Temp Increase (°C)	0.7		0.6		1.1	1.0	1.1		1.4		1.1	
40-60 kHz	Frequency (kHz)	52.04		59.98		59.11		59.83		44.47		59.09	
	Side Avg Temp Increase (°C)	9.7		12.8*		19.2*		9.8*		6.4	2.0	21.0*	
	Side Max Temp Increase (°C)	12.1		18.8*		25.8*		15.1*		8.5	2.4	26.9*	
	Top Avg Temp Increase (°C)	10.4		12.3*		19.4*		8.5*		8.2	8.2	22.7*	
	Top Max Temp Increase (°C)	10.9		17.4*		19.8*		10.8*		8.2	1.8	23.3*	
	Baseplate Temp Increase (°C)	12.9		25.2*		33.6*		24.0*		9.1	2.7	35.0*	
60-80 kHz	Frequency (kHz)	70.49		69.16		60.27		69.62		60.49		70.56	
	Side Avg Temp Increase (°C)	35.1		35.8		10.2*		35.8		10.7*		31.5	32.4
	Side Max Temp Increase (°C)	44.9		45.8		14.6*		47.0		14.5*		41.8	41.2
	Top Avg Temp Increase (°C)	32.1		33.1		9.6*		34.2		12.3*		33.1	33.3
	Top Max Temp Increase (°C)	34.5		38.8		13.3*		36.9		12.6*		33.8	34.6
	Baseplate Temp Increase (°C)	52.0		57.1		23.3*		58.5		18.4*		52.7	50.9

Table A.2. : Temperature increase for 1.27 cm height samples of various formulations with glass mica ceramic and PEEK thermal barriers attached beneath in response to harmonic excitation at the dominant resonant frequency within three subranges (1-20, 20-40, and 40-60 kHz).

1.27 cm Sample Height - Thermal Barrier							
	Sample Formulation	85-00		85-15		85-30	
	Sample Number	5	6	5	6	5	6
	Thermal Barrier Material	Ceramic	PEEK	Ceramic	PEEK	Ceramic	PEEK
1-20 kHz	Frequency (kHz)	15.36	15.54	15.47	15.51	15.58	15.70
	Side Avg Temp Increase (°C)	26.3		18.4	45.0	20.4	39.1
	Side Max Temp Increase (°C)	33.8	78.4[+]	21.7	64.4	30.9	56.5
	Top Avg Temp Increase (°C)	21.9	69.6	21.8		20.3	35.6
	Top Max Temp Increase (°C)	29.6	82.6	24.6		22.1	39.7
	Baseplate Temp Increase (°C)	10.3		7.0	11.2	9.8	10.6
20-40 kHz	Frequency (kHz)	33.19	21.34	22.02	22.42	21.85	22.02
	Side Avg Temp Increase (°C)	0.2	2.0	1.6	1.4	1.1	1.6
	Side Max Temp Increase (°C)	0.3	2.4	1.9	1.5	1.7	1.9
	Top Avg Temp Increase (°C)	0.4	1.8	1.5	1.1	0.9	1.5
	Top Max Temp Increase (°C)	0.4	2.3	1.3	1.1	0.8	1.0
	Baseplate Temp Increase (°C)	0.5	0.7	0.9	0.5	0.7	0.7
40-60 kHz	Frequency (kHz)	57.23	59.11	44.33	56.15		56.10
	Side Avg Temp Increase (°C)	6.0	10.5	12.2	6.7		8.1
	Side Max Temp Increase (°C)	10.2	16.4	19.0	11.1		14.1
	Top Avg Temp Increase (°C)	3.7	6.6	12.3	5.3		7.5
	Top Max Temp Increase (°C)	8.3	10.6	11.3	10.8		9.6
	Baseplate Temp Increase (°C)	11.9	22.6	6.7	13.9		14.1

B. HIGH-FREQUENCY MOCK ENERGETIC FREQUENCY RESPONSE REPEATABILITY

The frequency response functions for a representative mock sample of each formulation (85% solids loading with 0%, 15% and 30% aluminum additive content) are shown in Figures B.1 to B.3. The response was measured twice to verify repeatability in the mechanical response. As described in Chapter 3, the velocity was measured with time using the laser Doppler vibrometer in response to a swept sinusoidal input at the base of the cylindrical sample. The velocity data was then differentiated and transformed to produce the instantaneous acceleration versus instantaneous frequency as shown below. Minor discrepancies are present, however, the overall response appears to exhibit good correlation between the first test and the second test, especially near resonant frequencies.

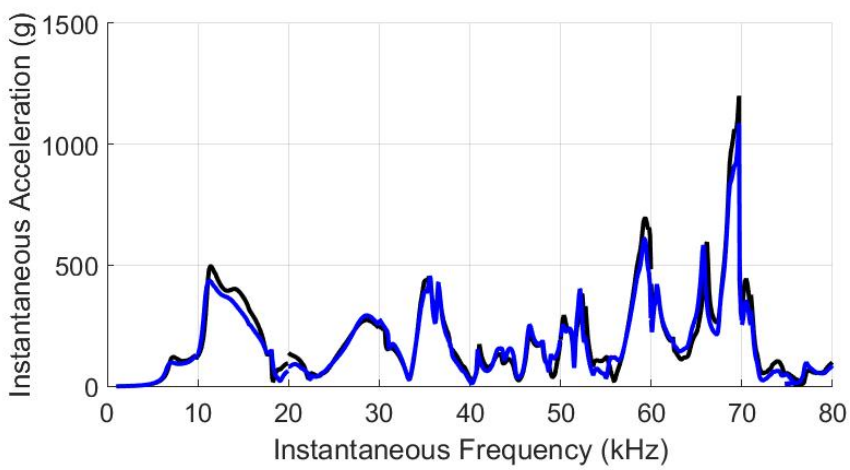

Figure B.1. : Instantaneous acceleration versus frequency for a 1.27 cm height sample prepared at 85% solids loading with 0% aluminum additive content recorded at two separate times to verify repeatability. The black line represents the response obtained first, and the blue line represents the response obtained second.

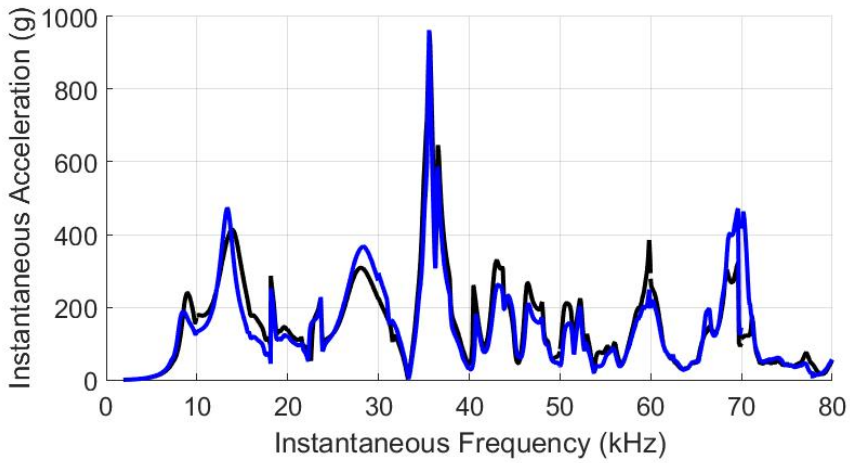

Figure B.2. : Instantaneous acceleration versus frequency for a 0.64 cm height sample prepared at 85% solids loading with 15% aluminum additive content recorded at two separate times to verify repeatability. The black line represents the response obtained first, and the blue line represents the response obtained second.

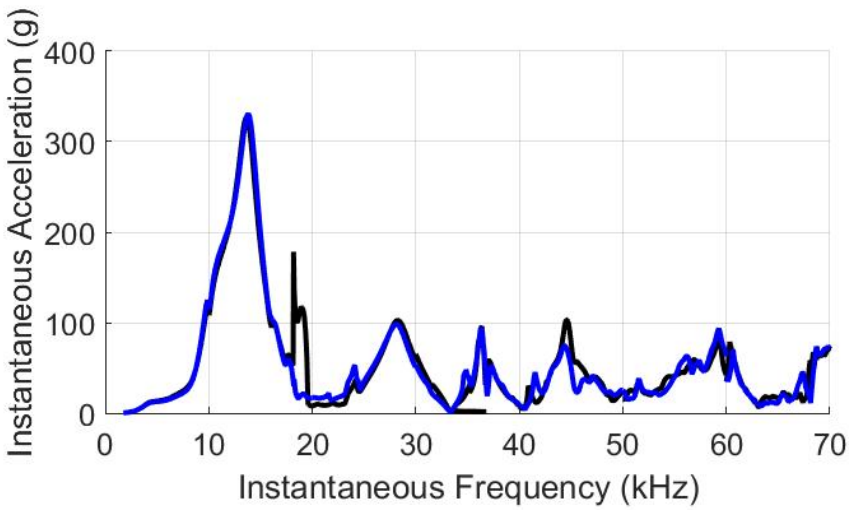

Figure B.3. : Instantaneous acceleration versus frequency for a 1.27 cm height sample prepared at 85% solids loading with 30% aluminum additive content recorded at two separate times to verify repeatability. The black line represents the response obtained first, and the blue line represents the response obtained second.

VITA

VITA

Allison R. Range completed her B.S. in Mechanical Engineering from Michigan Technological University in 2015. She graduated from Purdue University with her M.S.M.E. in 2018 and Ph.D. in 2019, both in the field of Mechanical Engineering. Her research interests are focused in the areas of mechanical vibration, dynamic systems, and acoustics with a variety of applications.

Journal Publications

- Allison R. Range, Nicole R. McMindes, Jeffrey F. Rhoads. The near-resonant thermomechanics of particulate composite mock energetic materials in response to high frequency (1 to 100 kHz) excitation. *Draft submitted.*
- Allison R. Range, Jacob T. Morris, Jeffrey F. Rhoads. The near-resonant thermomechanics of energetic and inert composite materials in response to high frequency excitation in elevated temperature environments. *Draft in progress.*

Book Chapter

- Allison R. Range, Nicole R. McMindes, Jaylon B. Tucker, Jeffrey F. Rhoads. The influence of formulation variation and thermal boundary conditions on the near-resonant thermomechanics of mock explosives. *Fracture, Fatigue, Failure and Damage Evolution, Volume 7*, 2017.

Conference Publication

- Lauren A. Cooper, Allison R. Range, Jeffrey F. Rhoads. The influence of macroscale stress concentrations on the near-resonant thermomechanics of mock energetic materials. *Summer Undergraduate Research Fellowship (SURF) Symposium, Paper 7*, 2017.

Conference Presentations

- Allison R. Range, Nicole R. McMindes, Jaylon B. Tucker, Jeffrey F. Rhoads. The influence of formulation variation and thermal boundary conditions on the near-resonant thermomechanics of mock explosives. *Annual Conference for the Society of Engineering Mechanics*, Indianapolis, IN.
- Allison R. Range, Nicole R. McMindes, Jeffrey F. Rhoads. The near-resonant thermomechanics of particulate composite mock explosives in response to high frequency excitation. *International Design Engineering Technical Conferences*, Quebec City, CA.
- Allison R. Range, Jeffrey F. Rhoads. The near-resonant thermomechanics of particulate composite energetic materials in response to high frequency excitation. *International Nonlinear Dynamics Conference*, Rome, Italy.

Technical Reports

- Jeffrey F. Rhoads, Steven F. Son, Patricia Davies, Marcial Gonzalez, Marisol Koslowski, Allison Range, Jelena Paripovic, Ankit Agarwal, Bogdan Tanasoiu, Johanna Palsdottir. Near-resonant thermomechanics of energetic and mock energetic composite materials. *Purdue University*, January 2016.
- Jeffrey F. Rhoads, Steven F. Son, Patricia Davies, Marcial Gonzalez, Marisol Koslowski, Allison Range, Jelena Paripovic, Ankit Agarwal, Akshay Dandekar, Lauren Cooper. Near-resonant thermomechanics of energetic and mock energetic composite materials, part 2. *Purdue University*, March 2018.